1966

Electrical properties of metallic sodium tungsten bronze

Lewis Dee Muhlestein
Iowa State University

MUHLESTEIN, Lewis Dee, 1938-
ELECTRICAL PROPERTIES OF METALLIC SODIUM TUNGSTEN BRONZE.

Iowa State University of Science and Technology, Ph.D., 1966
Physics, solid state

ELECTRICAL PROPERTIES OF METALLIC SODIUM TUNGSTEN BRONZE

by

Lewis Dee Muhlestein

A Dissertation Submitted to the
Graduate Faculty in Partial Fulfillment of
The Requirements for the Degree of
DOCTOR OF PHILOSOPHY

Major Subject: Physics

Approved:

Signature was redacted for privacy.

In Charge of Major Work

Signature was redacted for privacy.

Head of Major Department

Signature was redacted for privacy.

Dean of Graduate College

Iowa State University
Of Science and Technology
Ames, Iowa

1966

TABLE OF CONTENTS

LIST OF FIGURES

Page

LIST OF TABLES

ABSTRACT

The resistivities, Hall coefficients, and Seebeck coefficients of metallic Na_xWO_3 have been measured as functions of the sodium concentration (x-value) from x = 0.4 to x = 0.9 and as functions of the temperature from 4.2°K to 300°K. The resistivity and Hall coefficients showed an anomaly at x = 0.75 where the sodium atoms are ordered. These results are the first demonstration of ordering effects in any transport property of any tungsten bronze. At low temperatures the Seebeck coefficient consisted of a lattice contribution and a diffusion contribution. The lattice term had a part due to normal phonon-electron interactions, which decreased with increasing sodium concentration; and a part due to Umklapp phonon-electron interactions, which increased with increasing sodium concentration. The resistivities, Hall coefficients, and Seebeck coefficients are sensitive to the homogeneity of the single crystals. The electrical properties of homogeneous crystals did not follow the predictions of free electron theory.

I. INTRODUCTION

The nonstoichiometric compounds M_xWO_3 (where M represents an alkali metal) are commonly referred to as the alkali tungsten bronzes and since their discovery (Wohler, 1824 (1)) their properties have stimulated the interest of many investigators. Although other bronzes have been prepared and investigated, the alkali tungsten bronzes have received the most attention and, in particular, extensive data exists on sodium tungsten bronze, Na_xWO_3.

The x-ray analyses of Hagg (2) and Magneli (3) have shown that the crystal structure of Na_xWO_3 is the cubic perovskite structure for sodium concentrations (x-values) between x = 1.0 and x = 0.48.† For x between 0.48 and 0.25, the crystal structure of Na_xWO_3 is tetragonal with c/a = 0.3 and is usually designated as tetragonal I.†† For x between 0.25 and 0.05 the crystal structure is also tetragonal with c/a = 0.8 and is usually designated as tetragonal II. There is also a hexagonal structure which seems to overlap both of the tetragonal structures; and below x = 0.05 there are other changes in the crystal structure of Na_xWO_3.

---

†There exists some discrepancy in the literature concerning the values of x at which the structural changes occur. Indeed, Ribnick *et al.* (4) have shown that there is some overlap in the phase transitions. The values of x which shall be given here for the phase transitions will be those values which seem to occur most in practice.

††Ribnick *et al.* (4) have changed the designation of the two tetragonal structures originally used by Magneli (3). Here Magneli's original designation will be used.

Early investigations (5-8) showed that for sodium concentrations between x = 1.0 and x = 0.48 (the cubic structure) Na_xWO_3 exhibits a metallic behavior. Later (9) the range of the metallic behavior was extended to include the tetragonal I structure. For sodium concentrations between x = 0.25 and x = 0.0 (the tetragonal II and the lower symmetry structures) Na_xWO_3 exhibits the behavior characteristic of a semiconductor or an insulator (9). Hence, if the sodium concentration is varied, the properties of Na_xWO_3 can be changed from metallic behavior to the behavior characteristic of a semiconductor or an insulator. Thus, the intriguing aspect of Na_xWO_3, both to the theorist and to the experimentalist, has been this ability (in theory) to control the number of conduction electrons. Unfortunately however, the inability to grow good single crystals (especially in the low sodium concentration range); and (until recently) the inability to accurately determine the x-value of the crystals with low sodium concentrations have limited the experimental data primarily to the cubic range. Even for the cubic Na_xWO_3 the data has often been contradictory or inconclusive. The present investigation is an attempt to re-examine some of the electrical transport properties of metallic Na_xWO_3 as a function of the sodium concentration and to extend the measurements to lower values of x. The transport properties which were measured were the electrical resistivity, the Hall coefficient and the Seebeck coefficient. The results are compared to the results of previous investigations and discussed in terms of the various models which have been proposed for Na_xWO_3.

II. REVIEW OF EXPERIMENTAL DATA AND THEORETICAL MODELS

A. Experimental Data

1. Transport properties

As early as 1949 Straumanis and Dravnieks (5) measured the electrical resistivity of cubic polycrystalline Na_xWO_3. The resistivity of cubic single crystals were measured in 1951 by Huibregtse et al. (6). These investigations showed that cubic Na_xWO_3 had a high electrical conductivity and a positive temperature coefficient of resistivity. Brown and Banks (7) (1951) then showed that the resistivity of Na_xWO_3 had a linear temperature dependence. This resistivity data, together with the Hall coefficients which were measured by Gardner and Danielson (8)(1954), indicated that cubic Na_xWO_3 exhibited metallic behavior, and that each sodium atom contributes one electron to the conduction band.

However, the resistivity which had been measured by Brown and Banks (7) and by Gardner and Danielson (8) showed a definite minimum in the resistivity versus the sodium concentration at $x = 0.75$. Brown and Banks interpreted the minimum in the resistivity in terms of an equilibrium between the undissociated sodium atoms and the sodium ions plus free electrons; while Gardner and Danielson suggested that the minimum was due to the ordering of the sodium atoms. However, Ellerbeck et al. (10)(1961) showed that the minimum in the resistivity was due to the inhomogeneous crystals which were used by the previous investigators; and that when homogeneous single crystals were used for measurements

there was no minimum in the curve, resistivity versus sodium concentration. In fact, Ellerbeck et al. found no evidence of any anomaly at x = 0.75 even though partial ordering of the sodium atoms had been seen at x = 0.75 by Atoji and Rundle (11)(1960) in their neutron diffraction work. However, Mackintosh (12)(1962) pointed out that the experimental evidence to that date did not necessarily rule out the possibility of a maximum in the conductivity at x = 0.75; and suggested that further measurements be made in the region of the superlattice structure.

The electronic specific heat of several Na_xWO_3 samples with sodium concentrations from x = 0.89 to x = 0.56 was measured by Vest et al. (13)(1958). Using the approximation that $\gamma = \frac{1}{3}\pi^2k^2VN(E_f)$, Vest et al. calculated the density of states at the Fermi level as a function of the sodium concentration. They found a sharp increase in the density of states at x = 0.75 which was attributed to the Fermi surface approaching the Brillouin zone boundary. However, the density of states which was calculated from the magnetic susceptibility measured by Greiner et al. (14)(1962) did not show any such increase at x = 0.75. Rather, the density of states as determined from the magnetic susceptibility seemed to be a monotonically increasing function of x and did not vary as $x^{\frac{1}{3}}$ as predicted by the free electron model.

McNeill and Conroy (15)(1962) attempted to extend the measurements of the electrical properties of Na_xWO_3 to lower sodium concentrations. Their low x-value crystals were prepared by diffusing the sodium out of higher x-value crystals. The properties associated with decreasing just

the sodium concentration presents an interesting problem in itself, but this does not represent the true picture of Na_xWO_3. Their low x-value crystals were still cubic whereas for Na_xWO_3 the crystal structure for x between 0.48 and 0.25 is tetragonal. Hence, it is questionable whether the data obtained by McNeill and Conroy really applies to Na_xWO_3.

The Seebeck coefficients of cubic Na_xWO_3 were measured by Shanks et al. (9)(1963) at 300°K. They found that the Seebeck coefficients seemed to vary as $x^{-\frac{2}{3}}$ as predicted by the free electron model. Shanks et al. concluded that for the electronic properties of Na_xWO_3 the free electron model was applicable even though the free electron model did not account for the thermodynamic properties.

2. Nuclear magnetic resonance

Perhaps the most striking experimental result was the nuclear magnetic resonance of ^{23}Na in cubic Na_xWO_3 which was measured by Jones et al. (16)(1962). They found essentially no paramagnetic Knight shift in the ^{23}Na resonance. A negligible Knight shift indicated that there was essentially no interaction of the sodium nuclei with the conduction electrons. This result may arise from the occurrence of either a radial or an angular node in the conduction band wave functions at the sodium atom positions.

Narath and Wallace (17)(1962) observed the room temperature ^{183}W nuclear megnatic resonance in several cubic Na_xWO_3 samples and in WO_3. They found a small negative ^{183}W Knight shift. The absence of a positive ^{183}W Knight shift in Na_xWO_3 ruled out the the possibility of any major

contribution of the tungsten 6s states to the conduction band. Narath and Walláce explained the magnitudes of the observed ^{183}W Knight shifts by an exchange polarization of the core s electrons at the tungsten sites by conduction electrons near the top of the Fermi distribution. They further proposed that the observed increase of the ^{183}W Knight shifts with increasing sodium concentration suggested that non-s tungsten states contributed significantly to the conduction band.

In order to obtain the relative contribution of the conduction electrons to the relaxation rates of the sodium and the tungsten nuclei, Fromhold and Narath (18, 19) measured the spin-lattice relaxation rates for ^{23}Na (1964) and for ^{183}W (1966). They found that for ^{23}Na the product T_1T (T_1 is the spin-lattice relaxation time and T is the absolute temperature) was large (approximately 74 min. - °K) and nearly independent of the sodium concentration; while for ^{183}W T_1T had a strong x dependence and was much smaller (approximately 15 sec. - °K). The large difference between T_1T for ^{23}Na and T_1T for ^{183}W was in agreement with the ^{23}Na and ^{183}W Knight shifts and indicated that there is very little interaction of the sodium nuclei with the conduction electrons. Fromhold and Narath concluded that the tungsten nuclei interact significantly with the conduction electrons through the core s electrons indicating that the non-s tungsten states contribute significantly to the conduction band of Na_xWO_3.

B. Theoretical Models

1. Free electron model

The free electron model assumes that the conduction electrons

are formed into Bloch states which extend throughout the whole crystal. Thus, the electrons are considered to be free to move throughout the crystal under the action of a constant potential energy. The energy in k-space is then given by

$$E(\underline{k}) = \frac{\hbar^2}{2m^*} \underline{k}^2 \quad , \tag{1}$$

so that the constant energy surfaces are spheres centered at the origin. The density of states, which in general can be written as (20)

$$N(E) = \frac{1}{4\pi^3} \int \frac{dS}{|\nabla_{\underline{k}} E|} \quad , \tag{2}$$

reduces for the free electron model to

$$N(E) = \frac{3}{2} n \frac{E^{\frac{1}{2}}}{E_f^{\frac{3}{2}}} \quad , \tag{3}$$

where n is the number of electrons per unit volume and E_f is the Fermi energy. The Fermi energy for free electrons is given by

$$E_f = (3\pi^2 n)^{\frac{2}{3}} \frac{\hbar^2}{2m^*} \quad . \tag{4}$$

The density of states at the Fermi energy in terms of the number of free electrons is given by

$$N(E_f) = \frac{3m^*}{\hbar^2} \left(\frac{1}{3\pi^2}\right)^{\frac{2}{3}} n^{\frac{1}{3}} \quad . \tag{5}$$

If we assume a relaxation time $\tau(\underline{k})$, the Boltzmann equation can be solved to obtain the transport properties. In general, the solutions contain complicated integrals which must be integrated over the Fermi surface. However, for the free electron approximation where the energy surfaces are given by Equation 1 and the relaxation time τ is isotropic, the solutions are relatively simple. In particular (for instance, see Ziman, Reference 20), the conductivity for the free electron approximation is given by

$$\sigma = \frac{ne^2}{m^*}\tau. \tag{6}$$

The Hall coefficient is given by

$$R = \frac{1}{ne} \quad , \tag{7}$$

while the diffusion contribution to the Seebeck coefficient is

$$S_d = \frac{\pi^2 k^2 T}{3\, e\, E_f} \quad . \tag{8}$$

If the Fermi energy, as given in Equation 4, is substituted into Equation 8, we can write the diffusion contribution to the Seebeck coefficient in terms of the number of free electrons as

$$S_d = \frac{2}{3}\left(\frac{\pi}{3}\right)^{\frac{2}{3}} \frac{m^* k^2 T}{e\hbar^2}\, n^{-\frac{2}{3}} \quad . \tag{9}$$

If it is now assumed that each sodium atom contributes one electron to a conduction band in Na_xWO_3, then the number of conduction electrons per unit volume is given by

$$n = \frac{x}{a^3} \quad , \tag{10}$$

where a is the lattice constant. With this assumption, the density of states at the Fermi energy; the Hall coefficient; and the diffusion contribution to the Seebeck coefficient can be written in terms of the sodium concentration as

$$N(E_f) = \frac{3m^*}{\hbar^2} \left(\frac{1}{3\pi^2}\right)^{\frac{2}{3}} \frac{x^{\frac{1}{3}}}{a} \quad , \tag{11}$$

$$R = \frac{a^3}{xe} \quad , \tag{12}$$

$$S_d = \frac{2}{3} \left(\frac{\pi}{3}\right)^{\frac{2}{3}} \frac{m^* k^2}{e\hbar^2} T \left(\frac{x}{a^3}\right)^{-\frac{2}{3}} . \tag{13}$$

The conductivity explicitly contains the relaxation time τ which has been assumed to be isotropic. The reciprocal of the relaxation time is proportional to the scattering probability. Since probabilities are additive, the reciprocal of the total relaxation time can be written as

$$\frac{1}{\tau} = \sum_i \frac{1}{\tau_i} \quad , \tag{14}$$

where the sum is over all possible scattering processes. For Na_xWO_3 it is quite possible that the total relaxation time is a function of the sodium concentration. Thus, the x-dependence of the conductivity will depend both on the x-dependence of the number of conduction electrons as well as on the x-dependence of the total relaxation time.

The density of states at the Fermi energy, the Hall coefficient and the diffusion contribution to the Seebeck coefficient do not contain the relaxation time explicitly. Hence, they should have the x-dependence given in Equations 11-13 if the energy surfaces are proportional to k^2 and an isotropic relaxation time exists.

2. Bonding of the WO_3 complex

The basic unit of Na_xWO_3 is the WO_3 octahedra with the tungsten atoms at the centers of the octahedra and the oxygen atoms situated at each of the corners of the octahedra. Figure 1, which is taken from the work of Magneli (3), shows the WO_3 octahedra with the sodium atoms or sites directly above the faces of the octahedra. Also shown in Fig. 1 is the projection of the cubic structure into the (001) plane. The unit cell is as shown with the lattice parameter given by $a = 3.7850 + 0.0818\ x$ (21,22). Thus, the distance between the tungsten atoms changes with sodium concentration; the relative change from $x = 1.0$ to $x = 0.48$ being about 1% ($\Delta a/a = 0.011$).

For the tetragonal I structure, the WO_3 octahedra have been rotated in the basal plane such that the tungsten-oxygen-tungsten angles are no longer 180 degrees (2, 4). Thus, the symmetry along the c axis remains about the same as the symmetry of the cubic structure; while the

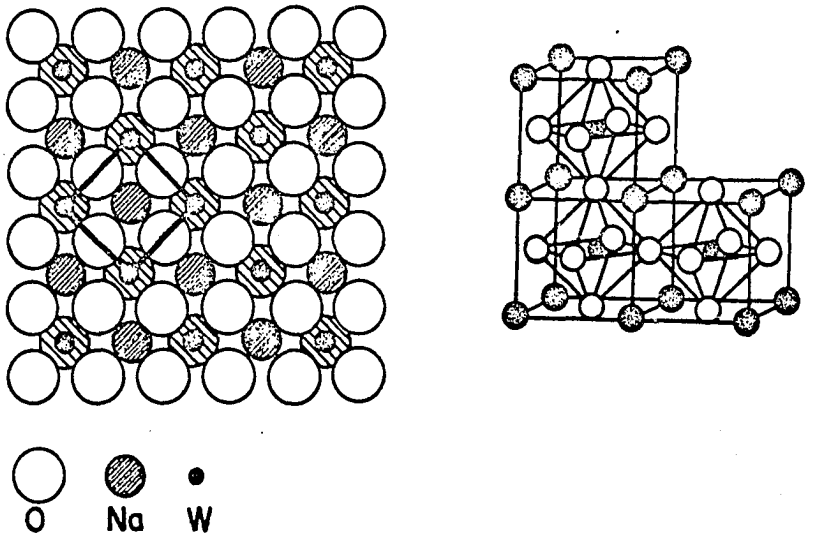

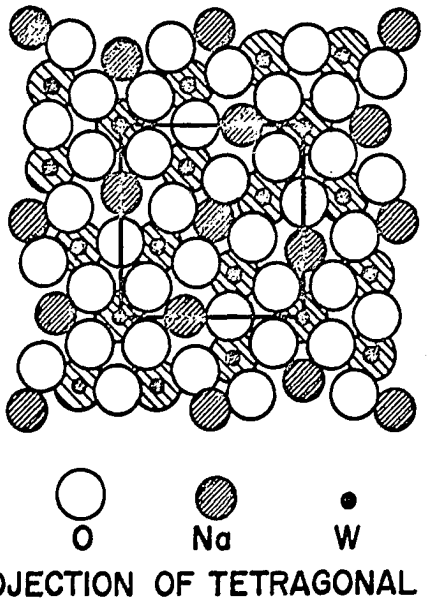

Fig. 1. Projection of the cubic and the tetragonal I structures of Na_xWO_3 into the (001) plane

symmetry in the basal plane has been changed considerably. Figure 1 also shows the projection of the tetragonal I structure into the basal plane. The sides of the unit cell in the basal plane are now approximately three times the original size; giving c/a = 0.3. The WO_3 octahedra now form three, four, and five member rings leaving "tunnels" along the c axis. These "tunnels" accommodate the sodium atoms or sodium sites.

For the WO_3 complex, the possible tungsten orbitals which are available for bonding are the $5d(t_{2g})^3$, the $5d(e_g)^2$, the $6s^1$ and the $6p^3$. The $5d(e_g)^2$, the $6p^3$ and the $6s^1$ orbitals form six octahedral hybrids which are directed octahedrally toward the six nearest neighbor oxygen atoms. The oxygen $2s^1$ and the $2p^1$ orbitals form diagonal hybrids which form covalent σ-bonds with the six tungsten octahedral hybrids. The remaining orbitals which are available for a conduction band are the tungsten $5d(t_{2g})^3$, and the remaining oxygen 2p along with the 3s and 3p sodium orbitals..

3. Tungsten 5d model

Sienko (23) proposed that the conduction band in Na_xWO_3 is formed by the direct overlap of the tungsten $5d(t_{2g})^3$ orbitals. The remaining oxygen 2p orbitals are filled localized levels. Each sodium atom contributes one electron to the conduction band. The value of x governs the extent to which the conduction band is filled.

The transition from cubic to tetragonal I has not been explicitly included in Sienko's model. However, the rotation of the WO_3 octahedra

would effect the overlap of the $5d(t_{2g})^3$ orbitals, and hence the conduction band.

The main objection to Sienko's model is the large tungsten-tungsten separation across the cube face in Na_xWO_3 along which the $5d(t_{2g})$ orbitals are directed ($R_{W-W} = 5.4$ A°). However, it may be possible for the $5d(t_{2g})$ orbitals to overlap not across the cube face, but along the cube edge† ($R_{W-W} = 3.8$ A°). Sienko allows for this possibility and suggests that under such conditions there would be π-bonding with the remaining oxygen 2p orbitals. This possibility is considered further in a model proposed by Goodenough (24). Goodenough's model is an extension of Sienko's model and shall be discussed later. It is, however, unlikely that the tungsten $5d(t_{2g})$ orbitals can overlap across the cube face in such a manner for a band to be formed since, as Mackintosh (12) has pointed out, the tungsten-tungsten distance across the cube face in Na_xWO_3 is 5.4 A° as compared to 2.7 A° for tungsten metal.

Sienko's model would account for the negligible ^{23}Na Knight shift observed in Na_xWO_3 by Jones et al. (16).†† The nuclear magnetic resonance

---

†It is felt that Sienko (23) intended the overlap of the $5d(t_{2g})$ orbitals to be along the cube edge rather than across the cube face as interpreted by his critics (12, 24).

††Sienko (23) suggested that the $5d(t_{2g})$ wave functions have angular nodes in the directions of the nearest-neighbor sodium sites. Thus, the $5d(t_{2g})$ model would predict a negligible ^{23}Na Knight shift. However, Narath and Wallace (17) point out that the $5d(t_{2g})$ wave functions in fact do not have such angular nodes. Nevertheless, Narath and Wallace show that for the $5d(t_{2g})$ wave functions the electron density at the sodium sites is small. Hence, Sienko's model still would account for a negligible ^{23}Na Knight shift.

data of Narath and Wallace (17) and Fromhold and Narath (18, 19) indicated that the non-s tungsten states contribute significantly to the conduction band of Na_xWO_3. Thus, Sienko's tungsten 5d model would also account for the nuclear magnetic resonance data.

Although Sienko's model qualitatively explains the nuclear magnetic resonance data, the model does not provide a quantitative explanation of the transport properties as a function of the sodium concentration. Also, Sienko's model does not account for the partial ordering of the sodium atoms at $x = 0.75$; nor does it account for the increase in the symmetry of the Na_xWO_3 crystal structure as the sodium concentration is increased.

Unless the $5d(t_{2g})$ wave functions overlapped significantly along the cube edge, the conduction band for Sienko's model would have a narrow band width. Thus, the conduction band would have a large density of states characteristic of d bands. In contrast, however, Na_xWO_3 is a relatively good conductor which would suggest a broad conduction band, and a low density of states.

4. Sodium 3p model

Mackintosh (12) proposed that the conduction band in Na_xWO_3 is formed by the direct overlap of the sodium 3p orbitals. The tungsten $5d(t_{2g})$ orbitals are assumed to be empty. The energy of the 3p level is assumed to fall relative to the energy of the 3s level and be even lower than the 3s level. In fact, the s and p bands are sufficiently separated in energy so that the wave function has predominantly p like symmetry with little s character. The value of x governs the extent

to which the conduction band is filled. The transition from metallic behavior to behavior characteristic of a semiconductor occurs when the sodium concentration is small enough so that the sodium 3p orbitals overlap very little with the nearest neighbor sodium atoms. The conduction electrons then become localized at the sodium ions.

Since the conduction band in Mackintosh's model is derived from the sodium 3p orbitals, the conduction band would have a broad band width and a low density of states. Hence, Mackintosh's model would account for Na_xWO_3 being a good conductor. Also, the sodium 3p model can qualitatively explain the increase in the symmetry of Na_xWO_3 with increasing sodium concentration; as well as the partial ordering of the sodium atoms at $x = 0.75$.

There are, at present, no inconsistencies between Mackintosh's model and the measured transport properties of Na_xWO_3. (Mackintosh's model will be discussed in connection with the results of the present investigation in Section V.) However, the sodium 3p model does not provide a quantitative explanation of the transport properties as a function of the sodium concentration.

The sodium 3p wave functions have radial nodes at the sodium nuclei. Hence, the sodium 3p model would account for the small ^{23}Na Knight shift observed in Na_xWO_3. The relaxation rates (which are proportional to $1/T_1$ where T_1 is the spin-lattice relaxation time) are nearly proportional to the square of the electronic specific heat. Hence, $1/T_1T$ would be proportional to the square of the density of states at the Fermi energy. The sodium 3p orbitals have nodal planes

passing through both the tungsten and the oxygen nuclei as well as the radial nodes at the sodium nuclei. Hence, for the ^{183}W and the ^{23}Na nuclei the sodium 3p model would predict a value of T_1T which is large and independent of x. For the ^{183}W nuclei, Fromhold and Narath (18) observed a value of T_1T which was small and x dependent; while for the ^{23}Na nuclei they observed a value of T_1T which was large and independent of x. Thus, the sodium 3p model does not account for all of the nuclear magnetic resonance data.

Measurements by Ferretti et al. (25) show that the perovskite $ReO_3(5d^5\ 6s^2)$ which has no cation sublattice is metallic and diamagnetic. The perovskite WO_3 $(5d^4\ 6s^2)$ which has one less outer electron per molecule is a semiconductor (26) and also diamagnetic. Goodenough (24) points out that these measurements show that metallic conductivity for materials with the perovskite structure (Na_xWO_3 included) does not depend on the population of sodium sites in the cation sublattice. Rather, the metallic conductivity is due to the addition of electrons to the already existing bands. Hence, the conduction band in Na_xWO_3 could not be formed completely by the overlap of the sodium 3p orbitals as proposed by Mackintosh's model.

In order to explain the negligible Knight shift in the ^{23}Na resonance, the sodium 3p model had to assume that the wave function had predominantly p like symmetry with little s character. This assumption required the energy of the 3p level to be not only lower but very much lower than the energy of the 3s level. Thus, it is questionable whether the wave functions could have predominantly p like symmetry as assumed by Mackintosh's model.

5. Tungsten 5d π-bond model

Goodenough (24) proposed a model in which the conduction band is formed by the π-bonding of the tungsten 5d(t_{2g}) orbitals with the oxygen 2p orbitals. As was pointed out earlier, Sienko (23) suggested this possibility in connection with his own model.

Figure 2 shows a one electron molecular orbit energy diagram for the cubic perovskite Na_xWO_3 as proposed by Goodenough. The tungsten $6p^3$, $6s^1$ and 5d(e_g) orbitals form octahedral hybrids which form bonding and antibonding σ bands with the $(s\ p_\sigma)^2$ digonal hybrids of oxygen. The sodium 3s and 3p orbitals from digonal hybrids which also form bonding and antibonding σ bands with the remaining oxygen 2p orbitals; the extent of these bonds depending on the number of sodium atoms present. The tungsten 5d(t_{2g}) orbitals then form bonding and antibonding π bands with the remaining p_π orbitals of oxygen. The number of available states at the levels marked p_π^+ and t_{2g} together with the number of states available in the π* band vary with x. For x less than 0.75 there are no localized t_{2g} states and the number of localized p_π^+ states varies with x. The sodium ions order at x = 0.75 and there are no localized orbitals. For x larger than 0.75 there are no localized p_π^+ states and the number of localized t_{2g} states increases with x. However, there is always a total of 24 available states below the π* conduction band which can be filled by the 24 + x outer electrons of Na_xWO_3. Hence, there are x electrons in the π* conduction band. For x larger than 0.75, according to this model, there are two types of carriers present: higher mobility π* electrons and lower mobility t_{2g} electrons.

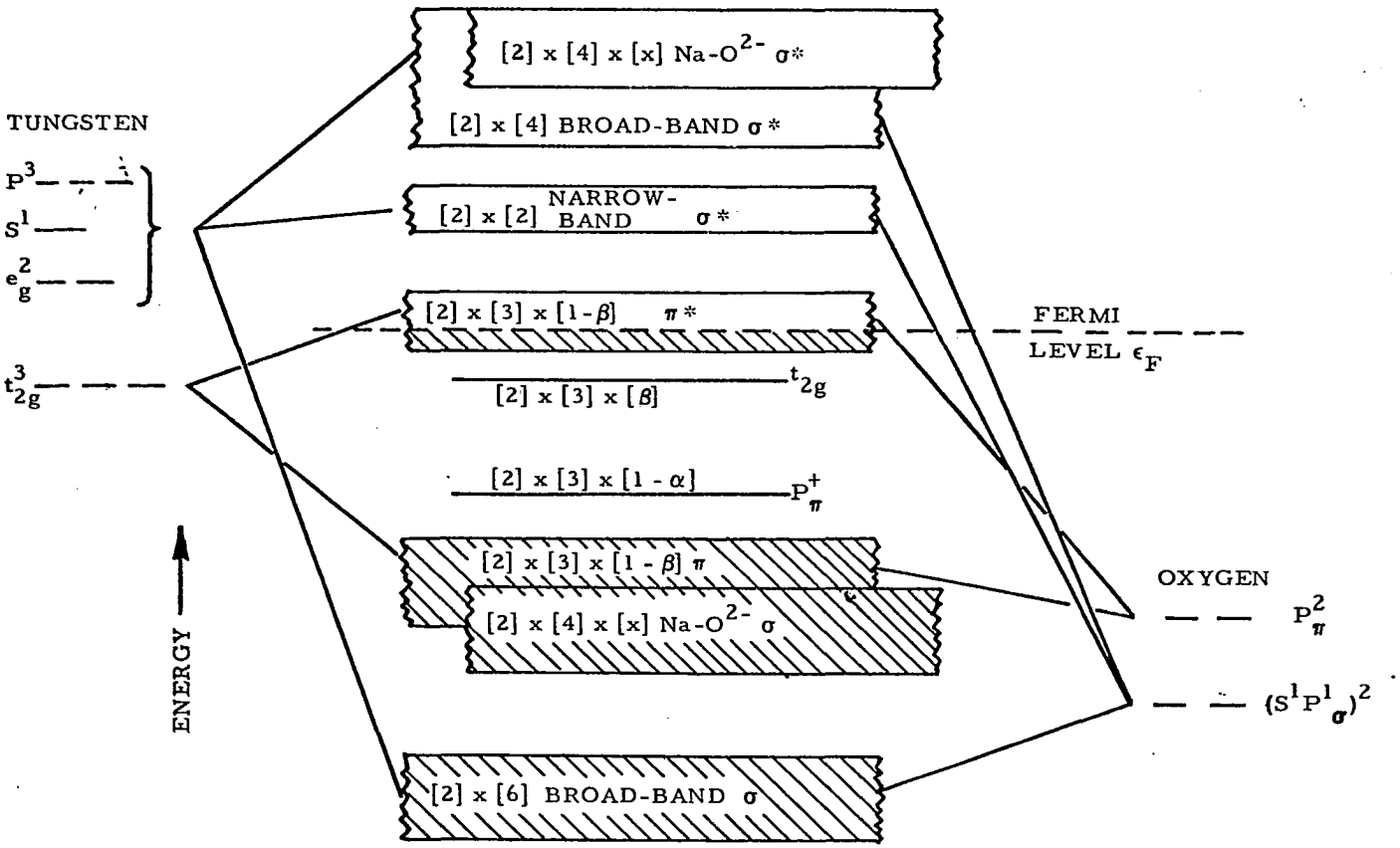

Fig. 2. One electron molecular orbit energy diagram for cubic perovskite Na_xWO_3

Goodenough suggests that the energy scheme in Fig. 2 qualitatively applies to the tetragonal I structures of Na_xWO_3. However, at lower x values (tetragonal II) the WO_3 octahedra are distorted with the tungsten atom no longer at the center of the octahedra. This distortion produces a permanent electric dipole moment which, according to Goodenough, will quench metallic conductivity.

Goodenough's model would account for the negligible ^{23}Na Knight shift observed in Na_xWO_3 as well as the nuclear magnetic resonance data of Fromhold and Narath (18, 19). The effect of the ordering of the sodium atoms at x = 0.75 is explicitly included in Goodenough's model in determining the localized states p_π^+ and t_{2g}. Also, Goodenough's model considers the changes in crystal structure as the sodium concentration is decreased. A qualitative explanation of the transport properties is obtainable from Goodenough's model. However, the model does not provide a quantitative explanation of the transport properties as a function of the sodium concentration.

Since Goodenough's model considers the conduction band in Na_xWO_3 to be formed by the π-bonding of the tungsten $5d(t_{2g})$ orbitals with oxygen 2p orbitals, the conduction band could have a narrow band width characteristic of d bands. However, Goodenough (24) points out that the competition between comparable tungsten π-bonding and sodium σ-bonding may cause the width of the conduction band to increase. Hence, Goodenough's model could conceivably account for a broad conduction band.

6. Nonuniform electron gas model

Fuchs (27) proposed a nonuniform electron gas model which was based

on the observed behavior of the density of states at the Fermi energy. For the nonuniform electron gas model the conduction electrons are assumed to concentrate at or near the sodium atoms, and to avoid the sodium vacancies. The effective volume occupied by the electrons is a fraction x of the entire volume of the crystal. Thus, the local conduction electron density is independent of x. Hence, the Fermi energy is also independent of x. Thus, an inherent property of the nonuniform electron gas model is that the density of states at the Fermi energy is proportional to x as was observed from the electronic specific heat measurements of Vest et al. (13) and the magnetic susceptibility measurements of Greiner et al. (14).

Fuchs observed that there was an inconsistency between the x-dependence of the density of states at the Fermi energy and the x-dependence of the Hall coefficients measured by Gardner and Danielson (8). For the nonuniform electron gas model the density of states at the Fermi energy is proportional to x irrespective of the shape of the conduction band. Thus, a parabolic conduction band which explained the observed Hall coefficients would be consistent with the nonuniform electron gas model. (The inconsistency between the observed density of states at the Fermi energy and the observed Hall coefficients shall be discussed again in Section V.)

The nonuniform electron gas model assumes that the sodium atoms are randomly located throughout the Na_xWO_3 crystal. Thus, the partial ordering of the sodium atoms at x=0.75 is neglected in this model. Further, the nonuniform electron gas model considers the conduction

process of Na_xWO_3 in terms of the clustering of the sodium atoms. The sodium sites are assumed to form a simple cubic lattice even for sodium concentrations less than 0.48. Thus, the changes in the crystal structure of Na_xWO_3 are also neglected in this model. (The effects of the change in crystal structure on the transport properties shall be considered in Section IV and discussed in Section V.)

Since the conduction electrons are assumed to be concentrated at or near the sodium atoms, the local conduction electron density is independent of x. Hence, the nonuniform electron gas model could explain the x-independent value of T_1T which was observed for the ^{23}Na nuclei by Fromhold and Narath (18). However, the nonuniform electron gas model cannot explain the small, x-dependent value of T_1T which was observed for the ^{183}W nuclei by Fromhold and Narath (19).

III. EXPERIMENTAL PROCEDURE

A. Growth and Preparation of Na_xWO_3 Single Crystals

The Na_xWO_3 single crystals were prepared by electrolytic reduction from a mixture of reagent grade sodium tungstate and tungsten trioxide. The electrolytic cell was a glazed ceramic crucible with a chromel wire cathode and a graphite anode. The temperature of the melt ranged from 700 to 800°C and the current ranged from 15 to 25 milliamperes.

The single crystals which were used for measurements were prepared in the following way. A wafer approximately 2 millimeters thick was cut from a larger piece of Na_xWO_3 single crystal. A rectangular shaped sample approximately 2 millimeters wide and from 5 to 8 millimeters long was then cut from the wafer. The entire perimeter of the wafer was cleaned in warm water containing sodium hydroxide; and analyzed by x-ray analysis and by neutron activation analysis (22) to obtain an average x-value of the single crystal. The single crystals were annealed for approximately 12 hours at 700°C and then cooled to room temperature at 50 degrees per hour. X-ray diffraction patterns of the tetragonal I single crystals were taken along the sample axis to determine the orientation of the sample.

Ellerbeck *et al.* (10) have demonstrated the necessity of using only homogeneous Na_xWO_3 single crystals. The test for sample homogeneity suggested by Ellerbeck was used on each of the Na_xWO_3 single crystals used in this investigation. Approximately eight independent electrical resistivity measurements were made on each Na_xWO_3 single crystal at

300°K. These electrical resistivity measurements were made from end to end and around the periphery of the sample. From the resistivity measurements an average resistivity, $\bar{\rho} = \frac{1}{N} \sum_i \rho_i$, and an average deviation, $\sigma = \frac{1}{N} \sum_i |\rho_i - \bar{\rho}|$, were determined. In order for a Na_xWO_3 single crystal to be considered electrically homogeneous, and thus suitable for measurements, the ratio of the average deviation to the average resistivity had to be less than 5% $(\Delta = \sigma/\bar{\rho} < 5\%)$. Table 1 lists the sample number, the average x-value, the average cross sectional area, the average resistivity, and the per cent deviation for each Na_xWO_3 single crystal used in this investigation.

Table 1. Sample numbers, x-values, and homogeneity data for the Na_xWO_3 single crystals

Sample number	x-value	Average area (mm^2)	Average ρ ($\times 10^{-6}$ ohm-cm)	% deviation
59-D	0.875 ± 0.047	4.974	20.44	5.1
261-E	0.874 ± 0.003	2.480	15.65	1.7
261-D	0.873 ± 0.004	2.104	16.03	1.3
70-D	0.854 ± 0.002	1.422	17.83	1.5
230-C2	0.817 ± 0.002	2.270	19.95	3.9
59-A	0.777 ± 0.002	3.331	20.85	1.6
230-B1	0.745 ± 0.047	3.341	21.28	2.4
242-B	0.730 ± 0.003	1.276	22.25	2.0

Table 1. Continued

Sample number	x-value	Average area (mm^2)	Average ρ ($\times 10^{-6}$ ohm-cm)	% deviation
277-B	0.717 ± 0.003	2.014	24.59	1.0
249-A1	0.698 ± 0.002	1.884	26.61	1.7
138-A2	0.662	2.077	31.22	3.3
235-J	0.617 ± 0.002	4.423	34.90	4.4
94-D	0.590 ± 0.002	5.288	39.29	1.6
234-A	0.565 ± 0.003	3.097	45.25	2.9
258-D	0.551 ± 0.003	2.459	48.54	4.2
281-H	0.513 ± 0.002	1.536	58.63	3.2
244-A1	0.512 ± 0.002	5.267	58.83	3.9
109-B2b (// c)	0.451 ± 0.018	0.701	103.2	7.8
109-A4 (// c)	0.437 ± 0.026	0.491	110.7	5.8
105-B2a (// c)	0.423 ± 0.013	0.938	122.6	8.4
105-A (⊥ c)	0.457 ± 0.023	0.736	351.4	6.5
105-Aa (⊥ c)	0.432 ± 0.013	1.244	381.5	7.2
105-B1 (⊥ c)	0.423 ± 0.013	0.867	410.4	4.4
109-A3 (⊥ c)	0.405 ± 0.020	0.898	557.9	4.5

B. Resistivity and Hall Coefficients

A standard two probe technique was used to measure the resistivity at 300°K. The Hall coefficient and the resistivity (as a function of

the temperature) were measured for each crystal by a Hall apparatus which used an a.c. electric current and a d.c. magnetic field. This a.c. Hall apparatus was designed to measure a.c. voltages having magnitudes from 10^{-3} to 10^{-9} volts over a frequency range from 100 cycles per second to 150 kilocycles per second by either a null balance technique or a direct measurement technique.

Figure 3 shows a block diagram of the a.c. Hall apparatus. An a.c. signal of the desired frequency was obtained from a Hewlett-Packard model 203A signal generator. The a.c. signal was amplified by a Hewlett-Packard model 467A power amplifier which supplied the a.c. current to the sample. The magnitude of the a.c. current supplied to the sample was obtained from the voltage across a 0.1 ohm standard resistor.

The a.c. signal from the signal generator was also used as the reference signal for a Princeton Applied Research model JB-5 phase sensitive lock-in amplifier, as well as for two separate bucking circuits. The first bucking circuit contained a phase shifter (see Fig. 4) followed by a Dekatran model DT 35 voltage transformer; and was used to buck out any voltage which existed across the Hall probes in zero magnetic field. The second bucking circuit contained a phase shifter (see Fig. 4) followed by a Fluke model 883 AB differential voltmeter and a Dekatran model DT 72A decade transformer. The second bucking circuit was used to buck out the unknown signal coming from either the Hall probes, the resistivity probes, or the standard resistor. A null occurred when the bucking signal and the unknown signal were 180 degrees out of phase and of equal magnitude. The null was detected by the Princeton Applied

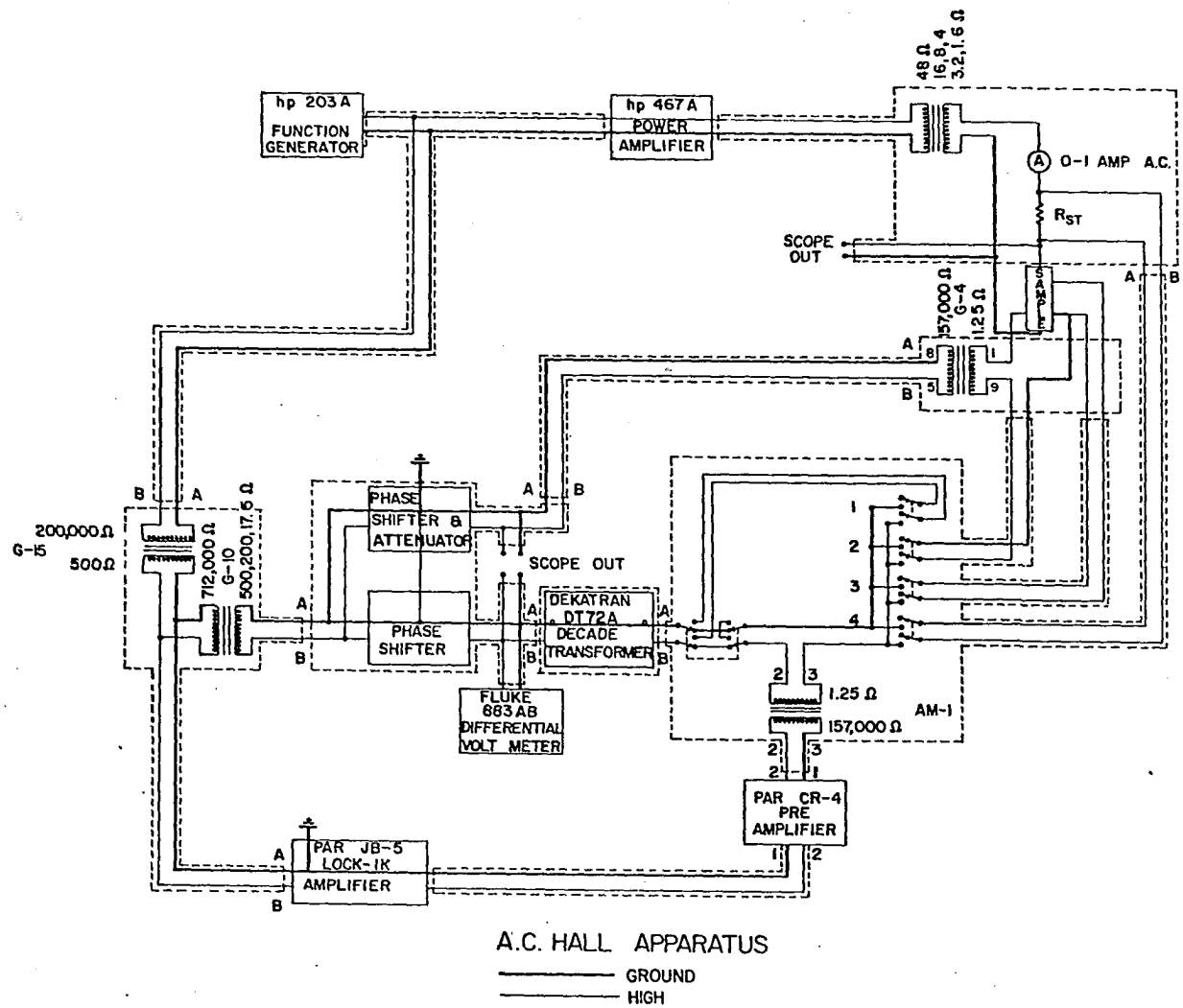

Fig. 3. Block diagram of the a.c. Hall apparatus

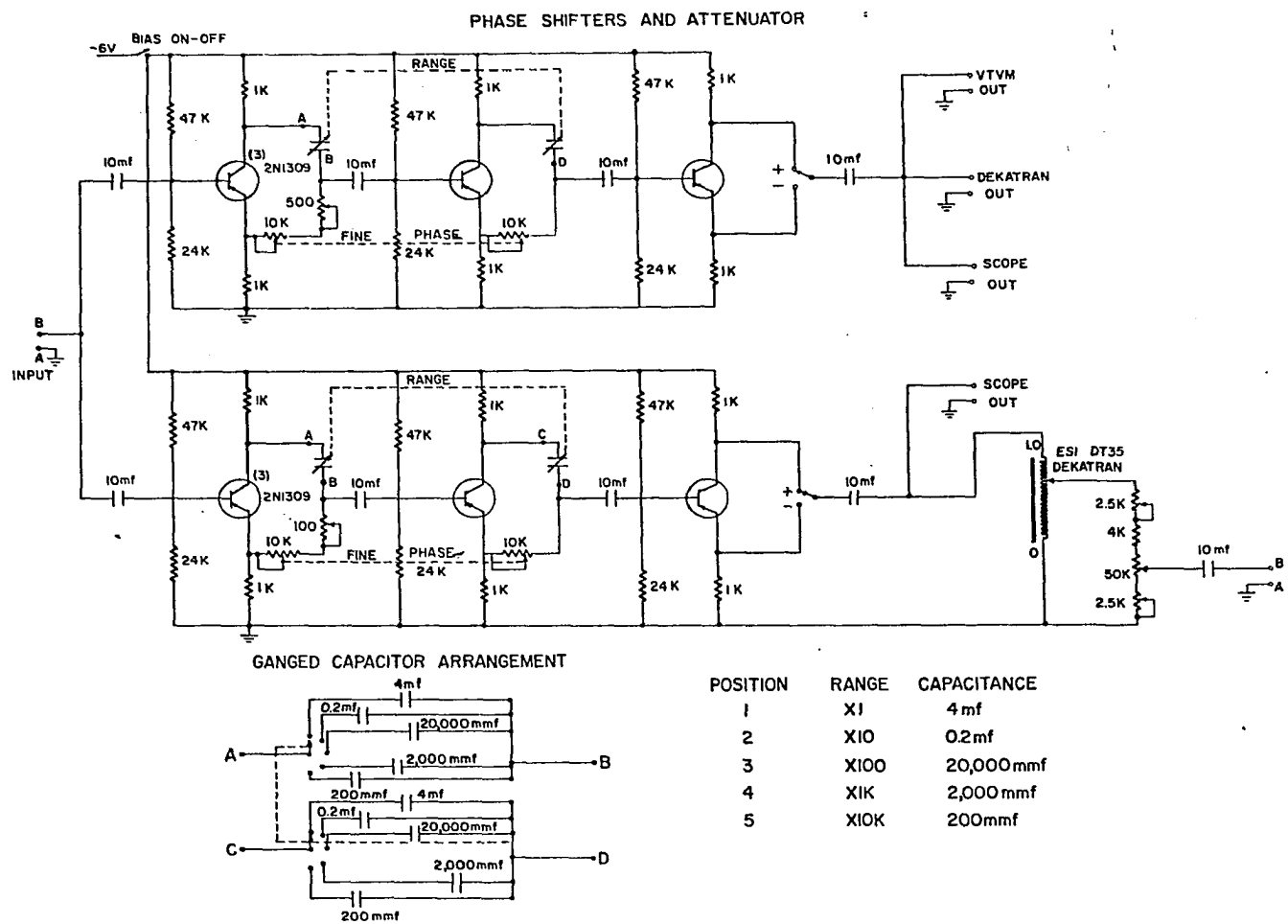

Fig. 4. Phase shifters and attenuator for the a.c. Hall apparatus

Research model CR-4 pre-amplifier and the model JB-5 lock-in amplifier. The magnitude of the unknown signal in rms volts was equal to the voltage measured by the differential voltmeter multiplied by the setting on the decade transformer. The Hall coefficients were determined from the equation

$$R = \frac{10^8 V_H (A R_{st})}{V_{st} d H} \quad cm^3/coulomb, \tag{15}$$

where V_H is the Hall voltage in volts; V_{st} is the voltage across the standard resistor in volts; A is the cross sectional area of the Na_xWO_3 single crystal in cm^2; R_{st} is the resistance of the standard resistor in ohms; d is the distance between the two Hall probes in centimeters; and H is the magnetic field in gauss. The resistivity was determined from the equation

$$\rho = \frac{V_\rho}{V_{st}} \frac{A R_{st}}{L} \quad \text{ohm-cm} \quad , \tag{16}$$

where V_ρ is the resistivity voltage in volts and L is the distance in centimeters between the resistivity probes. Since V_H, V_ρ, and V_{st} were measured by a null-balance technique, the gain of the amplifiers or the gain of the transformers did not enter into the equation for the Hall coefficients or the resistivity.

By means of a switch, an accurately known voltage from the second bucking circuit could be fed back into the pre-amplifier and the lock-in amplifier, thus providing a calibration for the detection system. The

unknown voltages could be measured directly. However, the null-balance technique proved to be much more effective in measuring the unknown voltages.

Figure 5 shows a detailed circuit diagram for the a.c. Hall apparatus. Hermetically sealed relays were used to switch between the unknown voltages. The transformers were Triad geoformers which were shielded with three mumetal shields interleaved with copper. To reduce inductive pick-up between the low level components of the a.c. Hall apparatus, each low level component was housed in a separate box which was magnetically shielded with Co-Netic magnetic shielding. The a.c. cables which connected the low level components consisted of number 20 copper wire threaded through insulation brain; Shieldflex flexible mumetal tubing covered with copper braid; and tygon tubing in that order. The Co-Netic magnetic shielding was a high permeability alloy developed by the Magnetic Shield Division of Perfection Mica Company for maximum attenuation of low intensity, low frequency a.c. signals. The Shieldflex flexible tubing was also a high permeability electro-magnetic alloy which was developed by Magnetic Metals Company. Thus, a continuous magnetic shield was formed around each low level component of the a.c. Hall apparatus.

In order to test the accuracy of the a.c. Hall apparatus and to be sure that each component of the apparatus was working satisfactorily, the following preliminary checks were made. First, the impedance of the standard resistor was checked as a function of the frequency. Between 100 cycles per second and 1.2 kilocycles per second the impedance

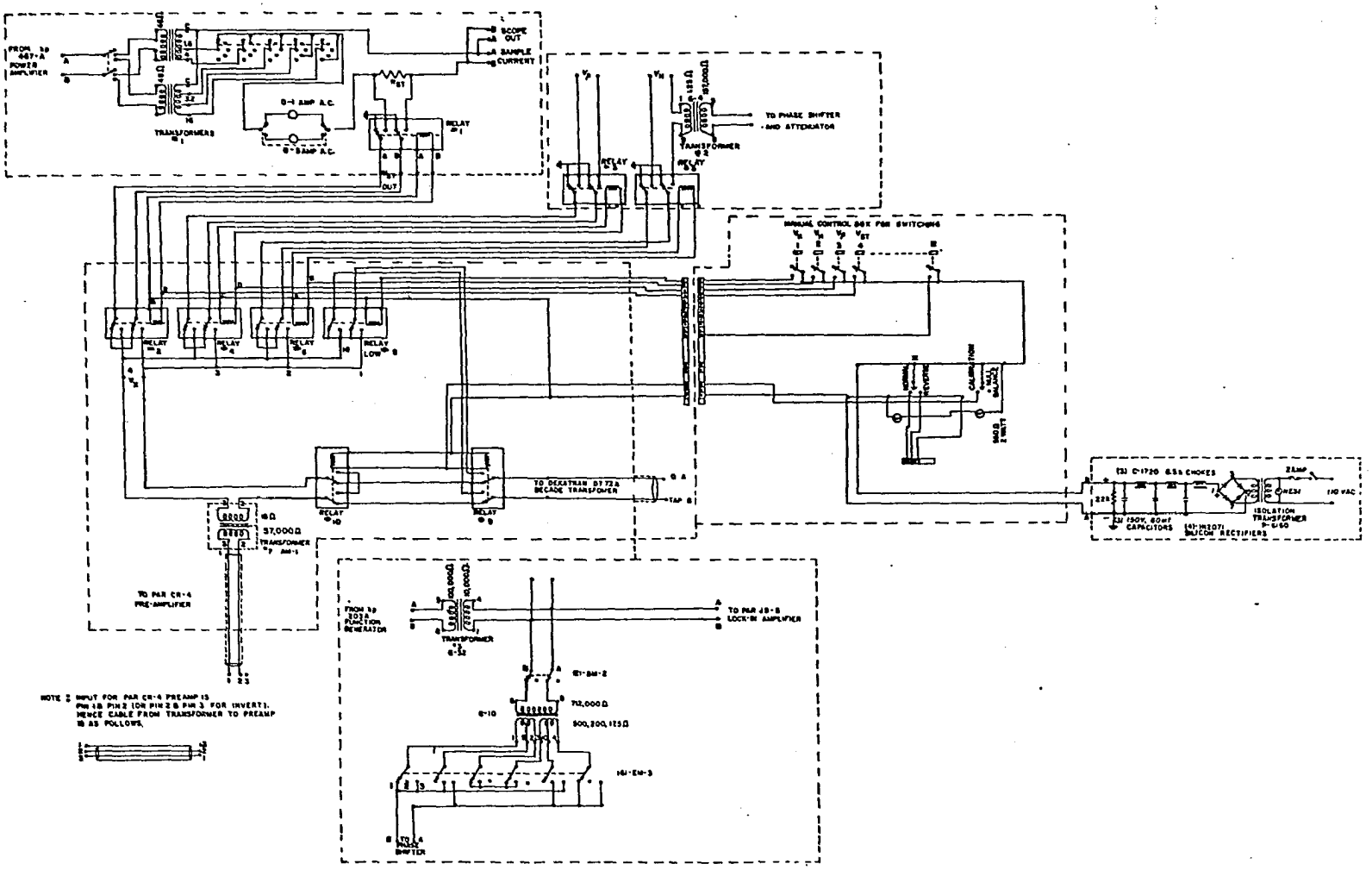

Fig. 5. Detailed circuit diagram for the a.c. Hall apparatus

of the standard resistor changed by less than 0.2% indicating that the impedance was purely resistive for these frequencies. Second, a calibration curve was determined for the Radio Frequency Laboratories model 1890 gaussmeter. The gaussmeter was used to measure the magnetic field and was calibrated against a 0.1% Rawson-Lush rotating coil gaussmeter which had previously been checked against nuclear magnetic resonance. Third, the Hall coefficients of a 99.999% copper sample and a 99.999% silver sample were measured at 300°K. The Hall coefficients and the resistivities which were measured are listed in Table 2 together with the Hall coefficients and the resistivities measured for copper and silver by other investigators.

Table 2. Hall coefficient and resistivity for copper and silver

	R ($\times 10^{-13}$ ohm-cm/gauss)		ρ ($\times 10^{-6}$ ohm-cm)	
	This study	Other	This study	Other
copper	5.39	5.5[a]	1.60 ± 0.01	1.69[b]
	5.71 ± 0.20	5.36[c]		1.55[a]
		5.4[d]		
silver	7.84 ± 0.18	8.46 ± 0.07[c]		1.63[b]
		8.40[a]	1.69 ± 0.01	1.50[a]

[a]Reference 28, p. 4-74.

[b]Reference 29, p. 2384.

[c]Reference 30.

[d]Reference 6.

Fourth, the Hall voltage of a gadolinium single crystal was measured as a function of the magnetic field. The results were compared to the d.c. results measured on the same gadolinium single crystal by Lee and Legvold (31). The two results differed by less than 6%. Since the Ettingshausen effect must be considered in the d.c. method, it was concluded that the results between the a.c. method and the d.c. method agreed as well as could be expected. With the completion of the above preliminary checks, it was concluded that the a.c. Hall apparatus was working properly.

The sample holder which was used to measure the a.c. Hall coefficients and the resistivity of Na_xWO_3 was similar in design to the sample holder which was used to measure the Seebeck coefficients (refer to Fig. 6). The heater which maintained the ambient temperature was made from 150 ohms of number 36 manganin wire wound on the center portion of the sample holder. A copper-constantan thermocouple and a 100 ohm carbon resistor were placed directly under the heater and acted as sensing elements for the temperature controller (see Appendix A). A copper-constantan and a copper-gold (0.02% iron) thermocouple were glued securely under the section of the sample holder which contained the sample and were used to measure the temperature of the sample. In order to thermally anchor the thermocouples to the sample holder, each thermocouple was wound on a small copper spool and glued securely with G.E., No. 7031, insulating varnish.

The three potential leads were number 36 copper wire and were twisted together to reduce inductive pick-up. A small coaxial cable

was used for the current leads. The twisted potential leads and the coaxial cable were thermally anchored on two mutually perpendicular copper spools.

As was pointed out by Kevane et al. (32) and later by Lavine (33), the major problem connected with an a.c. Hall apparatus is the presence of spurious voltages due to vibrations. Lavine notes that if the magnetic field is uniform over the region of the sample holder, then there will be no induced voltage due to the vibrations in the Hall leads. However, there will be an induced voltage in the Hall leads due to the alternating current. This induced voltage is not dependent upon the magnetic field unless there is motion between the Hall loop and the current loop. Since the magnetic field was uniform over the region of the sample holder, vibrations of the Hall leads presented no major problem. However, to eliminate any motion between the Hall loop and the current loop the current loop was made as small as possible, and all leads were glued securely to the sample holder.

C. Seebeck Coefficients

The Seebeck coefficient S is defined by the equation

$$\underline{E} = - S \nabla T \tag{17}$$

where $\underline{E}$ is the electric field which is produced across a conductor by the presence of a temperature gradient. We consider the closed circuit consisting of the two copper potential leads and the sample. Equation 17

can be written as

$$\oint \underline{E} \cdot d\underline{l} = - \oint S \nabla T \cdot d\underline{l} \quad , \tag{18}$$

or

$$\oint \underline{E} \cdot d\underline{l} = - \oint S \, dT \quad . \tag{19}$$

If we integrate around the closed circuit we obtain

$$\Delta V_{xcu} = - \int_{T_1}^{T_2} (S_x - S_{cu}) \, dT, \tag{20}$$

where S_x is the Seebeck coefficient of the sample, S_{cu} is the Seebeck coefficient of the copper potential leads, and $T_2 - T_1 = \Delta T$ is the temperature gradient across the sample. If the temperature gradient, ΔT, is small compared to the ambient temperature of the sample, and if both S_x and S_{cu} do not vary rapidly over the small temperature gradient, then Equation 20 can be written as

$$\Delta V_{xcu} = - (S_x - S_{cu}) \Delta T \quad , \tag{21}$$

or

$$S_x = S_{cu} - \Delta V_{xcu} / \Delta T \quad . \tag{22}$$

The Seebeck coefficients of the copper potential leads were calibrated from 4.2°K to 340°K against the Seebeck coefficients of

lead determined by Christian et al. (34). The temperature gradient was measured by two copper-gold (0.02% iron) or two copper-constantan thermocouples which were placed directly at each end of the sample. The copper-gold (0.02% iron) thermocouples were used from 4.2°K to 30°K and the copper-constantan thermocouples were used from 30°K to 340°K. The thermocouple potentials were measured on a Leeds and Northrup type 7556 guarded six dial potentiometer with a Keithley type 148 nanovoltmeter as the null detector. The thermocouple potentials could be measured accurately to 0.1 microvolt.

To obtain the sensitivity curve for the copper-constantan and the copper-gold (0.02% iron) thermocouples, the original data for the calibration curve, Emf vs. T, were fitted to a polynominal of the form

$$\text{Emf} = A + B\,T + C\,T^2 + D\,T^3 , \tag{23}$$

by a least squares computer program. The points of the fitted curve differed from the corresponding points of the calibrated curve by less than 0.5 microvolts. The sensitivity, dE/dT vs. T, was then obtained by differentiation of the polynomial.

The potential ΔV_{xcu} was measured by a Rubicon type 2772 double potentiometer with a Guildline Instruments type 5214 photocell galvanometer amplifier and a Guildline Instruments type SR 21 secondary galvanometer as the null detector. The potential ΔV_{xcu} could be measured accurately to 0.01 microvolt.

A cross sectional view of the sample holder is shown in Fig. 6. The sample holder was milled from a 3/4 inch diameter copper cylinder and

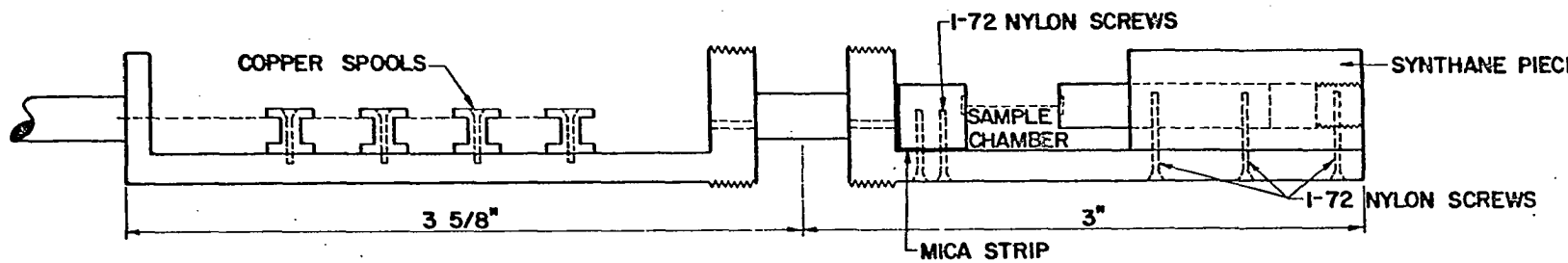

MATERIAL: COPPER UNLESS OTHERWISE STATED
SCALE: 1" = 1/2"

Fig. 6. Seebeck coefficient sample holder

consisted of two chambers. The first chamber was the sample chamber. The sample was soldered between a copper rectangular block and a copper cylinder. To electrically insulate the sample from the sample holder, the copper block was separated from the body of the sample holder by a mica strip, and the copper cylinder was housed in a cylindrical piece of synthane. A heater consisting of 70 ohms of number 36 manganin wire was wound on the copper cylinder, and produced the required temperature gradient across the sample. A copper-constantan and a copper-gold (0.02% iron) thermocouple were placed between the sample and the copper block and between the sample and the copper cylinder.

The second chamber contained eight small copper spools. In order to thermally anchor the thermocouples and the potential leads to the sample holder, each thermocouple wire and each potential lead was wound on a copper spool and was glued securely with G.E., No. 7031, insulating varnish.

The ambient temperature of the sample holder was maintained by a heater consisting of 100 ohms of number 32 manganin wire wound on the outside casing of the sample holder. The sensing element for the temperature controller was 120 ohms of number 42 copper wire which was wound directly under the heater.

IV. EXPERIMENTAL RESULTS

A. Resistivity

The room temperature resistivity of Na_xWO_3 is plotted as a function of sodium concentration in Fig. 7. Also shown in Fig. 7 is the room temperature resistivity of Na_xWO_3 measured by Gardner and Danielson (8) and the room temperature resistivity of Na_xWO_3 measured by Ellerbeck et al. (10). Ellerbeck et al. found that the difference (both in magnitude and in x-dependence) between their resistivities and the resistivities measured by Gardner and Danielson was due to the inhomogeneity of the crystals used by Gardner and Danielson. The eighteen Na_xWO_3 single crystals studied in the present investigation were electrically homogeneous (see Section III-A); and the resistivities of these Na_xWO_3 single crystals agreed with the resistivities which had been measured by Ellerbeck. There was, however, one notable difference. In the present investigation, each single crystal which had an x-value larger than 0.70 had a deviation from the average resistivity which was less than or equal to 2 per cent (with the exception of sample 230-C2, x = 0.817, where $\Delta = 3.9\%$; see Table 1). The resistivity of these homogeneous single crystals is shown in Fig. 7 in the insert. At x = 0.75 there is a definite change in the slope of the curve, resistivity versus sodium concentration. A closer examination of Ellerbeck's data also reveals this same change in slope.

In Fig. 8, the resistivity of the Na_xWO_3 single crystals is plotted as a function of the sodium concentration for three different

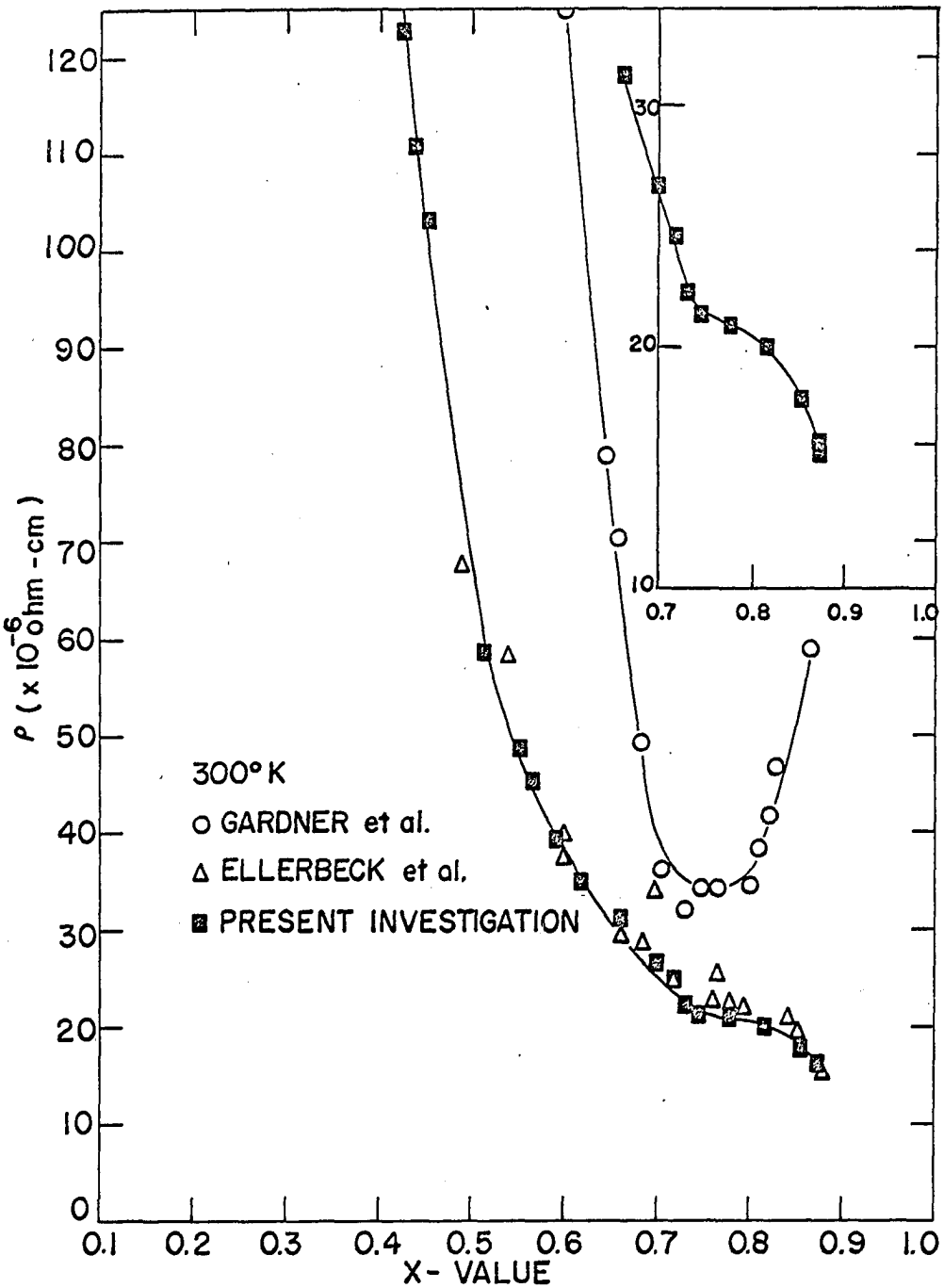

Fig. 7. Resistivity of Na_xWO_3 as a function of the sodium concentration at 300°K

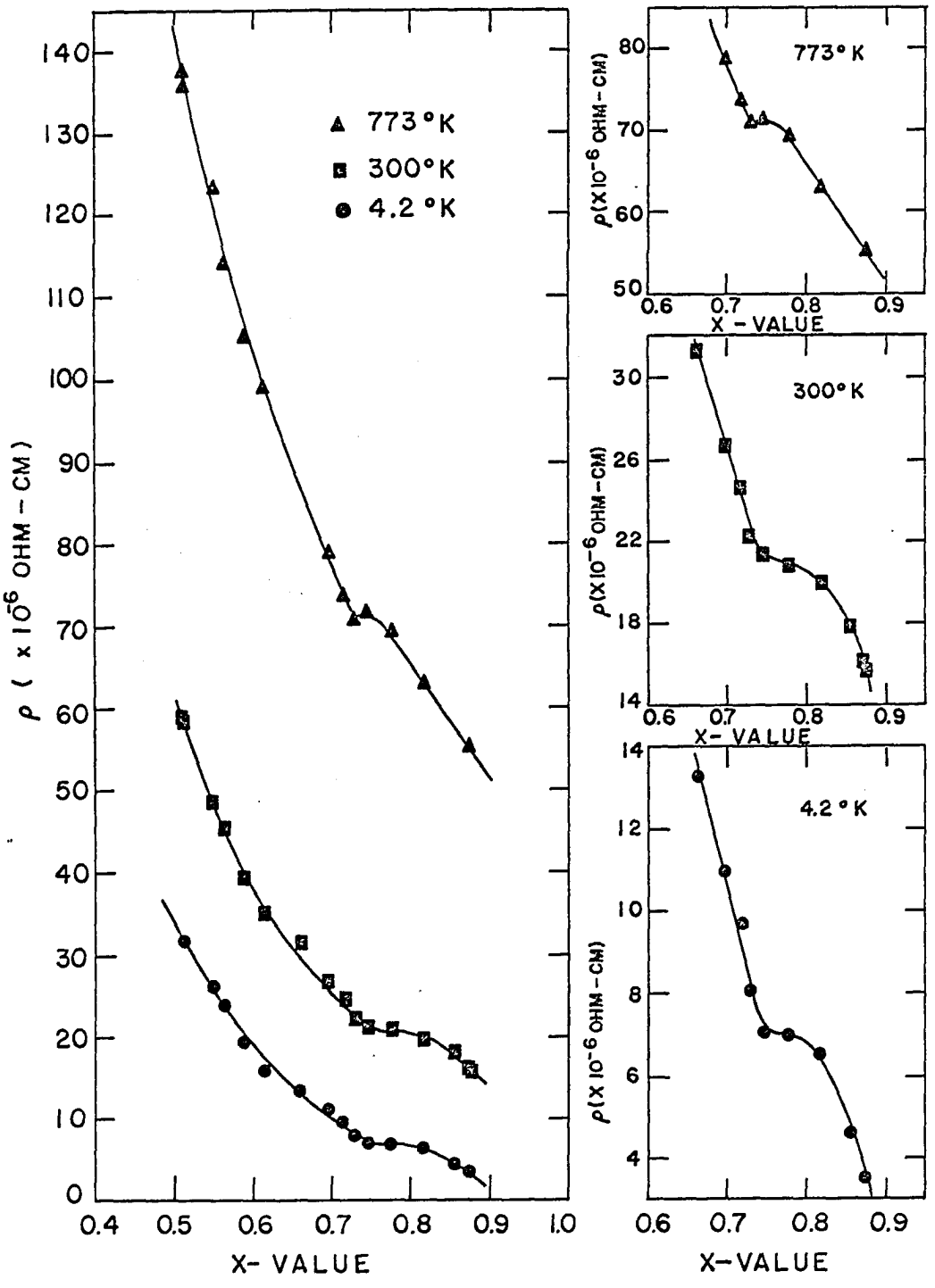

Fig. 8. Resistivity of Na_xWO_3 as a function of the sodium concentration at 4.2, 300, and 773°K

temperatures; 4.2, 300 and 773°K. An enlarged section of the resistivity versus sodium concentration from x = 0.6 to x = 0.9 is also shown in Fig. 8 for the three temperatures. The anomaly in the slope of the resistivity curve at x = 0.75 is evident for each of the three temperatures. This anomaly at x = 0.75 is also seen in the conductivity which is plotted as a function of the sodium concentration in Fig. 9. Figure 9 also shows an enlarged section of the conductivity versus sodium concentration from x = 0.7 to x = 0.9. For each of the three temperatures the conductivity shows the anomaly at x = 0.75. It is assumed that this anomaly in the conductivity at x = 0.75 is a consequence of the partial ordering of the sodium atoms.

If it is assumed that the contribution to the resistivity from the lattice vibrations is independent of the residual resistivity, then the total resistivity can be written as

$$\rho_T = \rho_{res} + \rho_{th} \quad , \tag{24}$$

where ρ_{res} is the temperature independent residual resistivity, and ρ_{th} is the temperature dependent thermal contribution. At 4.2°K the thermal contribution is negligible so that the measured resistivity is equal to the residual resistivity. It is further assumed that the contributions to the residual resistivity from impurities and lattice imperfections are small. This assumption seems to be valid for Na_xWO_3 since the impurity contribution and the contribution from lattice imperfections would have no definite x-dependence whereas the resistivity at 4.2°K shows a strong x-dependence. Thus, the major

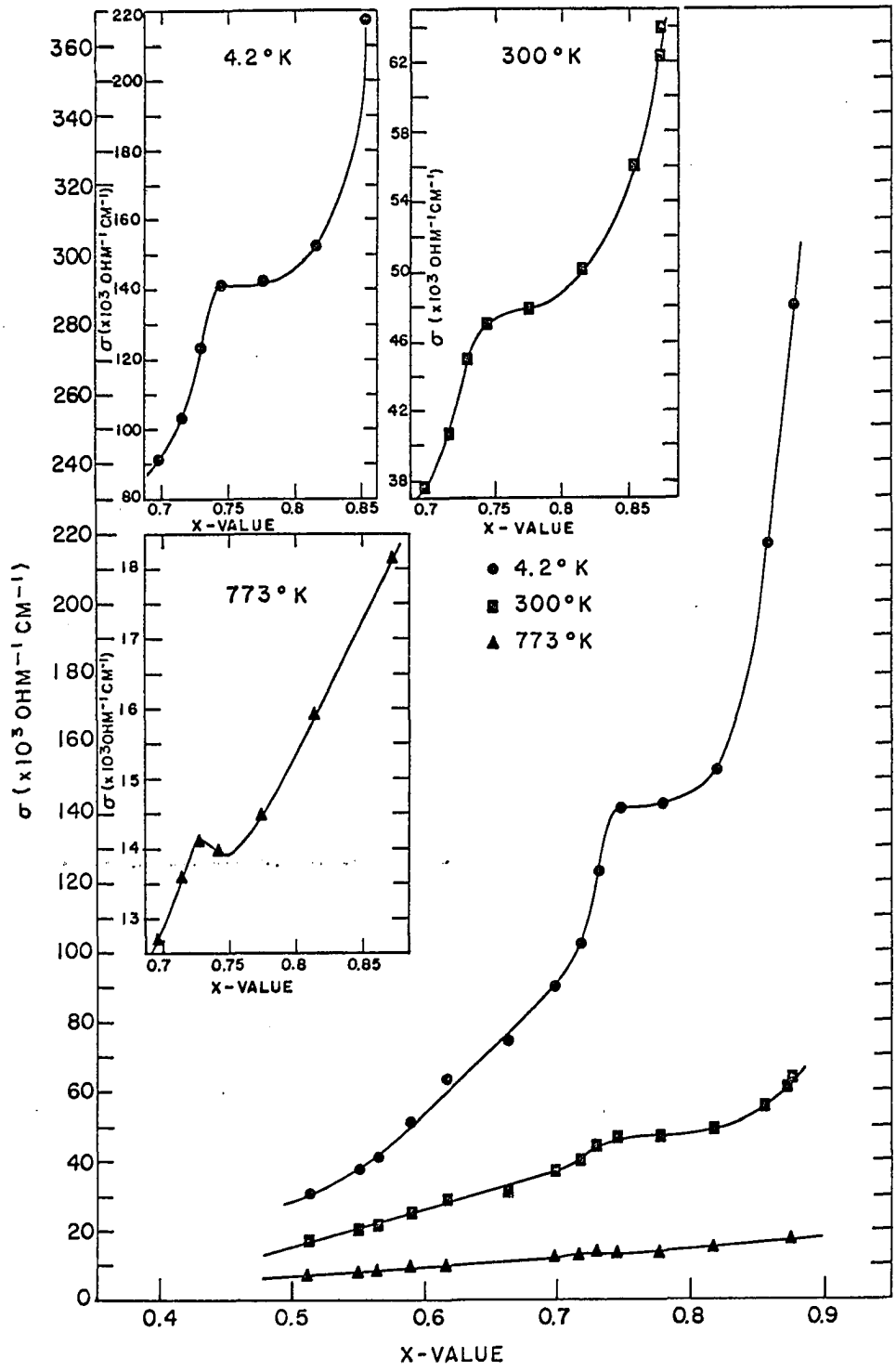

Fig. 9. Conductivity of Na_xWO_3 as a function of the sodium concentration at 4.2, 300, and 773°K

contribution to the residual resistivity would be the contribution from the electron-sodium vacancy scattering. It is apparent from Fig. 9 that the conductivity at 4.2°K increases rapidly with increasing sodium concentration. As pointed out by Ellerbeck, this effect suggests that the sodium vacancies do act as scattering centers. Further, the residual resistivity is large varying from 6% of the total resistivity at x = 0.874 to 24% of the total resistivity at x = 0.513.

The thermal contribution to the resistivity is assumed to be due to polar scattering by optical mode lattice vibrations. The thermal contribution as a function of the sodium concentration can be determined from Equation 24 and is plotted in Fig. 10 as a function of the sodium concentration. From Fig. 10, it can be seen that there is a maximum in the thermal resistivity at x = 0.75. This anomaly in the thermal resistivity would suggest that the partial ordering of the sodium atoms also affects the optical mode lattice vibrations.

The tetragonal I structure of Na_xWO_3 is anisotropic. Thus, the resistivity can be resolved into two independent components; $\rho_\perp$ and $\rho_{//}$ where $\rho_\perp$ is the resistivity perpendicular to the c axis (in the basal plane) and $\rho_{//}$ is the resistivity parallel to the c axis. The anisotropy in the tetragonal I structure is evident in Fig. 11 where the resistivity is plotted as a function of the sodium concentration at 300°K. The resistivity of the Na_xWO_3 single crystals with an axis parallel to the c axis increases in a manner similar to the increase in the resistivity of the cubic single crystals. However, the resistivity of the Na_xWO_3 single crystals with an axis in the basal plane is much

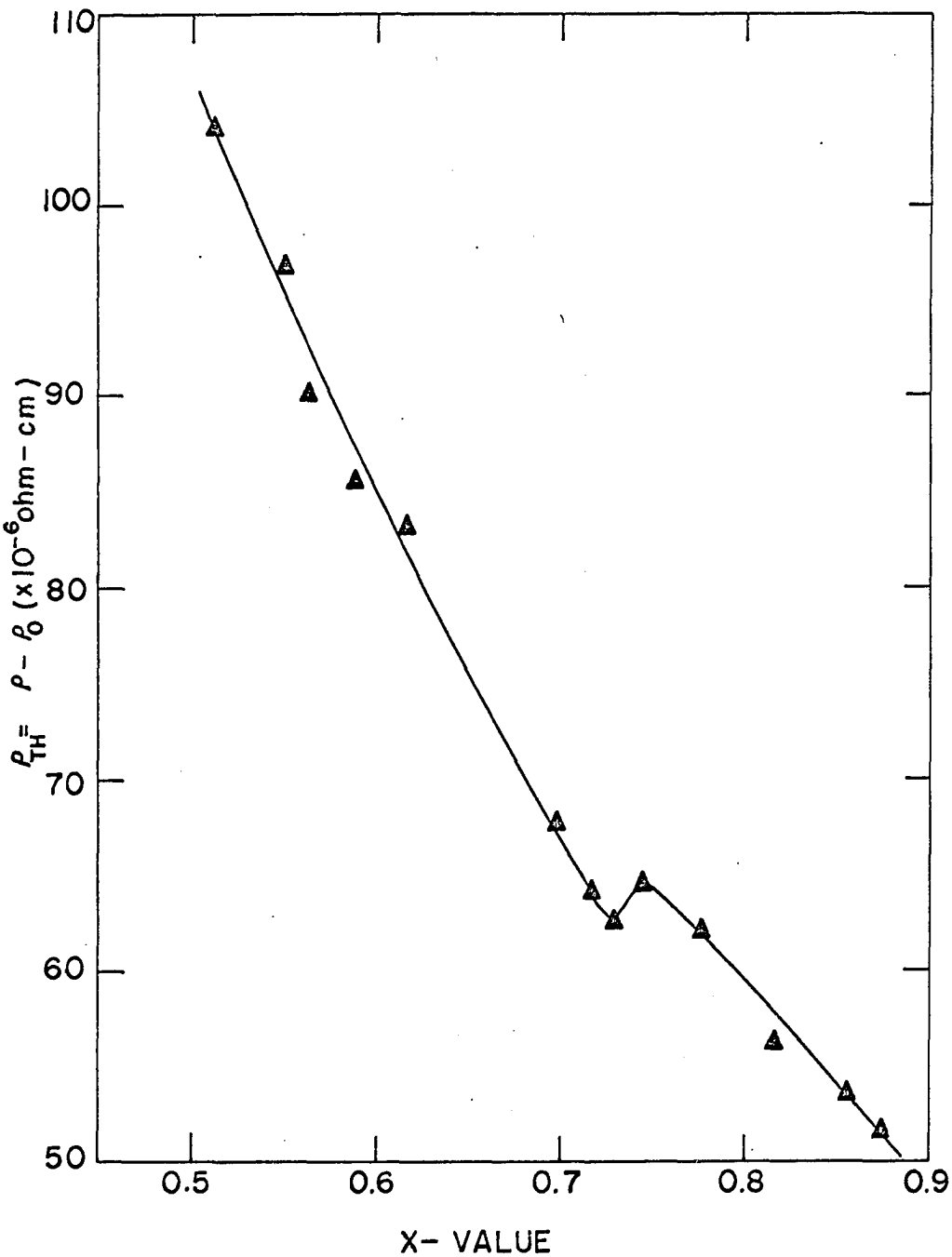

Fig. 10. Thermal contribution to the resistivity of Na_xWO_3 as a function of the sodium concentration

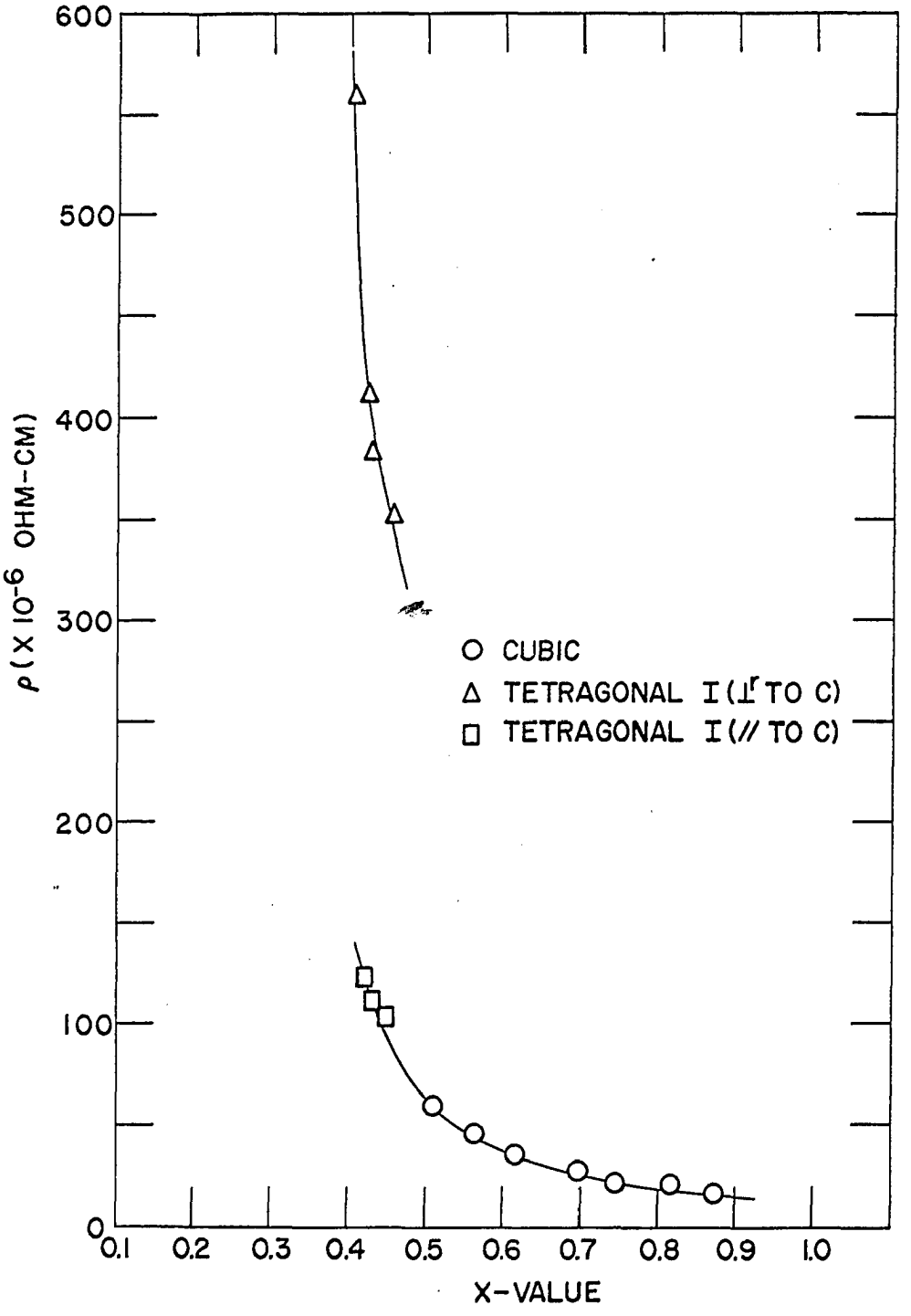

Fig. 11. Resistivity of Na_xWO_3 as a function of the sodium concentration at 300°K showing the anisotropy of the tetragonal I structure

larger, $\rho_{\perp} = 3.4\,\rho_{//}$. This behavior is expected since in the tetragonal I structure the WO_3 octahedra which share common corners have been rotated in the basal plane such that the tungsten-oxygen-tungsten angles are no longer 180 degrees (see Fig. 1). Thus, the symmetry along the c axis remains about the same as the symmetry of the cubic structure; while the symmetry in the basal plane has been changed considerably.

Figure 12 shows the conductivity of the Na_xWO_3 single crystals plotted as a function of the sodium concentration at 300°K. The anisotropy in the tetragonal I structure is also evident in the conductivity. If the conductivity parallel to the c axis and the conductivity in the basal plane are both extrapolated to zero conductivity, then the two curves in Fig. 12 suggests that Na_xWO_3 will become an insulator (or a semiconductor) for sodium concentrations in the neighborhood of 0.25 as suggested earlier by Shanks et al. (9).

Figure 13 shows the resistivity of two tetragonal I Na_xWO_3 single crystals as functions of the temperature. Sample 105-B2a, $x = 0.423$, has an axis along the c axis while sample 109-A3, $x = 0.405$, has an axis in the basal plane. The temperature dependence of the resistivity for sample 105-B2a is very similar to the temperature dependence of the resistivity for the cubic Na_xWO_3 (10). The resistivity for sample 109-A3 did, however, show a small but broad minimum at approximately 90°K. Both tetragonal I Na_xWO_3 single crystals had a large residual resistivity, and the thermal contribution to the resistivity is negligible as high as 40°K.

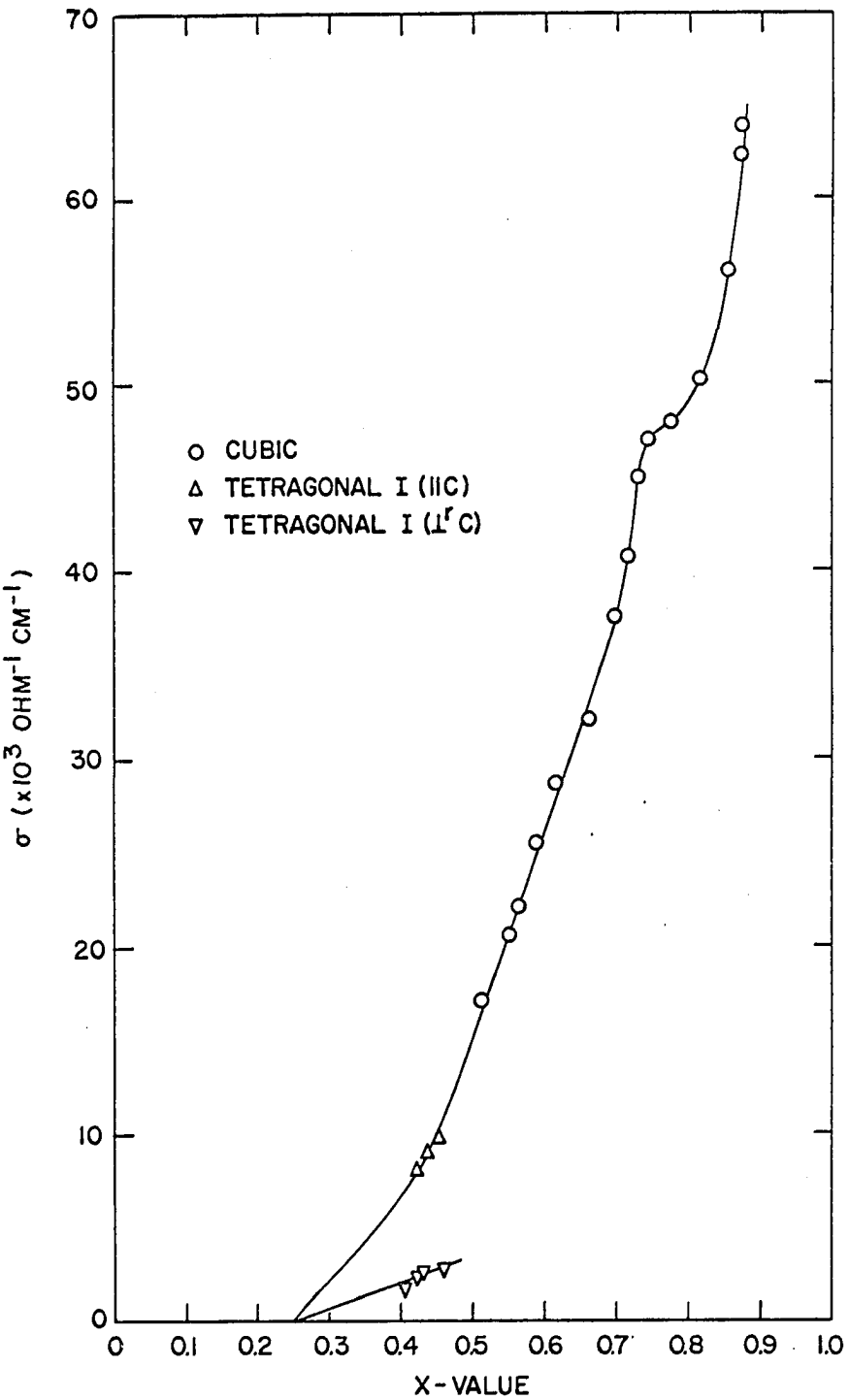

Fig. 12. Conductivity of Na_xWO_3 as a function of the sodium concentration at 300°K showing the anisotropy of the tetragonal I structure

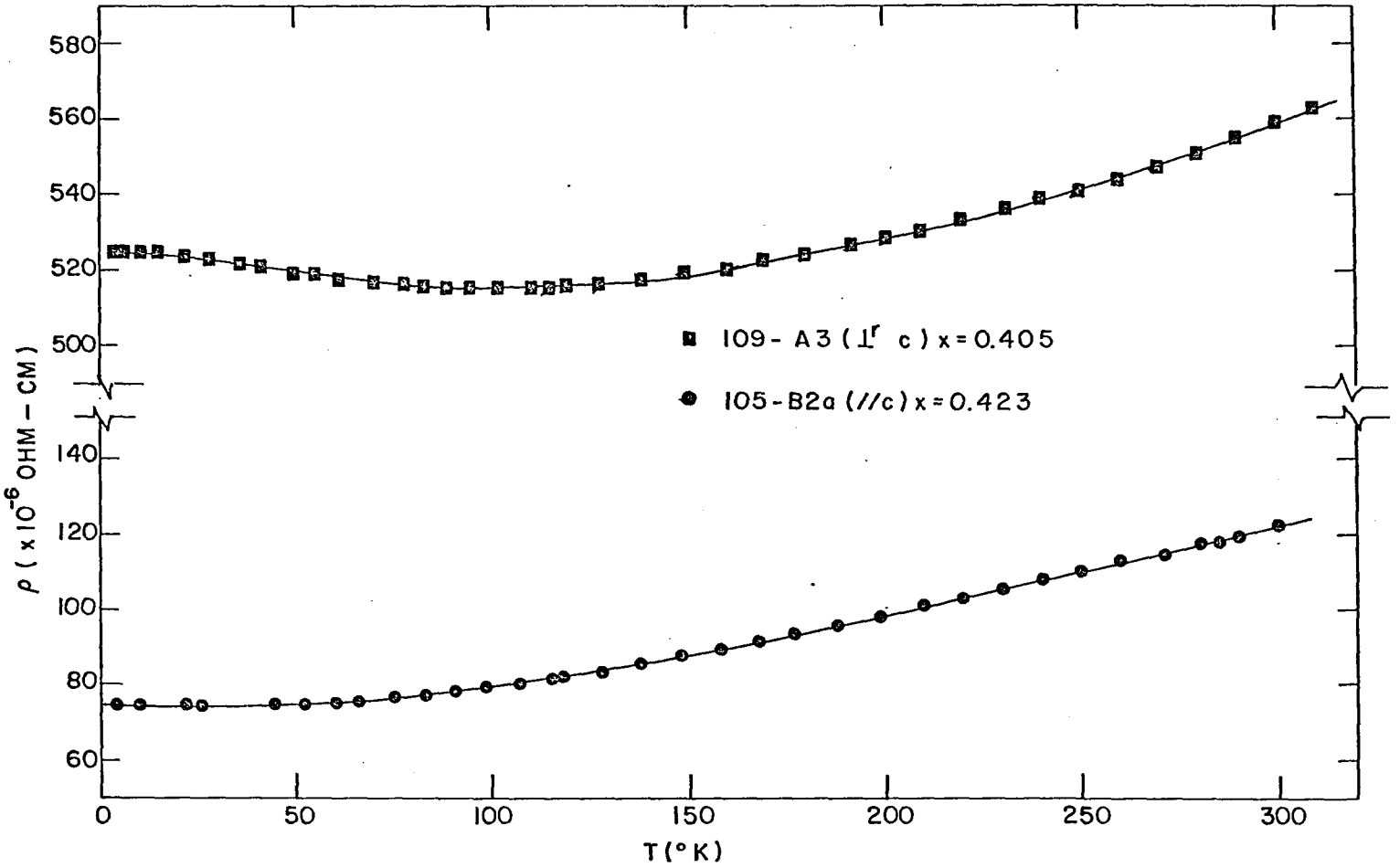

Fig. 13. Resistivity of two tetragonal I Na_xWO_3 single crystals as functions of the temperature from 4.2 to 300°K

B. Hall Coefficients

The room temperature Hall coefficients of Na_xWO_3 are plotted as a function of the sodium concentration in Fig. 14. Also shown in Fig. 14 are the Hall coefficients of Na_xWO_3 measured by Gardner and Danielson (8) as well as the Hall coefficients of two of Gardner's samples measured during the present investigation. These Hall coefficients, which were measured during the present investigation, are as much as 20% lower than the Hall coefficients which were measured by Gardner and Danielson. Also, the x-dependence of the Hall coefficients is different for the two investigations.

Huibregtse et al. (6) measured the correct Hall coefficient of a copper sample before measuring the Hall coefficient of one Na_xWO_3 sample ($x = 0.66$). Gardner and Danielson then compared the Hall coefficient of a similar Na_xWO_3 sample ($x = 0.658$) to the value which had been measured by Huibregtse et al. In the present research we checked the a.c. Hall apparatus by measuring the Hall coefficient of a copper sample before measuring the Hall coefficients of Na_xWO_3 (see Section III-B). Thus, the large difference between our Hall coefficients and the Hall coefficients measured by Huibregtse et al., and by Gardner and Danielson can not be attributed to the Hall apparatus which was used. Rather, the large difference in the Hall coefficients must be a consequence of the inhomogeneity of the samples used by Gardner and Danielson. Gardner (35) noted that in his measurements only a slight shift in the position of the Hall probes gave appreciably different results for the Hall coefficient. Such effects would be

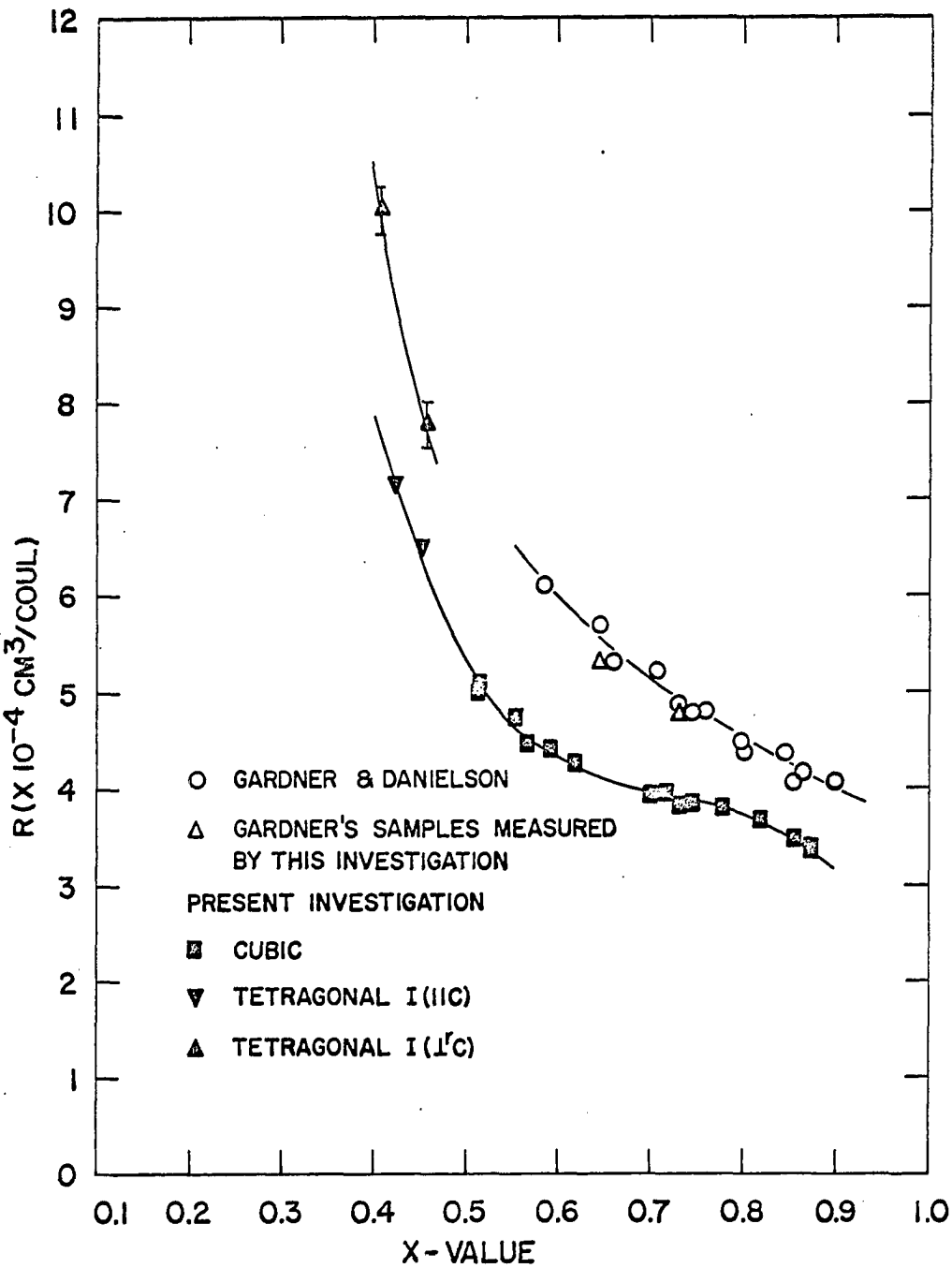

Fig. 14. Hall coefficients of Na_xWO_3 as a function of the sodium concentration

expected in the case of inhomogeneous samples. Further, the Hall coefficients of two of Gardner's original samples were measured during the present study. The results are plotted in Fig. 14 and are within the experimental error of Gardner's data. We conclude, therefore, that the reason for the difference between the Hall coefficients reported in the present investigation and those reported earlier by Gardner and Danielson must be the inhomogeneity of the samples used in the earlier investigation. Accordingly, the Hall coefficients, like the resistivity, are affected by the homogenity of the Na_xWO_3 single crystals.

The Hall coefficients of three Na_xWO_3 single crystals were measured as functions of the temperature from 4.2°K to 300°K. The results are shown in Fig. 15 where the Hall coefficients are plotted as a function of the temperature. Our results confirm the conclusion by Gardner and Danielson that the Hall coefficients of Na_xWO_3 are independent of temperature from 4.2°K to 300°K.

The number of sodium atoms per unit volume is given by $N_a = x/a^3$ where x is the sodium concentration and a is the lattice constant. Gardner and Danielson assumed the free electron value for the Hall coefficient and thus determined an effective number of electrons given by $n = 1/Re$. They then plotted the number of electrons as determined from the Hall coefficient as a function of the number of sodium atoms per unit volume. Their results are plotted in Fig. 16. From the one-to-one correspondence, Gardner and Danielson concluded that each sodium atom contributed one electron to a conduction band. Hence, the number of conduction electrons would also be given by $n = x/a^3$.

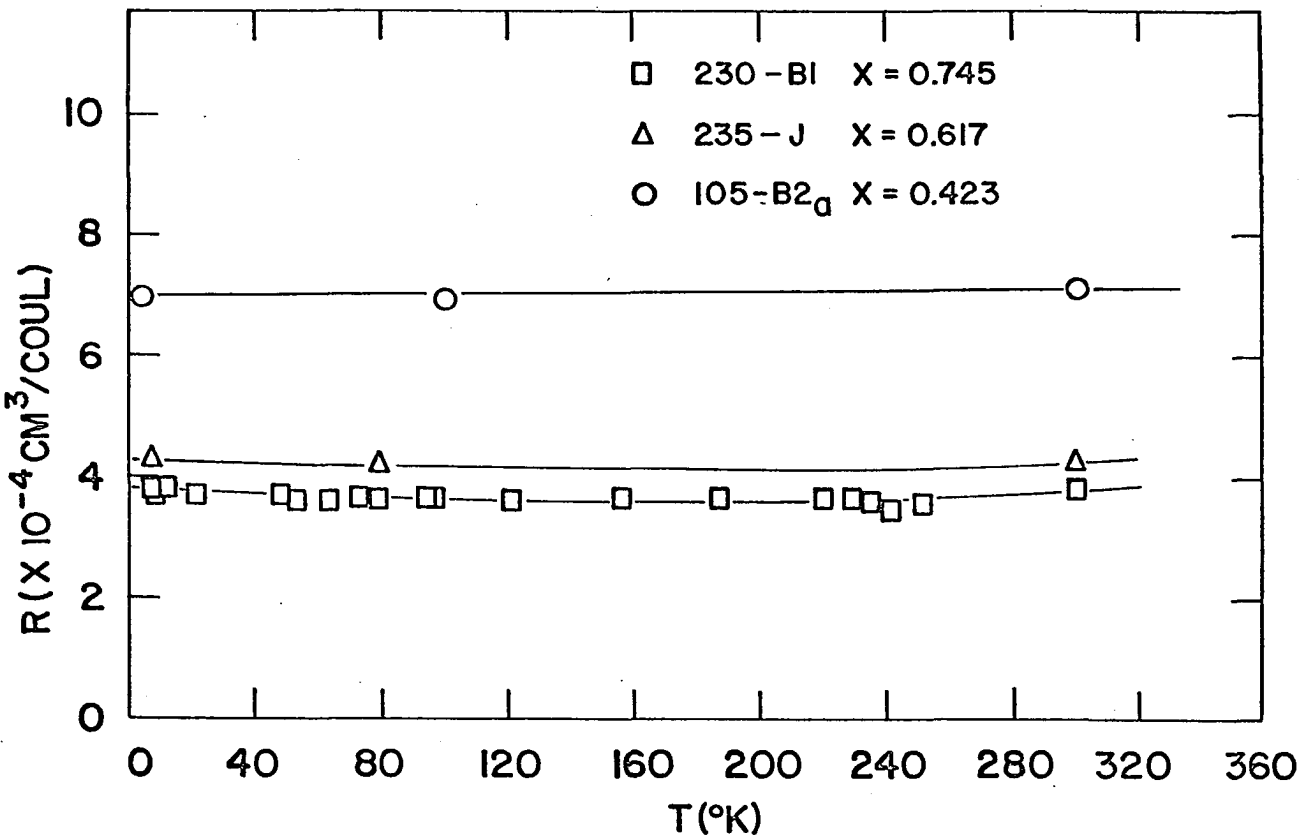

Fig. 15. Hall coefficients of three Na_xWO_3 single crystals as functions of the temperature from 4.2 to 300°K

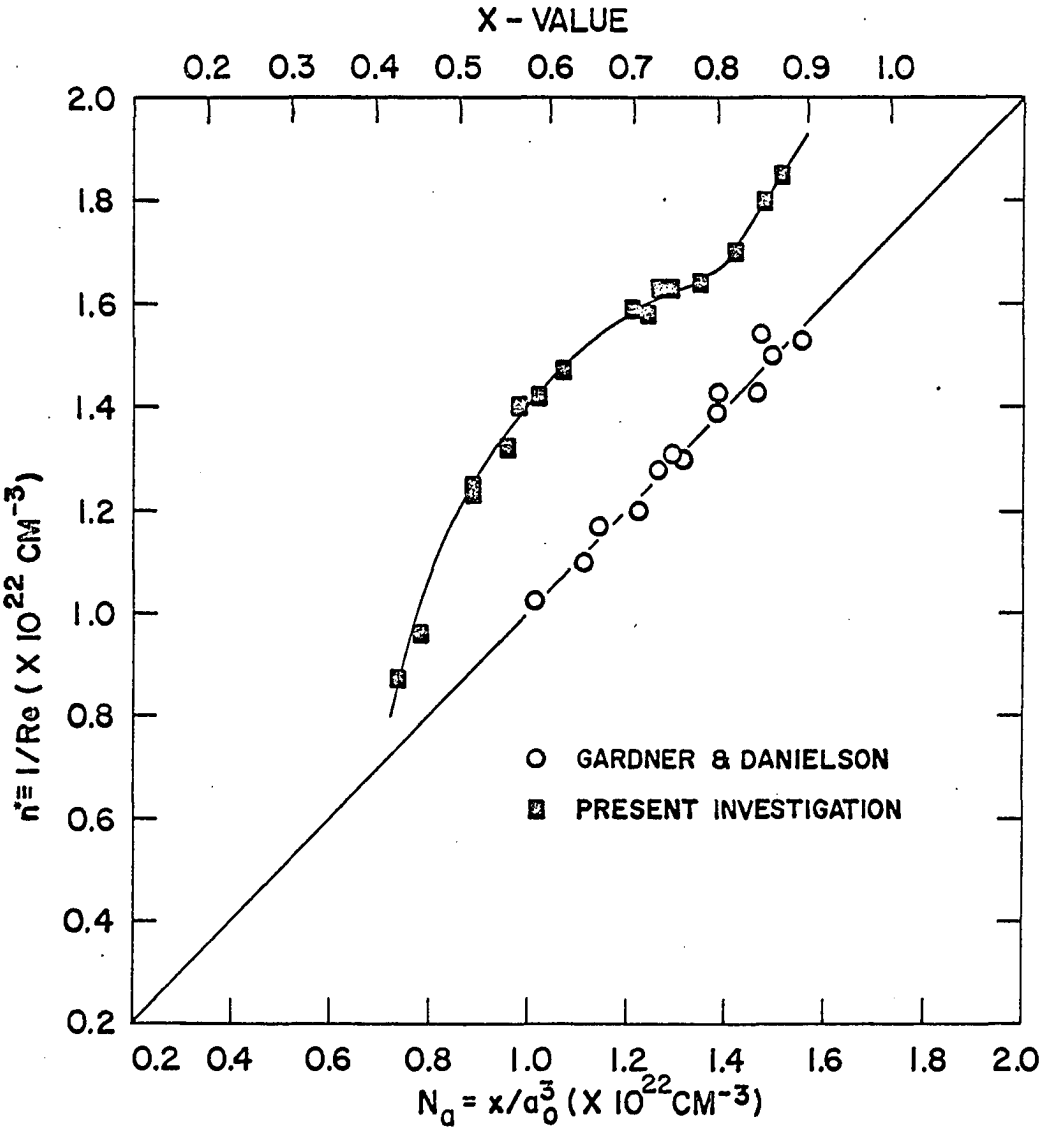

Fig. 16. Effective number of conduction electrons defined by n* = 1/Re as a function of the number of sodium atoms per unit volume

Figure 16 also shows the reciprocal product 1/Re plotted as a function of x/a^3 for the Hall coefficients of the homogeneous Na_xWO_3 single crystals that were measured during the present investigation. It is not evident from the Hall coefficients of homogeneous Na_xWO_3 single crystals that there is a one-to-one correspondence between the number of conduction electrons and the number of sodium atoms. However, the Hall coefficient is given by R = 1/ne only for the free electron approximation where the constant energy surfaces are proportional to k^2. The observed x-dependence of the Hall coefficients would suggest that the Hall coefficients for Na_xWO_3 are not given simply by R = 1/ne. (This result will be discussed further in Section V.) Further, for the tetragonal I structure (see Fig. 14) there is anisotropy in the Hall coefficients with $R_\perp / R_{//} = 1.2$.

The Hall mobility can be defined by the equation

$$\mu_H = R/\rho \quad , \tag{25}$$

where R is the measured Hall coefficient and ρ is the measured resistivity. In Fig. 17 the Hall mobility as defined by Equation 25 is plotted as a function of the sodium concentration at 300°K. Since the Hall coefficients are independent of temperature, (see Fig. 15) the Hall mobility at 773°K and 4.2°K would have much the same x-dependence as the conductivity at these temperatures. The anisotropy of the tetragonal I structure is also evident in the Hall mobility with $\mu_{//} / \mu_\perp = 2.86$. Also, at x = 0.75 there is an anomaly in the Hall mobility which is similar to the anomaly seen in the conductivity.

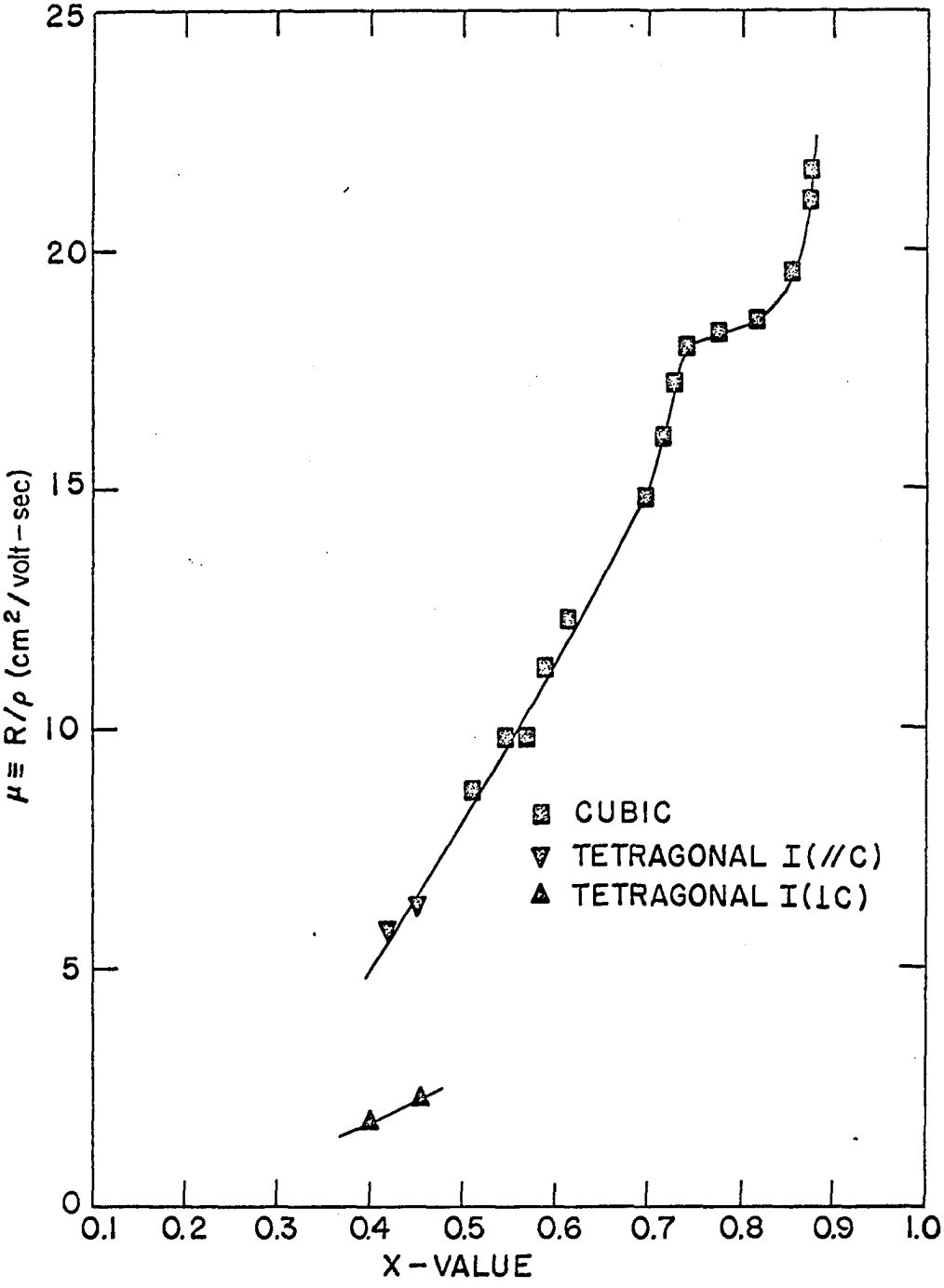

Fig. 17. Hall mobility of Na_xWO_3 defined by $\mu = R/\rho$ as a function of the sodium concentration

C. Seebeck Coefficients

The Seebeck coefficients of Na_xWO_3 were measured as a function of the temperature from 15°K to 340°K (see Fig. 18). The seven samples with x between 0.875 and 0.512 were cubic Na_xWO_3. The three samples with x between 0.457 and 0.405 were tetragonal I Na_xWO_3 with the axis of the sample in the basal plane. The Seebeck coefficients were negative, indicating, in agreement with the Hall data, that the carriers were electrons. The small magnitude of the Seebeck coefficients indicated metallic behavior.

In Fig. 19 the Seebeck coefficients of the same Na_xWO_3 single crystals are plotted as functions of the temperature from 15°K to 60°K on an expanded scale. Besides the usual diffusion contribution to the Seebeck coefficients, which is proportional to the temperature, there is another contribution which is believed to be a lattice or a "phonon-drag" contribution. To separate the diffusion contribution and the lattice contribution, the total Seebeck coefficient is assumed to be the sum of the diffusion contribution and the lattice contribution (36). The diffusion contribution is proportional to the temperature. Hanna and Sondheimer (37) have shown that the lattice contribution from normal electron-phonon processes increases from low temperatures as T^3 and decreases at higher temperatures as T^{-1}. Similarly, Bailyn (38) has shown that the lattice contribution from Umklapp electron-phonon processes also increases as T^3 and decreases at higher temperatures as T^{-1}. Thus, we assume that the total lattice contribution decreases as T^{-1} for temperatures larger than $\theta_D/10$. The total Seebeck coefficient

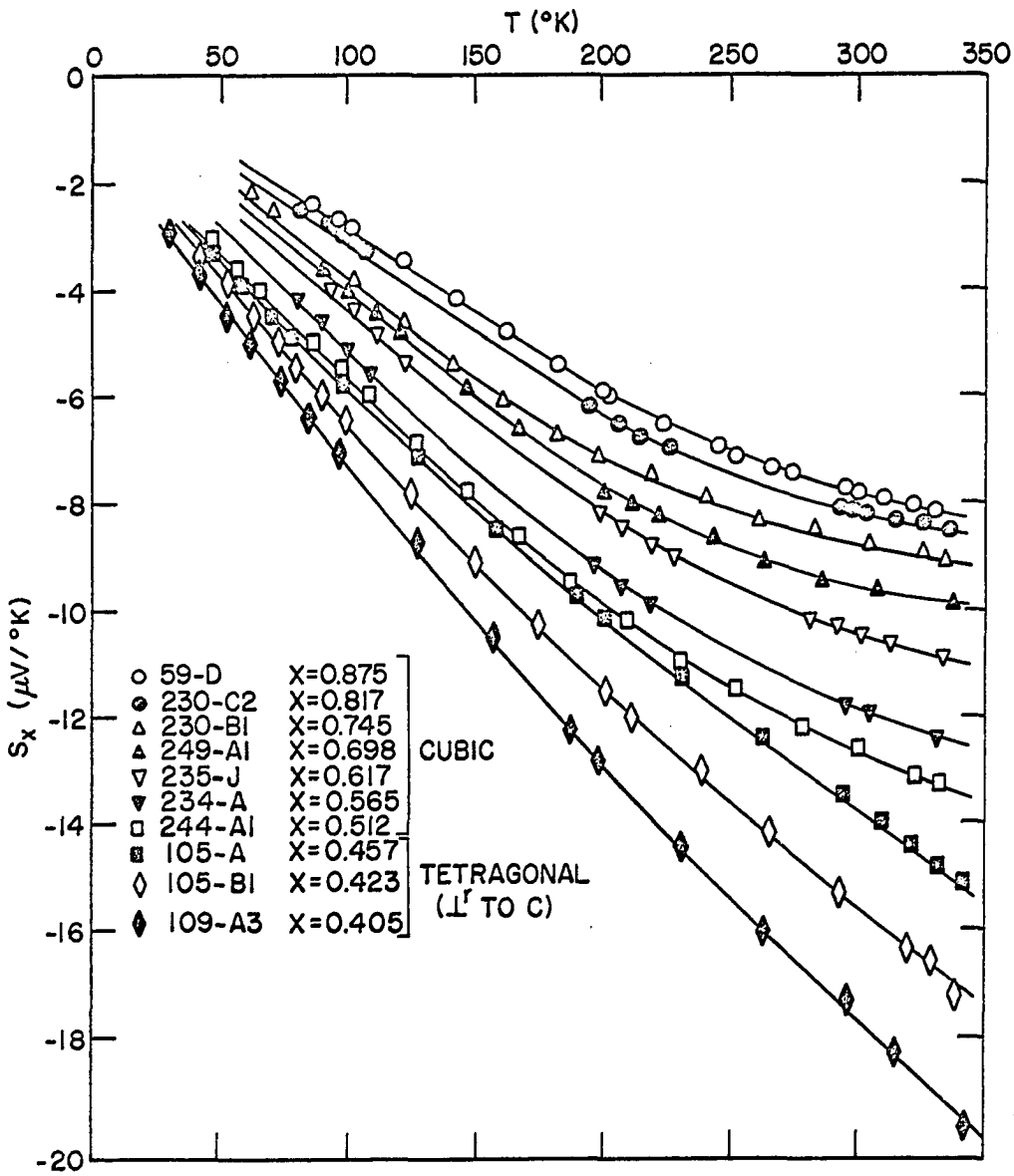

Fig. 18. Seebeck coefficients of Na_xWO_3 as functions of the temperature from 50° to 340°K

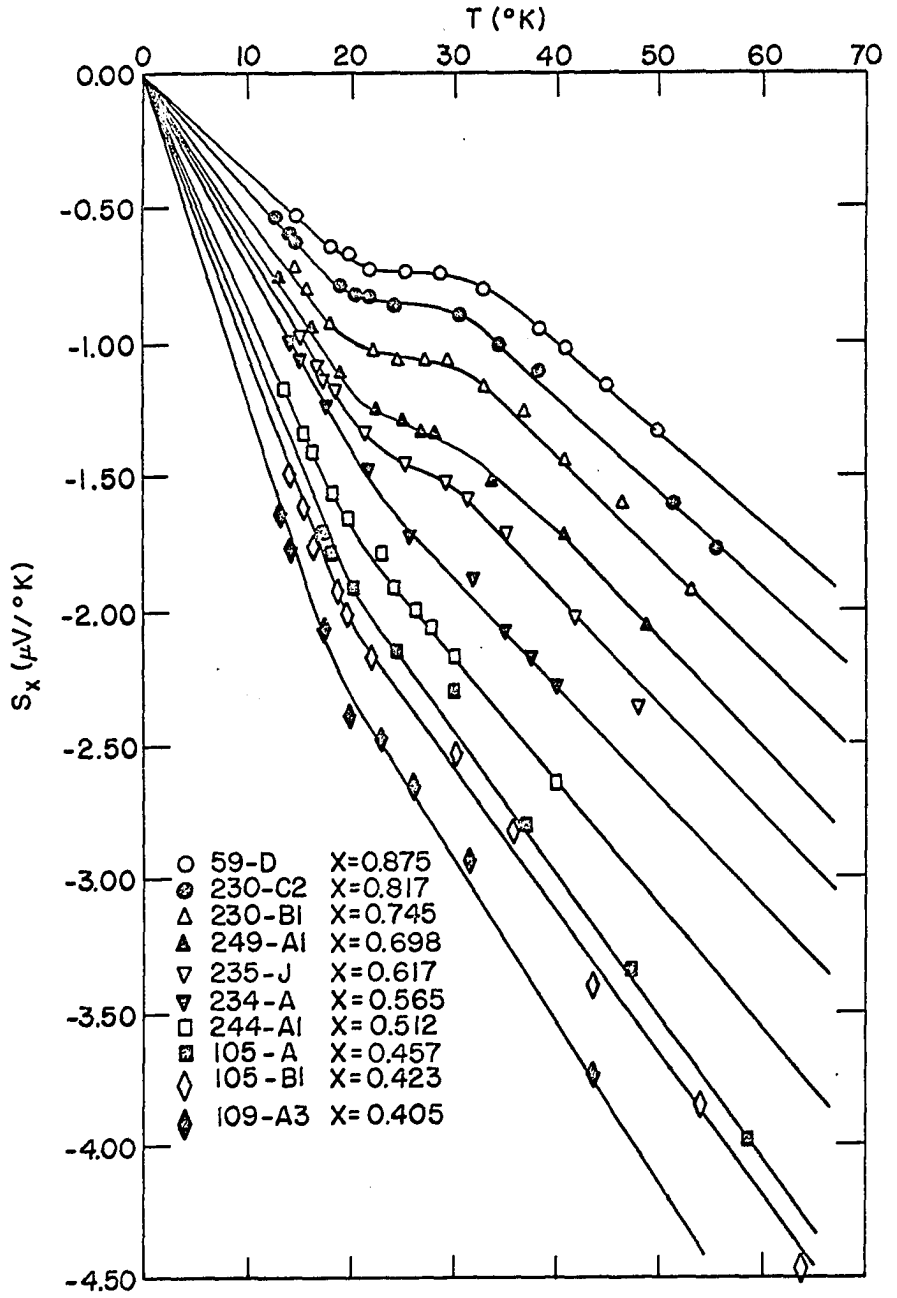

Fig. 19. Seebeck coefficients of Na_xWO_3 as functions of the temperature from 15 to 60°K

can then be written as

$$S = A\,T + B\,T^{-1} \quad , \tag{26}$$

for temperatures larger than $\theta_D/10$, or

$$S\,T = B + A\,T^2 \quad . \tag{27}$$

The slope A of the curve S T vs. T^2 will give the diffusion contribution to the Seebeck coefficient, and the lattice contribution can then be determined from

$$S_g = S - A\,T \quad , \tag{28}$$

where S is the total measured Seebeck coefficient.

In Fig. 20 the total Seebeck coefficients, the calculated diffusion contribution and the resulting lattice contribution are plotted as functions of the temperature from 15°K to 60°K for sample 59-D, which had a sodium concentration of x = 0.875.

The lattice contribution for each Na_xWO_3 single crystal was determined in this way. Figure 21 shows the lattice contribution as functions of the temperature from 15°K to 60°K. The lattice contribution for the high sodium concentrations is seen to consist of both a negative term and a positive term. Bailyn (38) showed that all normal electron-phonon processes gave a negative term to the Seebeck coefficient while

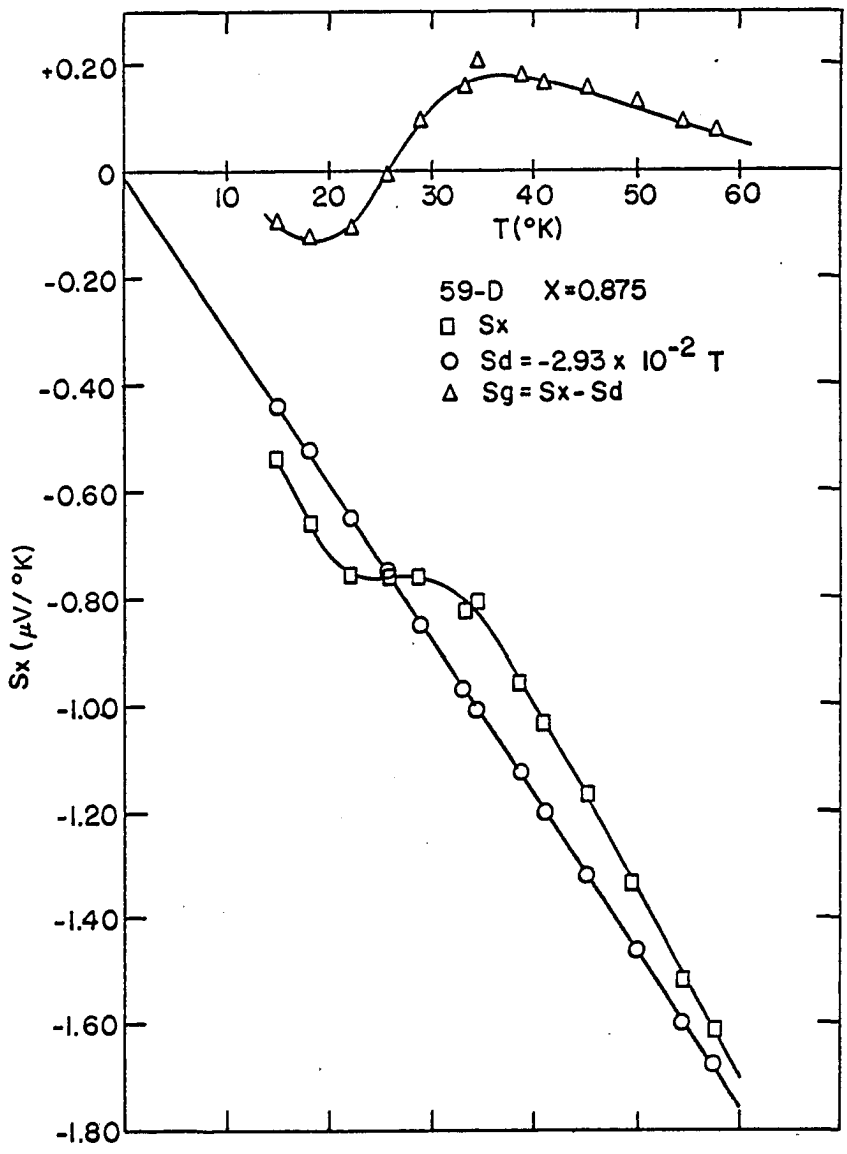

Fig. 20. Total Seebeck coefficients (S_x), diffusion contribution (S_d) and lattice contribution (S_g) as functions of the temperature for sample 59-D (x = 0.875)

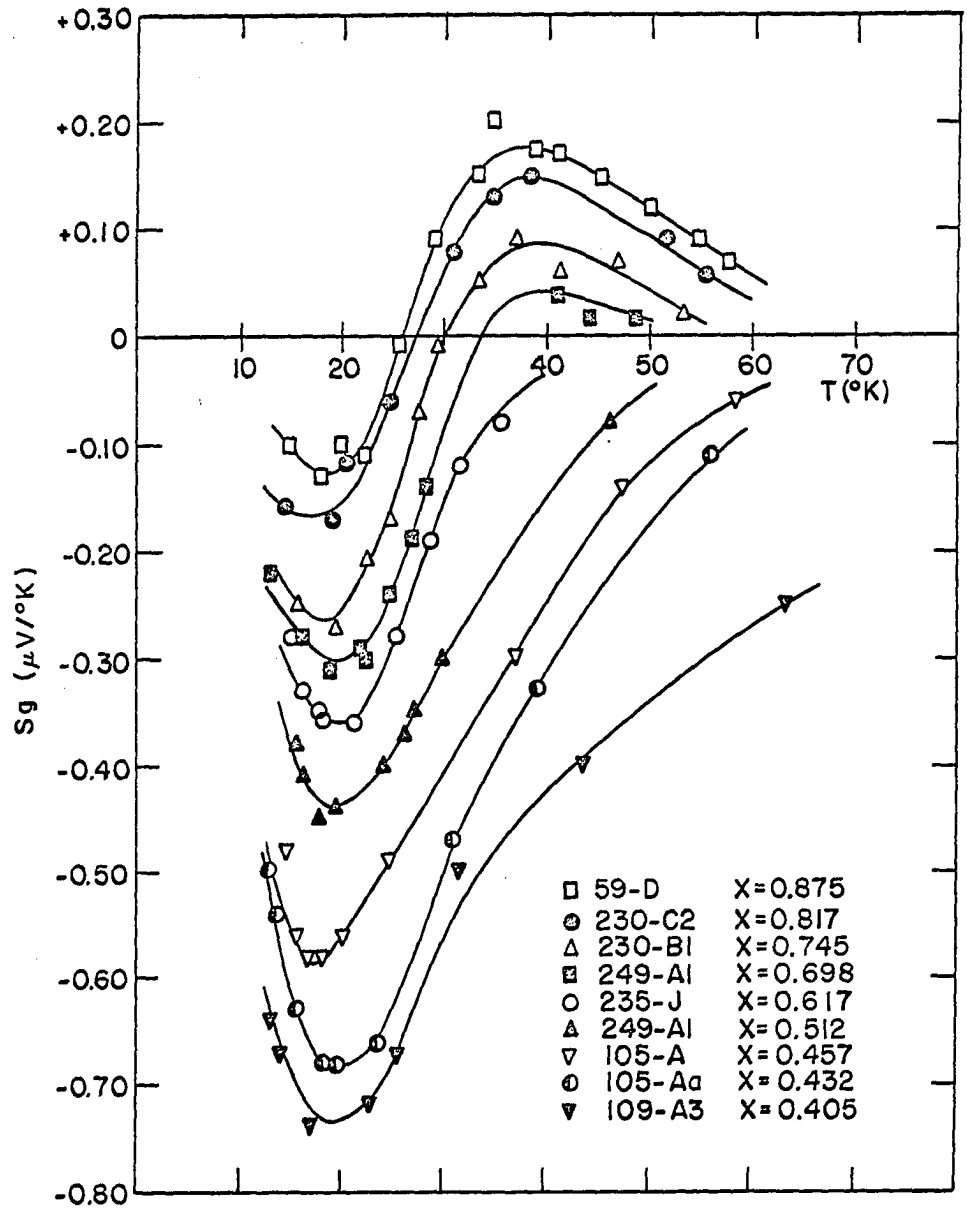

Fig. 21. Lattice contributions to the total Seebeck coefficients of Na_xWO_3 as functions of the temperature from 15 to 60°K

all Umklapp electron-phonon processes gave a positive term to the Seebeck coefficient. Thus, the negative term (which is of the same sign as the diffusion contribution) is considered to be due to normal electron-phonon processes (N-processes) while the positive term is considered to be due to Umklapp electron-phonon processes (U-processes). As the sodium concentration is decreased the Umklapp phonon-drag decreases while the normal phonon-drag increases.

In Fig. 22 the coefficients A, from which the diffusion contributions were determined, and the normal phonon-drag contributions at 19°K are plotted as functions of the sodium concentration. Both contributions increase with decreasing sodium concentration. The diffusion contribution to the Seebeck coefficient does not depend explicitly on the details of the lattice. Hence, the diffusion contribution varies smoothly as the structure changes from cubic to tetragonal I at $x = 0.48$. However, the phonon-drag contribution is related to the details of the lattice and the structure change from cubic to tetragonal I is seen in the sharp increase in the phonon-drag contribution starting at $x = 0.48$.

The total Seebeck coefficients of the Na_xWO_3 single crystals are plotted in Fig. 23 as functions of the sodium concentration for six different temperatures. At room temperature the magnitudes of the Seebeck coefficients start to increase rapidly with decreasing sodium concentration. Shanks *et al.* (9) had found that the Seebeck coefficients at 300°K seemed to vary as $x^{-2/3}$ as predicted by the free electron model. However, because of the limited range of the values of x; the relatively small change in the magnitudes of the Seebeck coefficients;

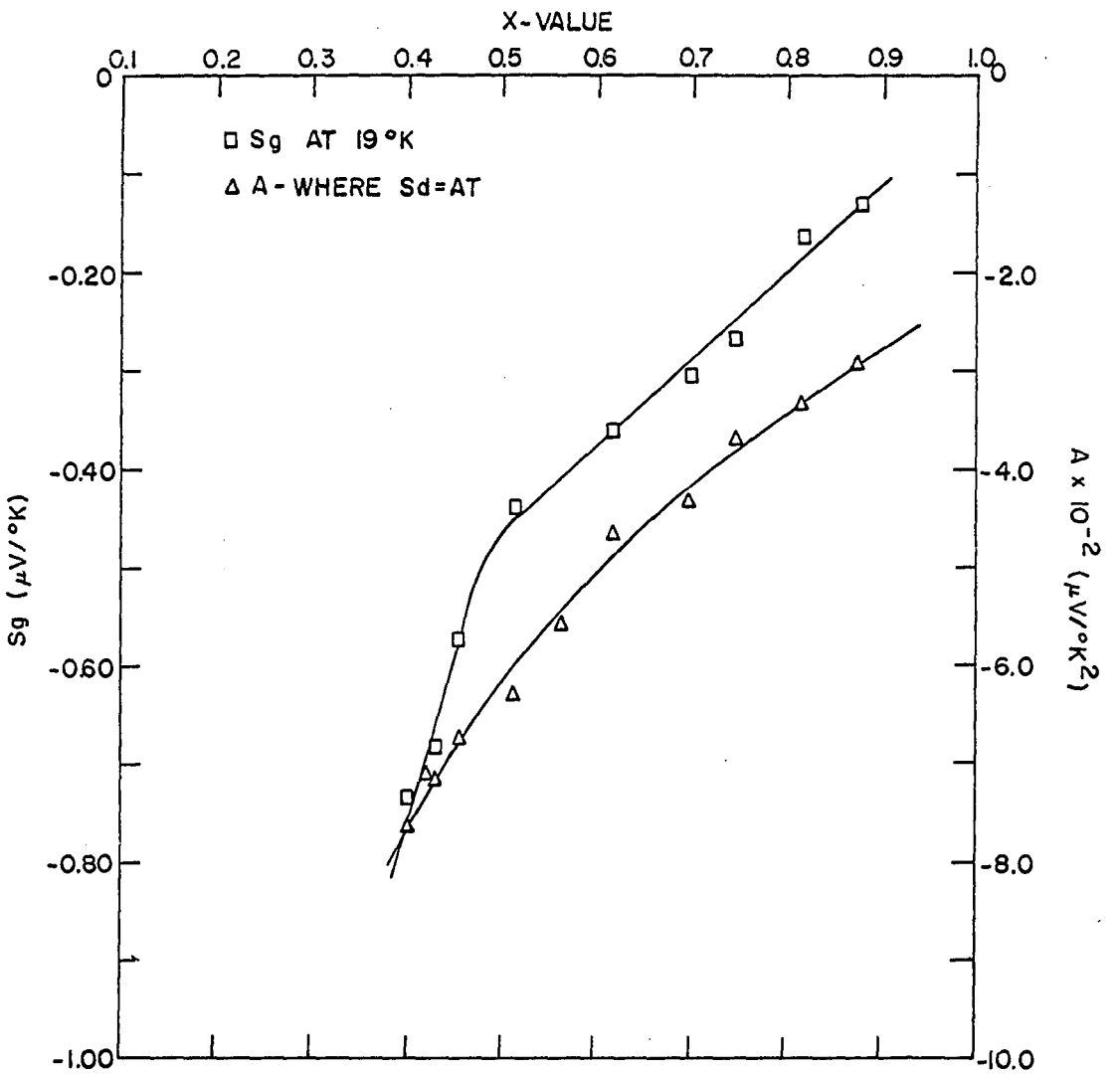

Fig. 22. Coefficients A and lattice contributions (S_g) at 19°K as functions of the sodium concentration

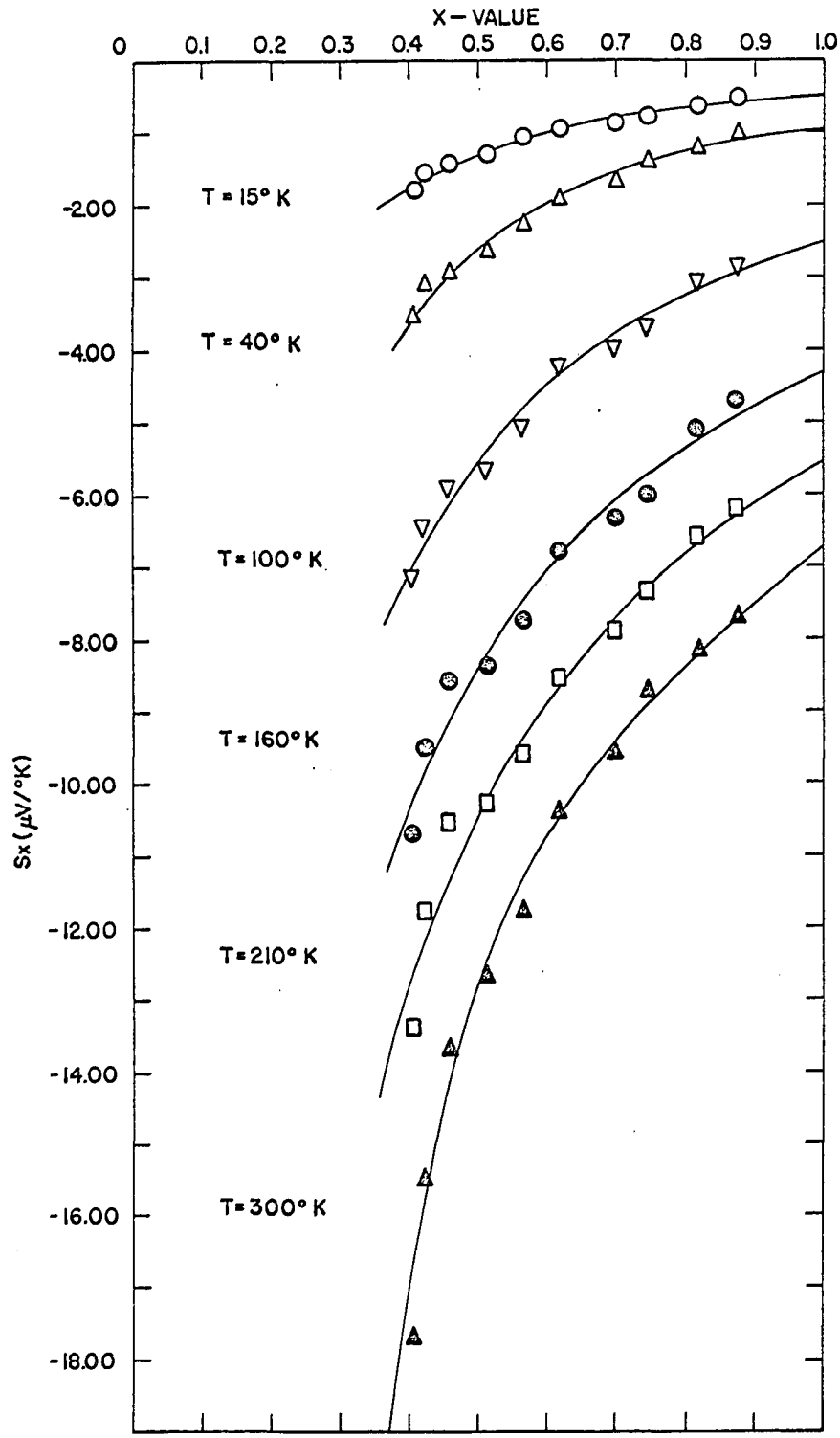

Fig. 23. Total Seebeck coefficients of Na_xWO_3 as functions of the sodium concentration for 15, 40, 100, 160, 210, and 300°K

and the scatter in the data the function x^{-n}, where n is a fraction, is quite insensitive to the exponent n. Thus, it is difficult to determine the exponent n from the experimental data. The results of the present investigation indicate that the Seebeck coefficients at 300°K vary faster than $x^{-2/3}$.

The anisotropy of the tetragonal I Na_xWO_3 was also evident in the Seebeck coefficients. At 300°K the ratio of the two independent components was found to be $S_\perp / S_{//} = 1.3$. In Fig. 24 the Seebeck coefficients of four tetragonal I Na_xWO_3 single crystals are plotted as functions of the temperature. Samples 105-B1 and 105-B2a have the same sodium concentration (x = 0.423), but sample 105-B1 has an axis which is in the basal plane while sample 105-B2a has an axis which is parallel to the c axis. Similarly for samples 105-A and 109-B2b where x = 0.457. Below 50°K each of the four tetragonal I Na_xWO_3 single crystals had a temperature dependence which was similar to that seen in Fig. 19.

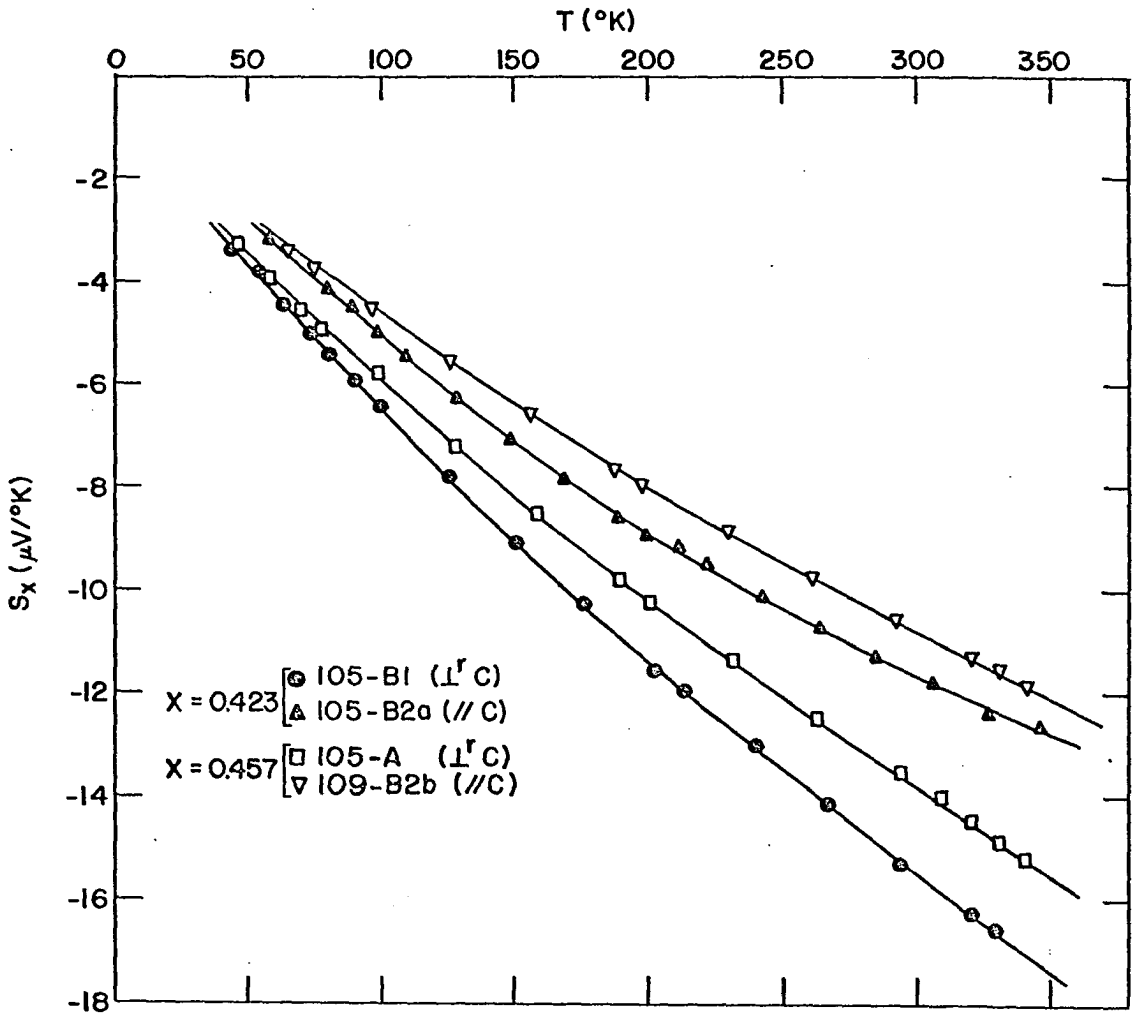

Fig. 24. Seebeck coefficients of four tetragonal I Na_xWO_3 single crystals as functions of the temperature from 50 to 340°K

V. DISCUSSION

A. Free Electron Model

An intriguing aspect of the study of Na_xWO_3 is the ability to control the number of conduction electrons. The question arises, "Can free electron theory be applied to these electrons?" In this approximation the constant energy surfaces are proportional to $\underline{k}^2$. The Hall coefficients measured by Gardner and Danielson (8) seemed to indicate that Na_xWO_3 could be described in terms of free electron theory. However, the density of states at the Fermi energy determined by Vest et al. (13) and the magnetic susceptibility of the electrons as determined by Greiner et al. (14) seemed to be in contradiction to the free electron model. Fuchs (27) noted that the free electron approximation could not explain the observed density of states at the Fermi energy. We shall now show that the results of the present investigation cannot be explained satisfactorily by the free electron approximation.

From the specific heat measurements at low temperatures, the intercept γ of the curve C/T versus T^2 is related to the density of states at the Fermi energy by the relation

$$\gamma = \frac{\pi^2}{3} k^2 V_m N(E_f) \quad . \tag{29}$$

For the free electron approximation, the density of states at the Fermi energy was given by Equation 5. Thus, the free electron value of

γ is defined by

$$\gamma_o = \frac{\pi^2}{3} k^2 V_m \frac{3m^*}{\hbar^2} \left(\frac{1}{3\pi^2}\right)^{\frac{2}{3}} n^{\frac{1}{3}} . \qquad (30)$$

If we assume that each sodium atom contributes one electron to the conduction band, then $n = x/a^3$. The effective mass can be written as $m^* = bm$ where m is the mass of a free electron and b is an adjustable parameter. If the numerical values of the physical constants are substituted into Equation 30, the free electron value of γ is given as

$$\gamma_o = 9.70 \times 10^{-5} \; a^2 \; b \; x^{\frac{1}{3}} \text{ joules mole}^{-1}\text{K}^{-2} , \qquad (31)$$

where a is the lattice constant given in Angstroms, and b is an adjustable parameter. The free electron value of γ can now be compared to the value of γ observed for Na_xWO_3 by Vest et al. (13). The comparison is best described by the ratio γ_{obs}/γ_o which is plotted as a function of the sodium concentration in Fig. 25. The adjustable parameter b was arbitrarily chosen such that $\gamma_{obs}/\gamma_o = 1$ when x = 0.73. If the value of b is chosen in this manner, then $m^* = 1.59$ m. From Fig. 25, it is evident that there is no value of b which can be chosen to make $\gamma_{obs}/\gamma_o = 1$ for all values of x. Hence, the observed values of γ do not correspond to the free electron values of γ.

The Hall coefficient for the free electron approximation was given by Equation 7 as $R = 1/ne$. If we assume that each sodium atom

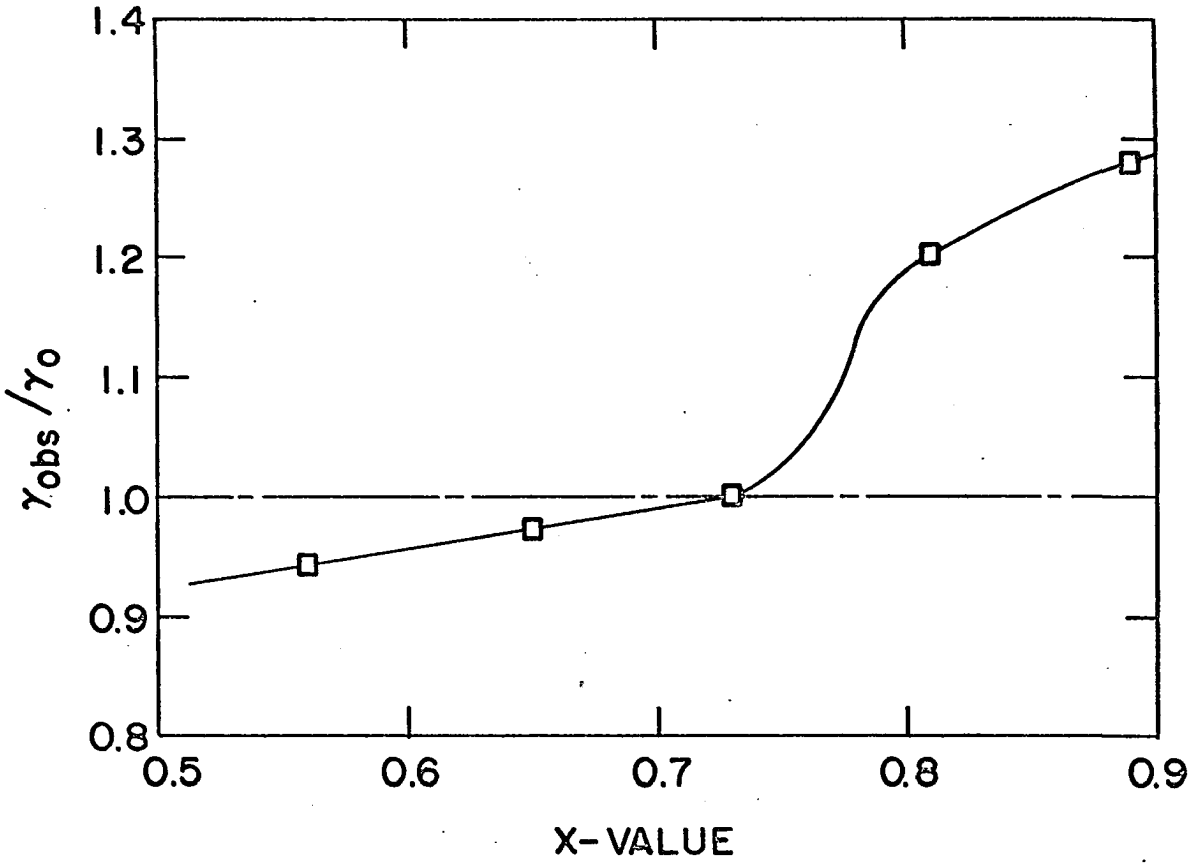

Fig. 25. The ratio of the observed value of γ (13) to the free electron value of γ as a function of the sodium concentration (The dashed line represents $\gamma_{obs}/\gamma_o = 1$)

contributes one electron to the conduction band, then the number of conduction electrons per unit volume is given by $n = x/a^3$. From the measured Hall coefficients of Na_xWO_3 the effective number of conduction electrons per unit volume can be defined as

$$n^* = 1/Re \quad . \tag{32}$$

The observed value of n* can be compared to the number of conduction electrons per unit volume expected from the free electron approximation. The comparison may be described by the ratio n^*/n_o which is plotted in Fig. 26 as a function of the sodium concentration. In the relation for n^*/n_o there are no adjustable parameters. Hence, from Fig. 26 it is evident that the observed values of 1/Re do not correspond to the number of conduction electrons expected from the free electron approximation.

Also for the free electron approximation, the diffusion contribution to the Seebeck coefficient was given by Equation 9. If we assume that each sodium atom contributes one electron to the conduction band, then the free electron value for the diffusion contribution can be defined by

$$S_o = \frac{2\pi^2}{3} \left(\frac{1}{3\pi^2}\right)^{\frac{2}{3}} \frac{m^* k^2 T}{e \hbar^2} a^2 x^{-\frac{2}{3}} . \tag{33}$$

The effective mass can again be written as $m^* = bm$ where m is the mass of a free electron and b is an adjustable parameter. If the numerical

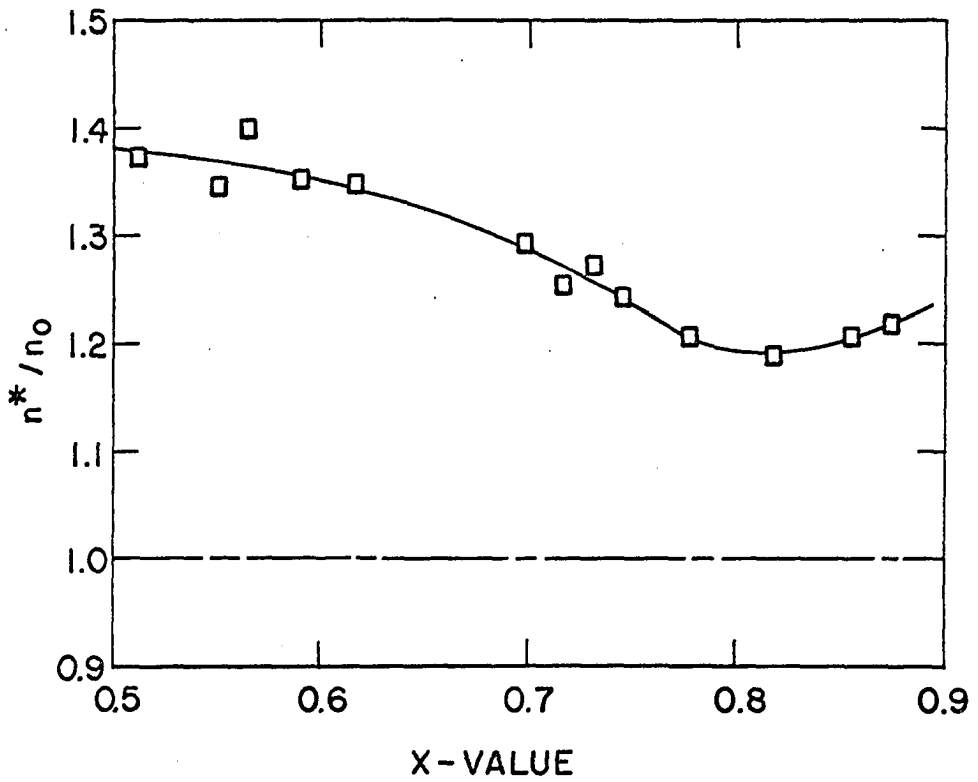

Fig. 26. The ratio of the observed effective number of conduction electrons defined by $n^* = 1/Re$ to the free electron number of conduction electrons as a function of the sodium concentration (The dashed line represents $n^*/n_o = 1$)

values of the physical constants are substituted into Equation 33, then the free electron value for the diffusion contribution is given by

$$S_o = 10.02 \times 10^{-9} \, b \, T \, x^{-\frac{2}{3}} \text{ volt/°K} . \qquad (34)$$

At 300°K the lattice contribution to the Seebeck coefficient should be negligible, and the measured Seebeck coefficient is just the diffusion contribution. Also, for low temperatures (less than $\theta_D/10$) the diffusion contribution can be separated from the lattice contribution (see Section IV-C). Hence, at both 300°K and at some low temperature (say 19°K) the measured diffusion contribution to the Seebeck coefficient can be compared with the free electron value. The comparison is seen in the ratio S_x/S_o which is plotted in Fig. 27 as a function of the sodium concentration. For both temperatures the adjustable parameter b was arbitrarily chosen such that $S_x/S_o = 1$ when $x = 0.512$. From Fig. 27 it is evident that there is no value of b which could be chosen so as to make $S_x/S_o = 1$ for all values of x. Hence, the observed values of the diffusion contribution to the Seebeck coefficient do not correspond to the free electron values for the diffusion contribution.

For the free electron value of the density of states, the number of conduction electrons, and the diffusion contribution to the Seebeck coefficient we assumed that each sodium atom contributed one electron to the conduction band. That is, we assumed that each sodium atom was completely ionized. Is this assumption responsible for the discrepancy between the observed quantity and the free electron value?

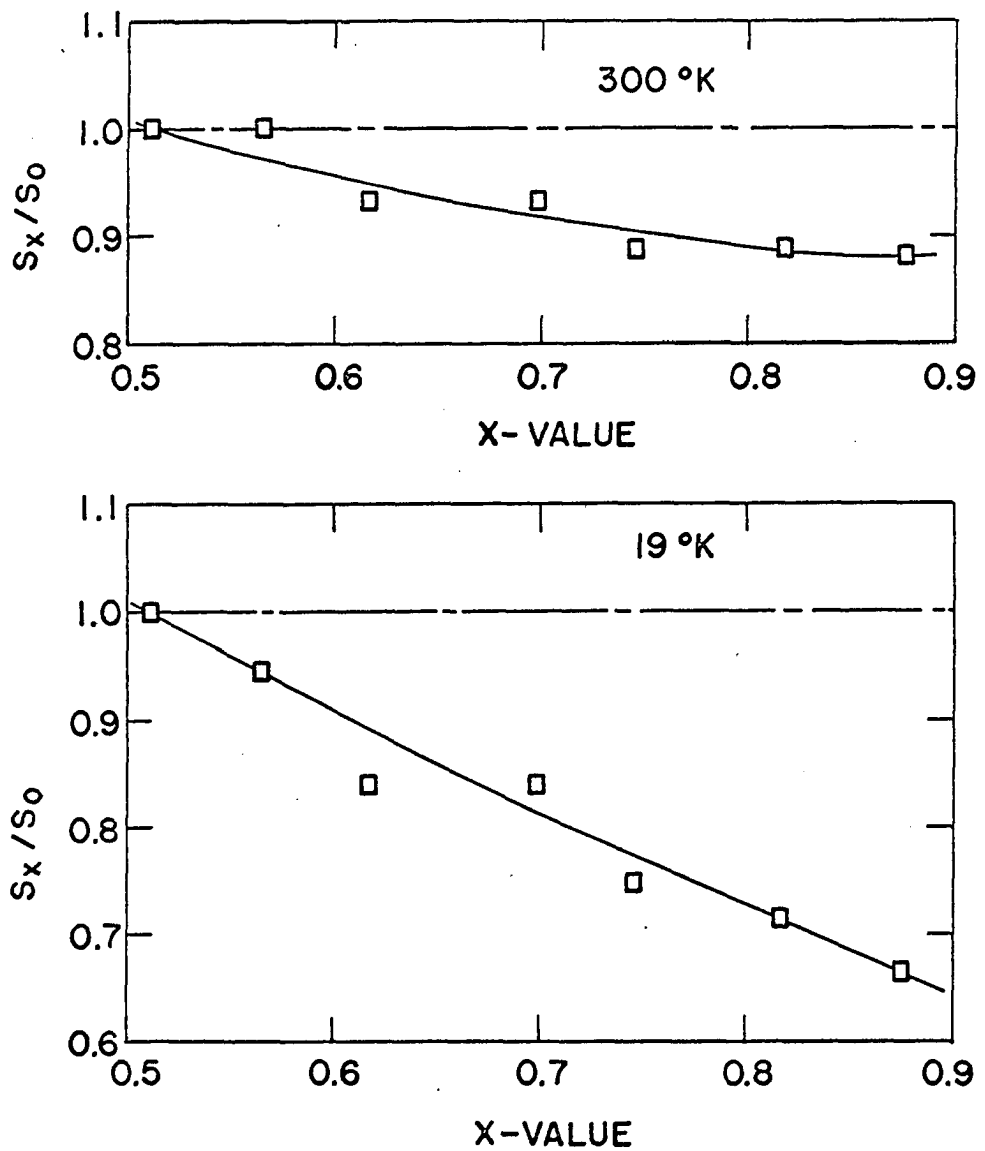

Fig. 27. The ratio of the observed diffusion contribution to the Seebeck coefficient to the free electron value of the Seebeck coefficient as functions of the sodium concentration (The dashed lines represent $S_x/S_o = 1$)

As was pointed out in Section II-A, Jones et al. (16) found essentially no paramagnetic Knight shift in the ^{23}Na resonance which indicated that there was essentially no interaction of the sodium nuclei with the conduction electrons. Further, Fromhold and Narath (18, 19) found a large, x-independent value of T_1T (T_1 is the spin-lattice relaxation time and T is the absolute temperature) for the ^{23}Na nuclei and a small, x-dependent value of T_1T for the ^{183}W nuclei. These nuclear magnetic resonance data show that the density of states at the sodium nuclei is small. If all of the sodium atoms were not completely ionized, then some of the electrons would still be in s states associated with the sodium nuclei. These s electrons associated with the sodium nuclei should produce a ^{23}Na Knight shift, as well as an x-dependent value of T_1T for the ^{23}Na nuclei. Since there is no paramagnetic ^{23}Na Knight shift and T_1T for the ^{23}Na nuclei is independent of x, it is reasonable to assume that each sodium atom is completely ionized. The conclusion one must make is that the number of "free" electrons is equal to the number of sodium atoms, but the electronic properties of Na_xWO_3 cannot be explained satisfactorily by the free electron approximation.

B. Density of States at the Fermi Energy

The density of states at the Fermi energy as determined from the electronic specific heat measurements of Vest et al. (13) showed a sudden increase at approximately x = 0.75 (see Fig. 28). However, the density of states at the Fermi energy as determined from the magnetic susceptibility measurements of Greiner et al. (14) seemed to increase

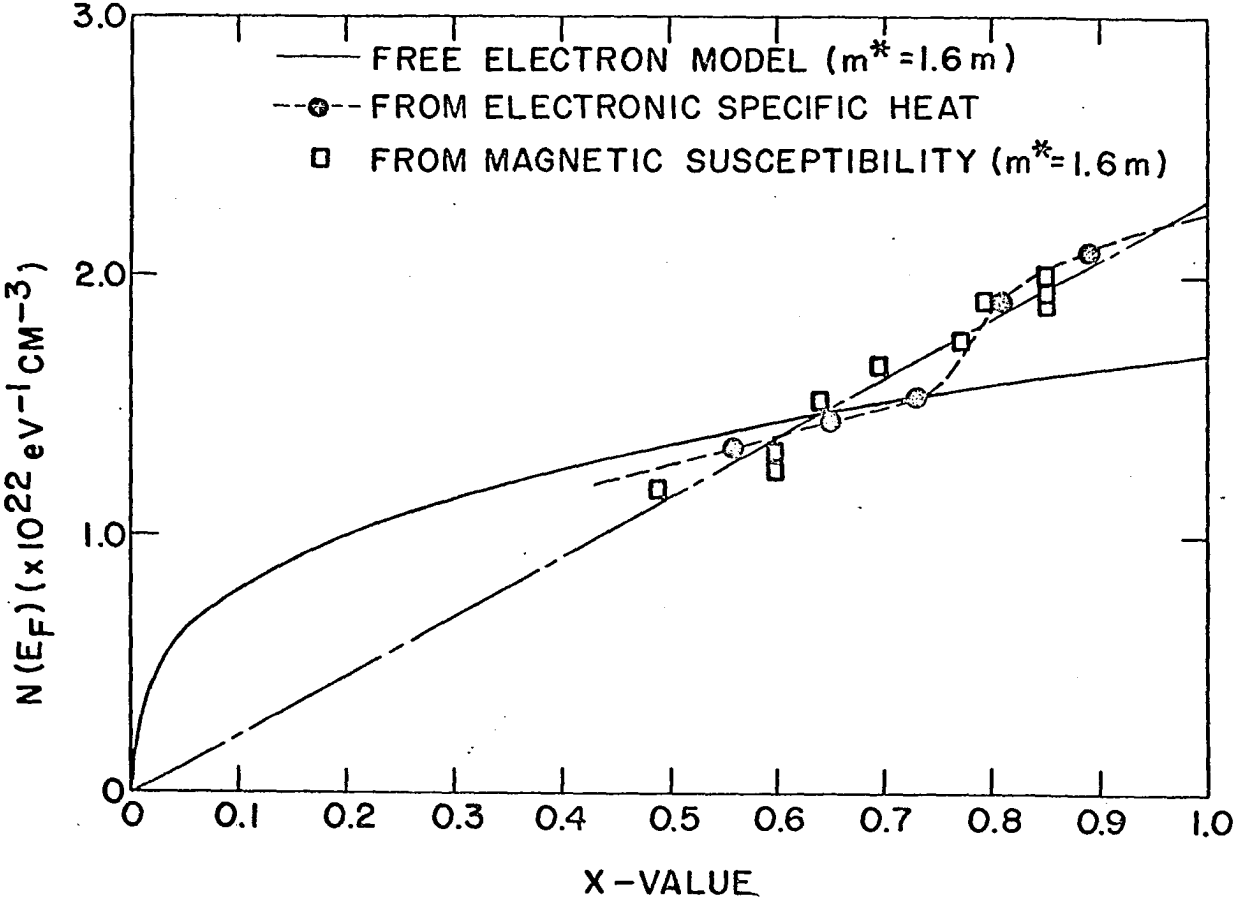

Fig. 28. The density of states at the Fermi energy as a function of the sodium concentration

linearly with x and showed no sudden increase at x = 0.75. The density of states was determined from the electronic specific heat by the relation

$$\gamma = \frac{\pi^2}{3} k^2 N(E_f) \quad , \tag{35}$$

where γ was the intercept of the curve C/T versus T^2. At low temperatures the specific heat is composed of an electronic contribution which is proportional to the temperature and a lattice contribution which is proportional to T^3. Thus, the total specific heat can be written as

$$C = \gamma T + \beta T^3 \quad , \tag{36}$$

or

$$C/T = \gamma + \beta T^2 \quad . \tag{37}$$

If the electrons obey Fermi-Dirac statistics, and if higher order terms in T^2 are neglected, the value of γ is related to the density of states at the Fermi energy by Equation 35 regardless of the shape of the Fermi surface.

On the other hand, the density of states at the Fermi energy, as determined from the magnetic susceptibility, is given by the relation

$$X_e = \mu_o^2 N(E_f) \left[1 - \frac{1}{3} \left(\frac{m}{m^*} \right)^2 \right] \quad , \tag{38}$$

where μ_o is the Bohr magneton. If the electrons obey Fermi-Dirac

statistics, and if higher order terms in T^2 are neglected, the Pauli spin paramagnetism is given by

$$X_p = \mu_o^2 N(E_f) \quad . \tag{39}$$

However, in addition to the paramagnetic effect due to the spins of the electrons, there is also a diamagnetic effect due to the precessional motion of the electrons. This diamagnetic correction is not negligible and is not very well known. For a conduction band, where the density of states is proportional to $E^{\frac{1}{2}}$ and the energy is porportional to $\underline{k}^2$ (that is, the free electron approximation), the diamagnetic correction is given by

$$X_L = -\frac{\mu_o^2}{3} N(E_f) \left(\frac{m}{m^*} \right)^2 \quad . \tag{40}$$

Thus, for the free electron approximation, the diamagnetic correction can be made, and the density of states is related to the magnetic susceptibility by Equation 38. However, we have shown that the free electron approximation does not account satisfactorily for the experimental data of Na_xWO_3. Thus, it is doubtful that Equation 40 gives the diamagnetic correction appropriate for the electrons in Na_xWO_3. Hence, the density of states at the Fermi energy would not be given correctly by Equation 38. It seems best to assume that the density of states at the Fermi energy is determined more correctly by the electronic specific heat measurements than by the magnetic susceptibility measurements.

However, a recent analysis of the sodium concentration for the Na_xWO_3 samples used by Vest et al. (13) for specific heat measurements indicated that the samples were very inhomogeneous in sodium concentration. The following table lists the average x-value as given by Vest et al. along with the range of x-values which were found by Shanks[1] for each sample.

Table 3. Average x-value and range of x-values for the Na_xWO_3 samples used by Vest et al. (13)

Average x-value	Range of x-values
0.56	0.560 - 0.586
0.65	0.650 - 0.716
0.73	0.704 - 0.755
0.81	0.797 - 0.836
0.89	0.850 - 0.892

Because of the relatively large spread in the sodium concentration, the values of γ which were obtained from the specific heat measurements should be considered weighted averages over ranges of sodium concentrations.

[1] Shanks, H. R., Ames Laboratory, Iowa State University of Science and Technology, Ames, Iowa. Range of x-values for specific heat samples. Private communication. 1966.

Nevertheless, the most reliable values for the density of states at the Fermi energy seem to be those determined from the electronic specific heat measurements.

C. Effects of Ordering

The neutron diffraction studies of Atoji and Rundle (11) indicated that there is a partial ordering of the sodium atoms at $x = 0.75$ and that a superlattice is formed. The lattice constant of the superlattice is twice the original lattice constant. If the unit cell of the superlattice is chosen such that a sodium site is situated at each of the corners, then there are no sodium atoms at the (000) and the $(\frac{1}{2}\frac{1}{2}\frac{1}{2})$ sodium sites.

Since the lattice constant of the superlattice is twice the original lattice constant, the periodicity of the lattice potential in which the electrons move will be twice the ordinary lattice spacing. Consequently, the Brillouin zones will be split in half, and there will be new planes (superzones) where the energy is discontinuous. The splitting of the Brillouin zone can be seen schematically in Fig. 29. Part (a) of Fig. 29 shows a simple, but nonspherical Fermi surface in a Brillouin zone with a reciprocal lattice vector $\underline{G}$. Part (b) of Fig. 29 shows how the superzones cut the original Fermi surface, and produce new discontinuities in the energy at the superzone boundaries. For Na_xWO_3 the symmetry of the ordered structure is body-centered cubic while the symmetry of the disordered structure is simple cubic. Thus, the primitive Brillouin zone is the body-centered cubic zone inscribed

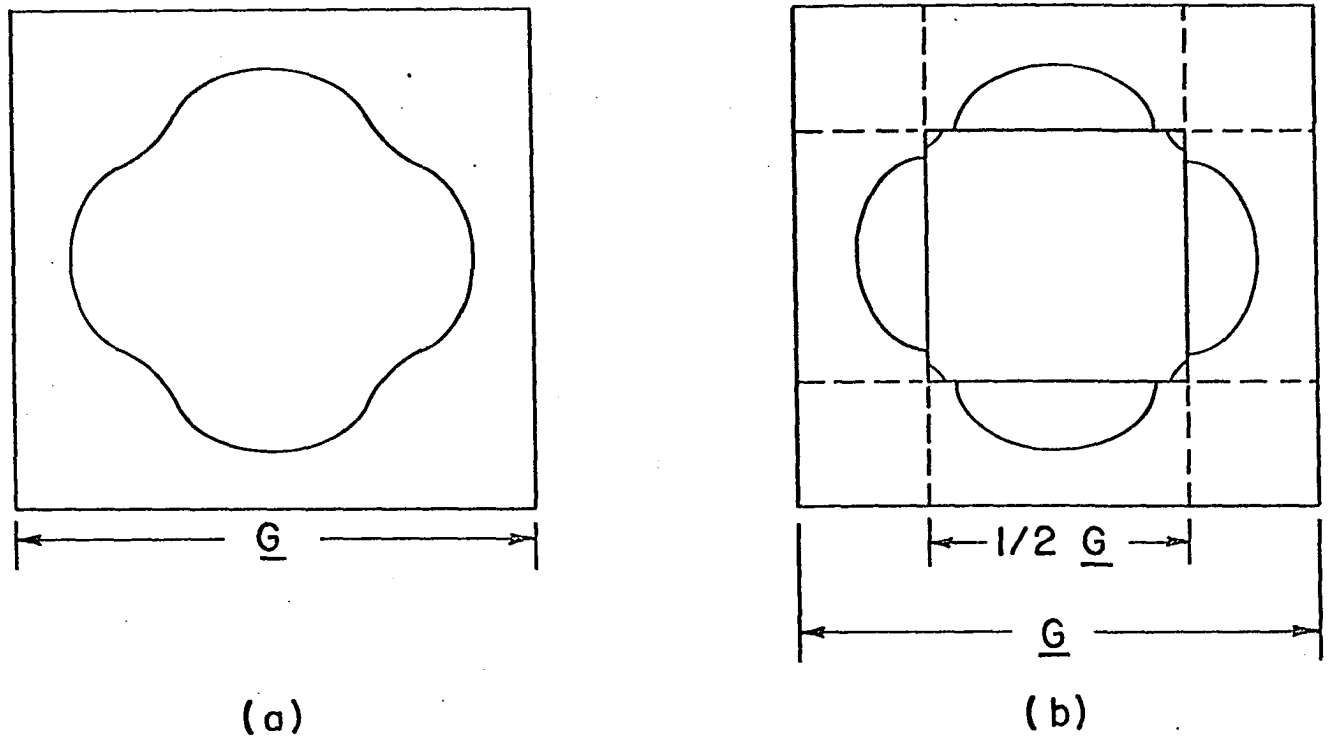

Fig. 29. A schematic representation showing the effect of the superzones

in the simple cubic zone. Hence, the Fermi surface of Na_xWO_3 would be cut by the superzones and there would be new discontinuities in the energy at the superzone boundaries.

The formation of superzones in connection with the ordering of Na_xWO_3 was first suggested by Mackintosh (12). Mackintosh pointed out that the sudden increase in the density of states at the Fermi energy at $x = 0.75$ could be due to the onset of ordering and the consequent appearance of superzones. Mackintosh further suggested that the continual increase in the density of states for x larger than 0.75 could be due to the fact that the electrons begin to occupy a second conduction band. In fact, after the ordering at $x = 0.75$, a second conduction band would be expected since the appearance of the superzones would have the same effect as if the electrons had almost filled the first zone and had begun to spill over into the second zone.

The sections of the Fermi surface contained in the first zone will have negative curvature (that is, $\frac{\partial^2 E}{\partial k^2}$ will be negative). The sections of the Fermi surface contained in the second zone will have positive curvature (that is, $\frac{\partial^2 E}{\partial k^2}$ will be positive). In the repeated zone scheme the sections of the Fermi surface which have negative curvature can be remapped into "hole-like" surfaces; while the sections of the Fermi surface which have positive curvature can be remapped into "electron-like" surfaces. In the band picture we say that we have two conduction bands: one which is nearly empty, where conduction is by electrons, and one which is nearly filled, where conduction is by holes.

Goodenough's tungsten 5d π-bond model predicted that above the

ordering at x = 0.75 two bands would be formed. In Goodenough's notation (see Fig. 2) the two bands are the π^* band and the t_{2g} band. However, the t_{2g} band could not be just a localized level as shown in Fig. 2. Rather, the t_{2g} band must be a narrow band which overlaps with the π^* band. Goodenough mentions that the t_{2g} level could be broadened by the competition between the comparable tungsten π-bonding and the sodium σ-bonding. In this case the energy gap between the π^* band and the t_{2g} band would disappear. Thus, the nearly filled band would be the t_{2g} band and the nearly empty band would be the π^* band.

The behavior of the conductivity of Na_xWO_3 can be explained qualitatively in the following manner. For x less than 0.75 we assume there is only one conduction band. The conductivity can be written as

$$\sigma = \frac{e^2}{12\pi^3 \hbar} \int \Lambda \, dS \quad . \tag{41}$$

Thus, the conductivity varies approximately as $\sum \Lambda_f$ where $\sum$ is the area of the Fermi surface and Λ_f is an average mean free path at the Fermi surface.

The mean free path is inversely proportional to the number of scattering centers. Since the residual resistivity is due to the scattering of electrons by sodium vacancies, at 4.2°K the mean free path would be inversely proportional to the number of sodium vacancies. The conductivity, therefore, varies approximately as

$$\sigma \sim \sum/(1-x) \quad . \tag{42}$$

We assume that each sodium atom contributes one electron to the conduction band. Therefore, it is reasonable to suppose that the area of the Fermi surface increases with increasing sodium concentration. Since Σ and $1/(1-x)$ both increase with increasing sodium concentration, the conductivity would increase with increasing sodium concentration as is found experimentally (see Fig. 9).

At $x = 0.75$, however, the sodium atoms are ordered and superzones are formed in the Brillouin zone. Elliott and Wedgwood (39) have shown that for rare earth metals where superzones are formed due to the periodicity of the magnetic moments the conductivity can be written as

$$\sigma = \sigma_o(1 - \delta) \quad , \tag{43}$$

where δ is proportional to the energy gap across the superzone boundaries. Thus, for rare earth metals there is a decrease in the conductivity at the ordering temperature.

When the sodium atoms order in Na_xWO_3 and superzones are formed, one would, therefore, expect that the conductivity could also be written as

$$\sigma = \sigma_o(1 - \delta) \quad , \tag{44}$$

where δ is proportional to the energy gap across the superzone boundaries. Thus, there may be a maximum in the conductivity at

$x = 0.75$. However, if the energy gap across the superzone boundaries is small, the conductivity may just level off.

Even when the sodium atoms are ordered ($x > 0.75$) the part of the conductivity which is independent of ordering (σ_o) should be given by Equation 42. That is, $\sigma_o \sim \Sigma/(1-x)$. For large x the factor $1/(1-x)$ will dominate the conductivity. Thus, for x larger than 0.75 the conductivity will increase rapidly with increasing sodium concentration.

Hence, one would expect that the conductivity of Na_xWO_3 would increase with increasing sodium concentration for x less than 0.75. In the vicinity of $x = 0.75$ there may be a maximum in the conductivity, or, depending on the magnitude of δ, the conductivity may just level off. For x larger than 0.75 the conductivity would increase rapidly with increasing sodium concentration. Figure 9 shows that these conclusions are in accord with the experimental results. These conclusions are also in agreement with Goodenough's model.

The Hall coefficient for a crystal with cubic symmetry and a nonspherical Fermi surface in low magnetic fields can be written as (40)

$$R = \sigma_H / \sigma_o^2 \quad , \tag{45}$$

where

$$\sigma_o = \frac{e^2}{12\pi^3 \hbar} \int_{F.S.} v_{\underline{k}} \tau_{\underline{k}} \, dS \quad , \tag{46}$$

and

$$\sigma_H = \frac{e^3}{4\pi^3} \int_{F.S.} \tau^2 \left\{ v_x^2 \, M_{yy}^{-1} - v_x v_y M_{yx}^{-1} \right\} \frac{dS}{v_{\underline{k}}} \quad . \tag{47}$$

In the above equations, the magnetic field is taken to be in the z direction, the current is taken to flow in the x direction, and the Hall voltage is measured in the y direction.

The inverse mass tensor is defined by

$$M_{yy}^{-1} = \frac{1}{\hbar^2} \frac{\partial^2 E}{\partial k_y^2} \quad , \tag{48}$$

and

$$M_{yx}^{-1} = \frac{1}{\hbar^2} \frac{\partial^2 E}{\partial k_y \partial k_x} \quad . \tag{49}$$

Thus, the Hall coefficient varies approximately as $eR \sim - M^{-1} / \sum v_f$ where $\sum$ is the area of the Fermi surface, v_f is an average velocity at the Fermi surface, and M^{-1} is the inverse mass tensor averaged over the entire Fermi surface.

For "electron-like" energy surfaces with positive curvature the effective mass tensor is positive; while for "hole-like" energy surfaces with negative curvature the effective mass tensor is negative. Thus, the sign of the Hall coefficient will depend on the sign of the inverse mass tensor.

For a distorted Fermi surface there may be sections of the surface which have positive curvature and sections of the surface which have negative curvature. The average inverse mass tensor will contain contributions from both sections of the surface and will be smaller than the inverse of the corresponding free electron mass. Also, the area of a distorted Fermi surface will be larger than the area of the

corresponding free electron sphere since the volume must remain the same. Thus, for a distorted Fermi surface the magnitude of the Hall coefficient would be smaller than the corresponding free electron value; and the reciprocal product 1/Re would give an effective number of conduction electrons which would be larger than the actual number of conduction electrons.

For Na_xWO_3, where the constant energy surfaces are not simply proportional to $\underline{k}^2$, one would expect that the effective number of conduction electrons determined from the Hall coefficients would be larger than the actual number of conduction electrons. Figures 16 and 26 show this conclusion to be in accord with the experimental results.

The behavior of the Hall coefficients, and hence the effective number of conduction electrons, as functions of the sodium concentration (see Fig. 16) can also be explained from Equations 45-47. Since the Hall coefficients vary approximately as $eR \sim - M^{-1} / \sum v_f$, the Hall coefficients do not explicitly contain the mean free path (or conversely the relaxation time). Thus, the Hall coefficients will not vary rapidly with changing sodium concentration.

It is assumed that the area of the Fermi surface increases with increasing sodium concentration. Since the Fermi surface becomes more and more distorted as it expands toward the zone boundary, the "hole-like" sections of the Fermi surface will increase and will contribute larger negative contributions to the average inverse mass tensor. Thus, the magnitude of the average inverse mass tensor will decrease with increasing sodium concentration and the area of the Fermi surface

will increase with increasing sodium concentration. Hence, the magnitude of the Hall coefficients will decrease with increasing sodium concentration; or the effective number of conduction electrons will increase with increasing sodium concentration as shown in Fig. 16.

At x = 0.75 the sodium atoms are ordered and another conduction band is formed. The band which is nearly empty, and conduction is by electrons, will contribute a negative contribution to the Hall coefficient. The band which is nearly filled, and conduction is by holes, will contribute a positive contribution to the Hall coefficient. The negative contribution to the Hall coefficient is dominant, but the magnitude of the Hall coefficient decreases faster for x larger than 0.75. This more rapid decrease in the Hall coefficient is seen in the sudden increase in the effective number of conduction electrons for x larger than 0.75 (see Fig. 16).

Ziman (41, 42) has pointed out that the lattice contribution to the Seebeck coefficient is very sensitive to any distortion of the Fermi surface and is one of the best indicies of the shape of the Fermi surface. If we consider only electron-phonon interactions, then the lattice contribution to the Seebeck coefficient can be written as (41)

$$S_g = -\frac{k}{e\, n_a} \frac{4\pi^4}{5} (T/\theta)^3 \frac{\langle \underline{K} \cdot \underline{q} \rangle}{\langle q^2 \rangle}, \qquad (50)$$

where $\underline{K} = \underline{k} - \underline{k}'$ and the terms in the brackets refer to averages over all electron-phonon scattering processes. When considering both normal electron-phonon processes (N-processes) and Umklapp electron-phonon

processes (U-processes), Bailyn (38) found that all N-processes gave a negative term to the Seebeck coefficient (that is, a term of the same sign as the diffusion term) while all U-processes provided a positive term. Thus, the sign of the lattice Seebeck coefficient is a delicate balance between the contribution of N-processes (giving a negative contribution) and U-processes (giving a positive contribution). This balance between the contribution of N-processes and U-processes depends on the form of the electron-phonon interactions and, thus, on the shape of the Fermi surface.

Consider a simple but nonspherical Fermi surface in the repeated zone scheme as shown in Fig. 30. The condition for N-processes is that

$$\underline{k}' - \underline{k} = \underline{q} \quad , \tag{51}$$

while for U-processes

$$\underline{k}' - \underline{k} - \underline{G} = \underline{q} \quad , \tag{52}$$

where $\underline{G}$ is a reciprocal lattice vector, $\underline{q}$ is the phonon wave vector, and $\underline{k}$ and $\underline{k}'$ are the initial and final wave vectors for the electron. The minimum value of $\underline{q}$ for which an U-process can occur is twice the distance in $\underline{k}$-space between the Fermi surface and the zone boundary. This distance is marked by q_{min} in Fig. 30. If k_f represents the wave vector at the Fermi surface nearest the zone boundary, then the

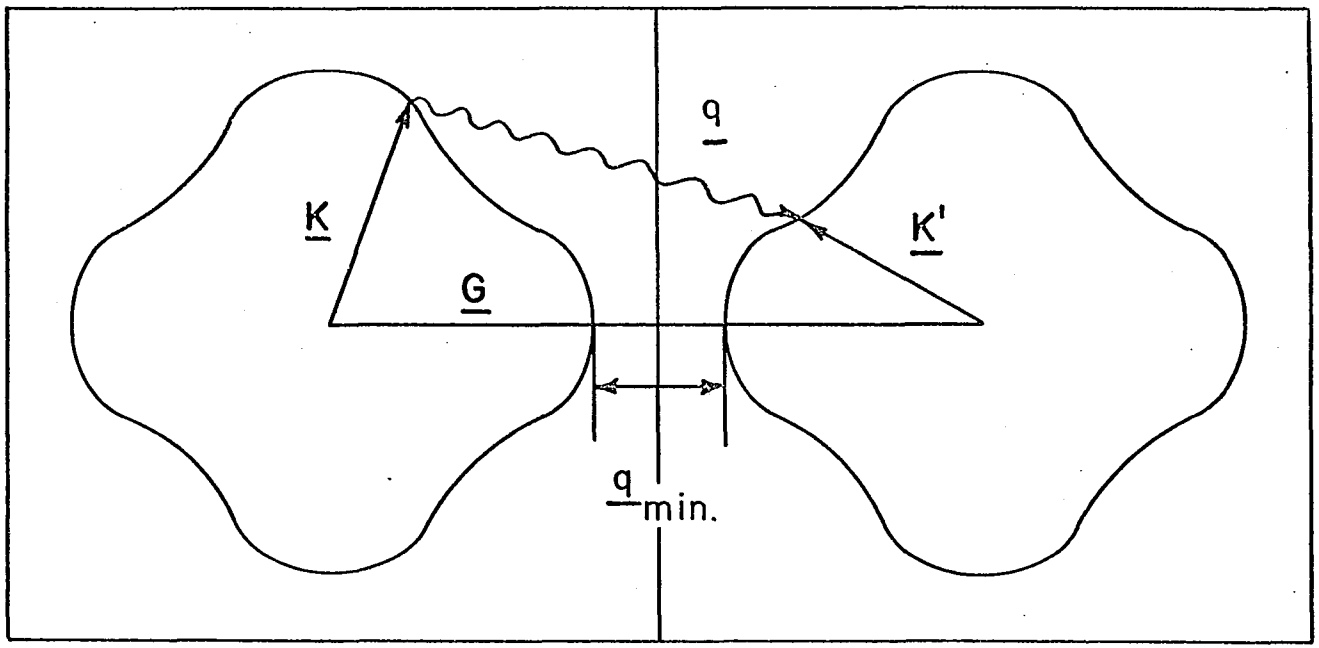

Fig. 30. A schematic representation showing the minimum value of $\underline{q}$ for which a U-process can occur

minimum distance can be written as

$$q_{min} = G - 2k_f \quad . \tag{53}$$

As the value of q_{min} decreases, the probability of U-processes occurring will increase. Thus, the contribution of U-processes to the lattice Seebeck coefficient will increase as q_{min} decreases.

Again we assume that the Fermi surface of Na_xWO_3 is nonspherical and that the Fermi surface increases with increasing sodium concentration. As the sodium concentration increases, the minimum distance, q_{min}, between the Fermi surface and the zone boundary decreases. The contribution of U-processes to the lattice Seebeck coefficient will, therefore, increase with increasing sodium concentration. Thus, the lattice contribution should show an increase in the positive phonon-drag contribution with increasing sodium concentration. This behavior is seen in the lattice contribution to the Seebeck coefficients of Na_xWO_3 (refer to Fig. 21). For low sodium concentrations there is only a negative contribution to the lattice Seebeck coefficient. However, as the sodium concentration increases, the positive phonon-drag contribution also increases.

When the sodium atoms order at x = 0.75 the superzones cut the Fermi surface. The probability of U-processes occurring should be about the same as the probability of N-processes occurring. Hence, for x larger than 0.75 one would expect (see Fig. 21) an almost equal contribution from both the U-processes and the N-processes.

When the sodium atoms order at x = 0.75, one would expect that the ordering would be reflected in an anomaly in both the lattice Seebeck coefficient and the diffusion Seebeck coefficient as functions of the sodium concentration. For most normal ordering processes, the ordering occurs as a function of the temperature. Thus, it is relatively easy to measure the Seebeck coefficient as a function of the temperature and to observe a change in the Seebeck coefficient at the ordering temperature.

However, for Na_xWO_3 the ordering occurs as a function of the sodium concentration and is, therefore, much more difficult to observe. Also, the effects of the ordering seem to be quite small. Because of the error associated with the experimental data, and the error associated with the analysis of the x-values; together with the fact that the x-values are not extremely close together for the Seebeck coefficients, it is very easy to completely miss the effects of ordering. The lattice Seebeck coefficients (see Fig. 22), the diffusion contributions at low temperatures (see Fig. 22) and the total Seebeck coefficients at 300°K (see Fig. 23) as functions of the sodium concentration do not show any anomaly at x = 0.75. However, the experimental data does not necessarily rule out the possibility of a small anomaly in the Seebeck coefficients at x = 0.75.

D. Other Models

The sodium 3p model, the tungsten 5d model, the tungsten 5d π-bond model, and the nonuniform electron gas model can each qualitatively

explain the general behavior of the transport properties as a function of the sodium concentration. For instance, each model would predict that the conductivity should increase with increasing sodium concentration; and each model would predict that the Hall coefficients should decrease with increasing sodium concentration. It was pointed out in Section II-B, however, that none of the models could quantitatively explain the behavior of the transport properties of Na_xWO_3 as a function of the sodium concentration. Since each model can qualitatively explain the general features of the transport properties, the transport properties cannot explicitly determine which model is more correct. Nevertheless, there are some areas where the transport properties can help to distinguish between the several models. These areas shall now be discussed.

For sodium concentrations less than $x = 0.5$ less than half of the sodium sites are filled. Further, in the tetragonal I structure the sodium sites in the basal plane are located in the four or five member rings (see Fig. 1). Thus, the distance between the sodium sites has been increased. Also, in the basal plane there is not a direct path between each of the nearest neighbor sodium sites. If the conduction band were formed by the direct overlap of the sodium 3p orbitals, there could be very little continual overlap of the sodium 3p orbitals in the basal plane. Thus, with less than 50 per cent of the sodium sites occupied, the sodium 3p model would suggest that the conductivity in the basal plane should be small. Hence, on the basis of the sodium 3p model, one would expect a larger anisotropy in the resistivity of

tetragonal I Na_xWO_3 than is observed experimentally ($\rho_\perp / \rho_{//} = 3.4$).

For the tetragonal I structure the WO_3 octahedra have been rotated in the basal plane. This rotation would effect the π-bonding of the tungsten $5d(t_{2g})$ orbitals with the oxygen 2p orbitals. In the basal plane there would be areas with greater overlap of the tungsten $5d(t_{2g})$ orbitals with the oxygen 2p orbitals, and areas with less overlap. The overall effect would be to disturb the π* conduction band in the basal plane and, hence, to reduce the conductivity in the basal plane. The conductivity in the basal plane would be smaller than the conductivity along the c axis. Hence, the tungsten 5d π-bond model could conceivably account for the magnitude of the anisotropy observed in the resistivity of tetragonal I Na_xWO_3.

VI. CONCLUSION

Ellerbeck et al. (10) were the first to demonstrate that the homogeneity of the Na_xWO_3 single crystals affected the electrical resistivity. We have shown that the homogeneity of the samples also affects the Hall coefficient and Seebeck coefficient. For the first time the effects of ordering of the sodium atoms were observed in the resistivities and Hall coefficients. The Seebeck coefficients, at low temperatures, contained a phonon-drag effect due to normal electron-phonon interactions and a phonon-drag effect due to Umklapp electron-phonon interactions. The normal phonon-drag decreased with increasing sodium concentration; while the Umklapp phonon-drag increased with increasing sodium concentration.

From the results of the present study, we conclude that free electron theory cannot be applied to the conduction electrons in Na_xWO_3. Thus, the question arises, "Which model does describe the electronic properties of Na_xWO_3?"

The nuclear magnetic resonance data suggests that the conduction band in Na_xWO_3 is formed from the tungsten non-s states. The most conceivable arrangement which would provide the largest overlap and hence the broadest conduction band would be the π-bonding of the tungsten $5d(t_{2g})$ orbitals with the oxygen 2p orbitals as suggested first by Sienko (23) and later extended by Goodenough (24). The experimental results of the transport properties do not disagree with this conclusion. In fact, the behavior of the transport properties can be understood qualitatively on the basis of the tungsten 5d π-bond model. Thus, if we

consider all the data which is available for Na_xWO_3, at the present the most satisfactory model would be the tungsten 5d π-bond model.

However, the tungsten 5d π-bond model, along with all of the other models, does not provide a quantitative theory which can be compared with the experimental results. With better experimental data now available, it is highly desirable to have a more quantitative theory. At the present state of band structure calculations, it is not too unreasonable to suggest that band structure calculations be attempted for the two ideal structures $Na_{0.75}WO_3$ and $NaWO_3$. Such calculations could determine the conduction band in Na_xWO_3 and allow one to describe the Fermi surface.

It would be desirable to remeasure the electronic specific heat. We have assumed that when the sodium atoms order, the Brillouin zone is cut in half by superzones, and another conduction band is formed. If this assumption is correct, the density of states at the Fermi energy should show a sudden increase at $x = 0.75$. The existing electronic specific heat data tends to verify this assumption. However, it would be very worthwhile to repeat the experiment with a larger number of homogeneous samples that are spaced closer together in sodium concentration.

VII. LITERATURE CITED

1. Wholer, F., Ueber das wolfram. Ann. Phys. 2, 345 (1824).

2. Hagg, G. Z., Na_xWO_3 cubic and tetragonal I. Z. Phys. Chem. B, 29, 192 (1935).

3a. Magneli, A., Crystal structure studies on tetragonal sodium tungsten bronze. Ark. Kemi 1, 269 (1949).

3b. Magneli, A. and Blomberg, B., Contribution to the knowledge of the alkali tungsten bronzes. Acta Chem. Scandinavica 5, 372 (1951).

4. Ribnick, A. S., Post, B., and Banks, E., Phase transitions in Na_xWO_3. Adv. Chem. Ser. 39, 246 (1963).

5. Straumanis, M. D. and Dravnieks, W., The sodium tungsten bronzes. II. The electrical conductivity of the bronzes. J. Amer. Chem. Soc. 71, 683 (1949).

6. Huibregtse, E. J., Barker, D. B., and Danielson, G. C., Electrical properties of sodium tungsten bronze. Phys. Rev. 84, 142 (1951).

7. Brown, B. W. and Banks, E., Conductivity of the sodium tungsten bronzes. Phys. Rev. 84, 609 (1951).

8. Gardner, W. R. and Danielson, G. C., Electrical resistivity and Hall coefficients of sodium tungsten bronze. Phys. Rev. 93, 46 (1954).

9. Shanks, H. R., Sidles, P. H., and Danielson, G. C., Electrical properties of the tungsten bronzes. Adv. Chem. Ser. 39, 237 (1963).

10. Ellerbeck, L. D., Shanks, H. R., Sidles, P. H., and Danielson, G. C., Electrical resistivity of cubic sodium tungsten bronze. J. Chem. Phys. 35, 298 (1961).

11. Atoji, M. and Rundle, R. E., Neutron diffraction study on sodium tungsten bronzes. J. Chem. Phys. 32, 627 (1960).

12. Mackintosh, A. R., The electronic structure of metal tungsten bronzes. J. Chem. Phys. 38, 1991 (1963).

13. Vest, R. W., Griffel, M., and Smith, J. F., Electronic specific heat of sodium tungsten bronze. J. Chem. Phys. 28, 293 (1958).

14. Greiner, J. D., Shanks, H. R., and Wallace, D. C., Magnetic susceptibility of Na_xWO_3. J. Chem. Phys. 36, 772 (1962).

15. McNeill, W. and Conroy, L. E., Electrical properties of some dilute cubic sodium tungsten bronzes. J. Chem. Phys. 36, 87 (1962).

16. Jones, W. H., Garbaty, E. A., and Barnes, R. G., Nuclear magnetic resonance in metal tungsten bronzes. J. Chem. Phys. 36, 494 (1962).

17. Narath, A. and Wallace, D. C., Nuclear magnetic resonance in cubic sodium tungsten bronzes. Phys. Rev. 127, 724 (1962).

18. Fromhold, A. T. and Narath, A., Transient nuclear magnetic resonance study of the conduction band of metallic Na_xWO_3: Na relaxation. Phys. Rev. 136, A487 (1964).

19. Fromhold, A. T. and Narath, A., Transient nuclear magnetic resonance study of the conduction band of metallic Na_xWO_3: 183W relaxation. [To be published in Phys. Rev. ca. 1966].

20. Ziman, J. M., Electrons and phonons. London, England, Clarendon Press. 1960.

21. Brown, B. W. and Banks, E., The sodium tungsten bronzes. J. Amer. Chem. Soc. 76, 963 (1954).

22. Reuland, R. J. and Voigt, A. F., Activation analysis for sodium in the sodium tungsten bronzes. Analyt. Chem. 35, 1263 (1963).

23a. Sienko, M. J., Thallium-tungsten bronze: a solid state defect structure. J. Amer. Chem. Soc. 81, 5556 (1959).

23b. Sienko, M. J., Electrical and magnetic properties of the tungsten and vanadium bronzes. Adv. Chem. Ser. 39, 224 (1963).

24a. Goodenough, J. B., Transition metal oxides with metallic conductivity. Bull. Soc. Chim. France 4, 1200 (1965).

24b. Goodenough, J. B., Covalency criterion for localized vs. collective electrons in oxides with the perovskite structure. J. Appl. Phys. Supplement 37, 1415 (1966).

25. Ferretti, A., Rogers, D. B., and Goodenough, J. B., The relation of the electrical conductivity in single crystals of rhenium trioxide to the conductivities of Sr_2MgReO_6 and Na_xWO_3. J. Phys. Chem. Solids 26, 2007 (1965).

26. Crowder, B. L. and Sienko, M. J., Some solid state studies of tungsten trioxide and their significance to tungsten bronze theory. J. Chem. Phys. 38, 1576 (1963).

27. Fuchs, R., Electronic properties of the tungsten bronzes. J. Chem. Phys. 42, 3781 (1965).

28. Bardeen, J., Conduction: metals and semiconductors. In Condon, E. U. and Odishaw, H., eds. Handbook of physics. pp. 4-73 - 4-102. New York, New York, McGraw-Hill Book Company, Inc. 1958.

29. Handbook of chemistry and physics. 39th ed. Cleveland, Ohio, Chemical Rubber Publishing Co. 1958.

30. Jan, J. P., Galvanomagnetic and thermomagnetic effects in metals. Solid State Phys. 5, 1 (1957).

31. Lee, R. S. and Legvold, S., Hall effect in Gd single crystals. Bull. Am. Phys. Soc. 11, 447 (1966).

32. Kevane, C. J., Legvold, S., and Spedding, F. H., The Hall effect in yttrium, lanthanum, cerium, praseodymium, neodymium, gadolinium, dysprosium, and erbium. Phys. Rev. 91, 1372 (1953).

33. Lavine, J. M., Alternate current apparatus for measuring the ordinary Hall coefficient of ferromagnetic metals and semiconductors. Rev. Sci. Instr. 29, 970 (1958).

34. Christian, J. W., Jan, J. P., Pearson, W. B., and Templeton, I. M., Thermoelectricity at low temperatures. VI. A redetermination of the absolute scale of thermoelectric power of lead. Proc. Roy. Soc. A245, 213 (1958).

35. Gardner, W. R., Electrical resisitivity and Hall effect in sodium tungsten bronze. Unpublished Ph.D. thesis. Ames, Iowa, Library, Iowa State University of Science and Technology. 1953.

36. MacDonald, D.K.C., Thermoelectricity: an introduction to the principles. New York, New York, John Wiley and Sons, Inc. 1962.

37. Hanna, I. I. and Sondheimer, E. H., Electron and lattice conduction in metals. Proc. Roy. Soc. A239, 247 (1957).

38. Bailyn, M., Transport in metals: effect on the nonequilibrium phonons. Phys. Rev. 112, 1587 (1958).

39. Elliott, R. J. and Wedgwood, F. A., Theory of the resistance of rare earth metals. Proc. Phys. Soc. 81, 846 (1963).

40. Ziman, J. M., Ordinary transport properties of the noble metals. Adv. Phys. 10, 1 (1961).

41. Ziman, J. M., The thermoelectric power of the alkali metals at low temperatures. Phil. Mag. 4, 371 (1959).

42. Ziman, J. M., Ordinary transport properties and the shape of the Fermi surface. In Harrison, W. A. and Webb, M. B., eds. The Fermi surface. pp. 296-305. New York, New York, John Wiley and Sons, Inc. 1960.

VIII. ACKNOWLEDGMENTS

It is a pleasure to thank my major professor, Dr. G. C. Danielson, for his encouragement and guidance during my graduate study. I would also like to thank Dr. A. L. Trego, Dr. R. Fuchs, Dr. J. B. Goodenough and Dr. A. Narath for their helpful discussions. I would especially like to thank Dr. A. Narath for making his results of the ^{183}W relaxation times available to me before they were published.

I have appreciated the help of Mr. P. H. Sidles and Mr. O. M. Sevde in connection with the design and maintenance of much of the electrical equipment. Special thanks and appreciation is given to Miss J. E. Brown who helped prepare the Na_xWO_3 samples and take the resistivity data.

I would especially like to thank my wife Leda, and my two sons, Kerry and Mylan. Their love and encouragement helped make my graduate study a very worthwhile and enjoyable experience.

IX. APPENDIX A: TEMPERATURE CONTROLLER

The temperature controller, which was used to maintain the equilibrium temperatures, is shown in a block diagram in Fig. 31. The temperature controller was designed to use either resistive sensing elements or thermocouple sensing elements. For the Seebeck coefficients, a carbon resistor was used as a sensing element between 4.2°K and 40°K. A copper resistor was used as a sensing element between 40°K and 340°K. For the Hall coefficients, a carbon resistor was also used as a sensing element between 4.2°K and 40°K. A copper-constantan thermocouple was used as a sensing element between 40°K and 340°K.

The resistance bridge circuit for the resistive sensing elements is shown in Fig. 32. The thermocouple bridge circuit for the thermocouple sensing elements is shown in Fig. 33. The servo amplifier circuit is shown in Fig. 34 and the heater power supply is shown in Fig. 35.

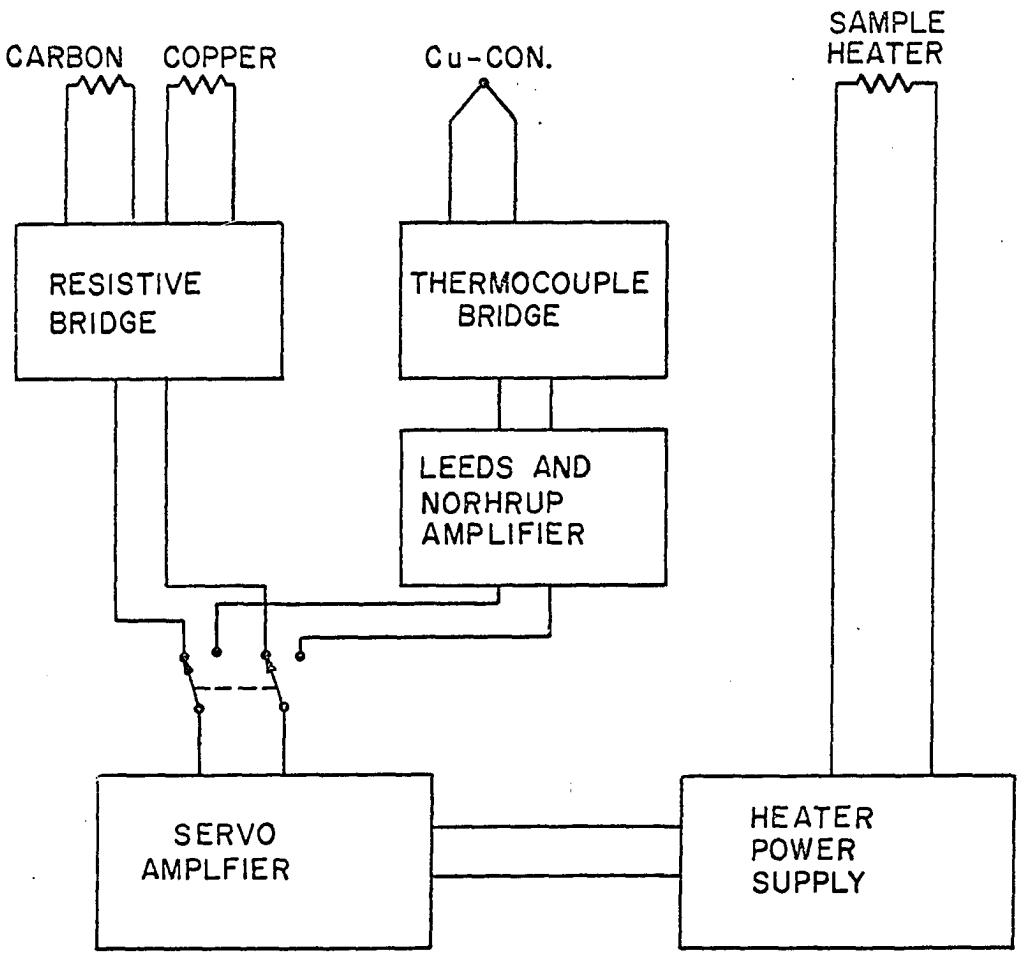

Fig. 31. Block diagram of the temperature controller

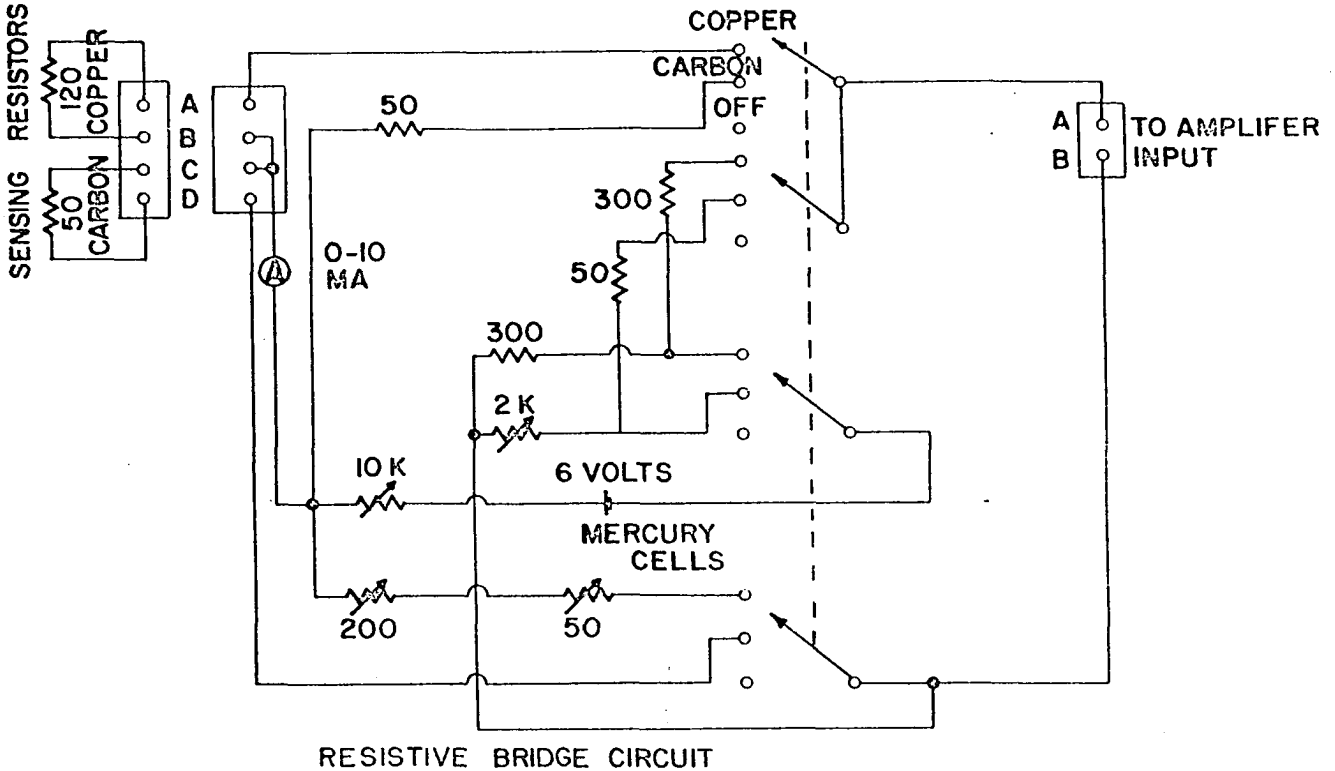

Fig. 32. Resistance bridge circuit for the resistive sensing elements

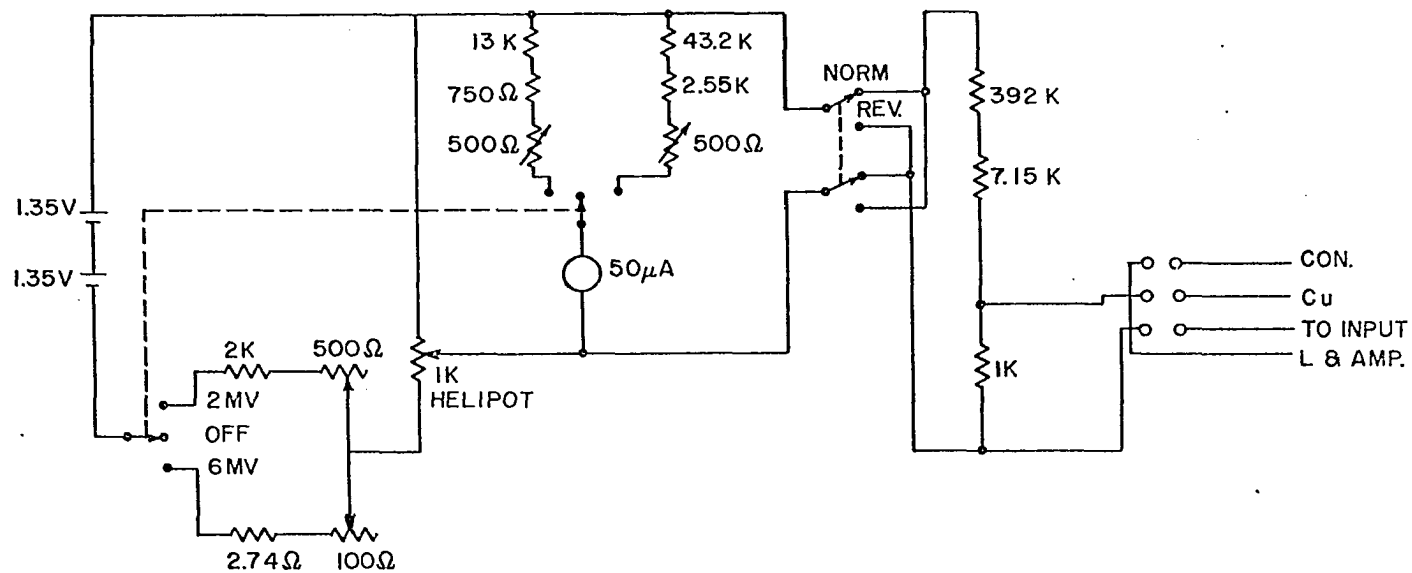

THERMOCOUPLE BRIDGE CIRCUIT

ALL FIXED RESISTORS ARE PRECISION RESISTORS

Fig. 33. Thermocouple bridge circuit for the thermocouple sensing elements

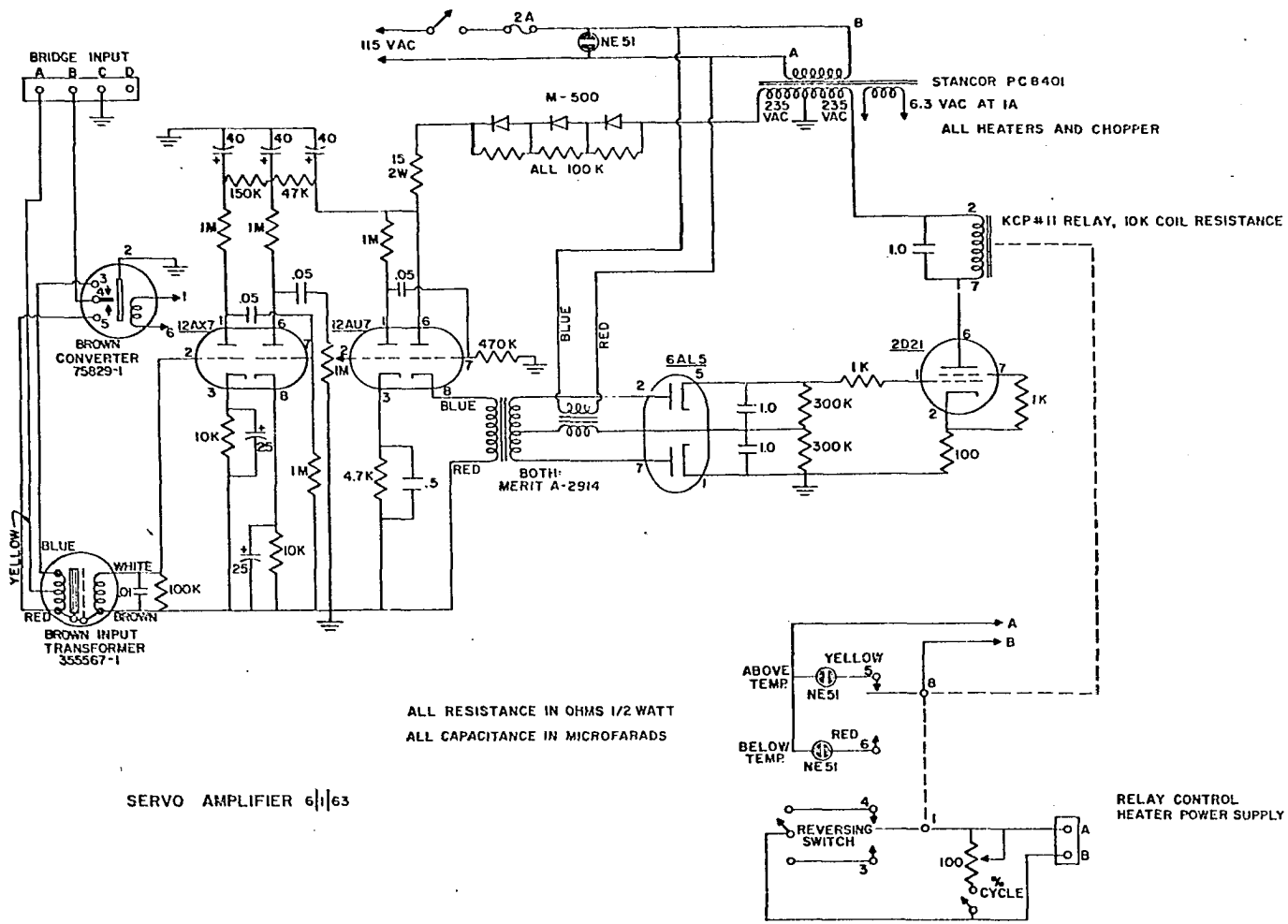

Fig. 34. Servo amplifier circuit

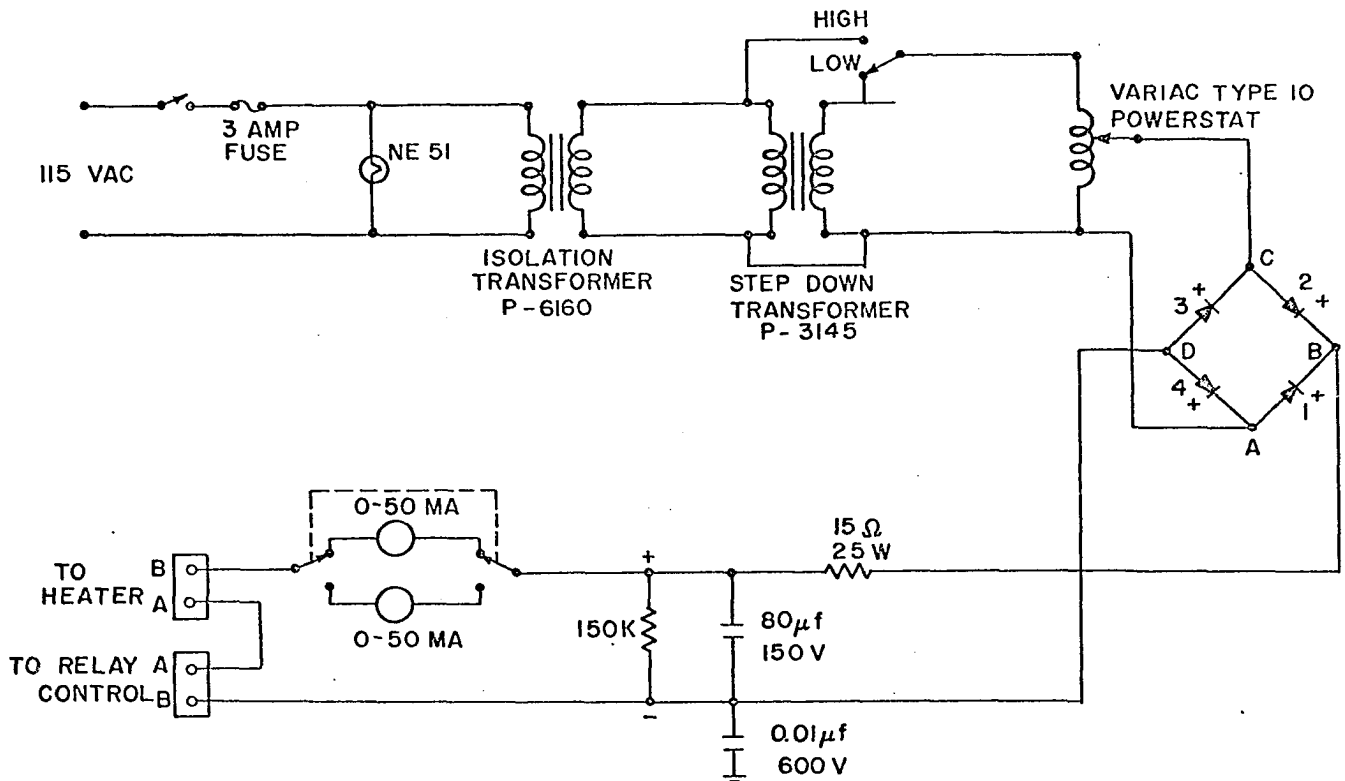

Fig. 35: Heater power supply

X. APPENDIX B: EXPERIMENTAL DATA

Table 4. Resistivity of cubic Na_xWO_3 single crystals at 4.2, 300, and 773°K

Sample number	x-value	ρ (x 10^{-6} ohm-cm) 773°K	300°K	4.2°K
261-E	0.874	55.12	15.65	3.50
261-D	0.873	56.74	16.03	
70-D	0.854		17.83	4.60
230-C2	0.817	62.79	19.95	6.55
59-A	0.777	69.11	20.85	7.02
230-B1	0.745	71.48	21.28	7.07
242-B	0.730	70.82	22.25	8.10
277-B	0.717	73.48	24.59	9.71
249-A1	0.698	78.70	26.61	10.99
138-A2	0.662		31.22	13.30
235-J	0.617	98.84	34.90	15.68
94-D	0.590	104.9	39.29	19.39
234-A	0.565	113.9	45.25	23.79
258-D	0.551	122.8	48.54	26.10
281-H	0.513	135.7	58.63	31.86
244-A1	0.512	137.4	58.83	

Table 5. Hall coefficients of Na_xWO_3 at 300°K

Sample number	x-value	f(L/w)[a]	R(x 10^{-4} cm^3/coulomb)
261-E	0.874	0.998	-3.38 ± 0.02
261-D	0.873	0.999	-3.37 ± 0.03
70-D	0.854	0.998	-3.47 ± 0.03
230-C2	0.817	0.990	-3.68 ± 0.02
59-A	0.777	0.995	-3.80 ± 0.02
230-B1	0.745	1.000	-3.82 ± 0.04
242-B	0.730	0.995	-3.83 ± 0.03
277-B	0.717	1.000	-3.95 ± 0.02
249-A1	0.698	1.000	-3.93 ± 0.05
235-J	0.617	0.975	-4.26 ± 0.03
94-D	0.590	1.000	-4.41 ± 0.03
234-A	0.565	0.990	-4.46 ± 0.03
258-D	0.551	0.988	-4.73 ± 0.05
281-H	0.513	1.000	-5.09 ± 0.04
244-A1	0.512	0.992	-4.99 ± 0.05
109-B2 (// c)	0.451	0.985	-6.54 ± 0.29
105-B2a (// c)	0.423	0.995	-7.18 ± 0.13
105-A (⊥ c)	0.457	0.996	-7.78 ± 0.24
109-A3 (⊥ c)	0.405	0.990	-10.02 ± 0.26

[a]Shape correction factor, Reference 30, p. 20.

Table 6. Seebeck coefficients of Na_xWO_3 at 15, 40, 100, 210 and 300°K

Sample number	x-value	S_x (x 10^{-6} volts/°K) 15°K	40°K	100°K	210°K	300°K
59-D	0.875	-0.54	-1.02	-2.85	-6.20	-7.80
230-C2	0.817	-0.64	-1.21	-3.07	-6.58	-8.18
230-B1	0.745	-0.79	-1.43	-3.70	-7.35	-8.75
249-A1	0.698	-0.89	-1.70	-3.98	-7.90	-9.60
235-J	0.617	-0.97	-1.95	-4.25	-8.55	-10.42
234-A	0.565	-1.07	-2.29	-5.08	-9.60	-11.80
244-A1	0.512	-1.31	-2.67	-5.67	-10.30	-12.70
105-A (⊥ c)	0.457	-1.44	-2.98	-5.92	-10.55	-13.70
105-Aa (⊥ c)	0.432	-1.68	-3.23	-6.11	-11.09	-14.40
105-B1 (⊥ c)	0.423	-1.56	-3.12	-6.45	-11.78	-15.50
109-A3 (⊥ c)	0.405	-1.81	-3.56	-7.15	-13.40	-17.70
109-B2b (// c)	0.451	-1.10	-2.32	-4.70	-8.30	-10.75
105-B2a (// c)	0.423	-1.22	-2.41	-5.05	-9.20	-11.62

Table 7. Resistivity of tetragonal I Na_xWO_3 single crystals at 300°K

Sample number	x-value	ρ (x 10^{-6} ohm-cm)
109-B2b (// c)	0.451	103.2 ± 8.0
109-A4 (// c)	0.437	110.7 ± 6.4
105-B2a (// c)	0.423	122.6 ± 10.3
105-A (⊥ c)	0.457	351.4 ± 22.8
105-Aa (⊥ c)	0.432	381.5 ± 27.5
105-B1 (⊥ c)	0.423	410.4 ± 18.1
109-A3 (⊥ c)	0.405	557.9 ± 25.1

Table 8. Anisotropy of tetragonal I Na_xWO_3 single crystals at 300°K

Ratio of lattice constants (c/a)	Resistivity ($\rho_{//}/\rho_{\perp}$)	Hall coefficients ($R_{//}/R_{\perp}$)	Mobility ($\mu_{//}/\mu_{\perp}$)	Seebeck coefficients ($S_{//}/S_{\perp}$)
0.31	0.29	0.48	2.86	0.76